UNIVERSITÀ
DEGLI STUDI
FIRENZE

DOTTORATO DI RICERCA IN SCIENZE CHIMICHE

CICLO XXVI

COORDINATORE Prof. PIERO BAGLIONI

"CHEMICAL CHARACTERIZATION OF ATMOSPHERIC AEROSOL COLLECTED IN THE CENTRAL MEDITERRANEAN SEA: STUDY OF NATURAL AND ANTHROPIC SOURCES"

Settore Scientifico Disciplinare CHIM/01

Dottorando
Dott.ssa Miriam Marconi

Tutore
Prof. Roberto Udisti

Coordinatore
Prof. Piero Baglioni

Anni 2011/2016

INTRODUCTION

Atmospheric aerosols are estimated to have negative effects on human health and to play a relevant role in climate, also affecting the hydrological cycle and the atmospheric radiative balance through scattering, absorption, and emission of radiation and by acting as cloud condensation nuclei (IPCC 2007; di Sarra et al., 2011; Levin et al. 1996). Thus the effect that atmospheric aerosol produce on climate is among the main priorities to reduce uncertainties in future climate projections: in this view assessing its chemical composition is one of the major topic in the study of climate change.

The Mediterranean Basin, due to its vicinity with African deserts and industrialized areas of continental Europe, is one of the regions heavily influenced by aerosols and its atmosphere appears to be one of the most polluted in the world (Kouvarakis et al., 2000; Lelieveld and Dentener, 2000). Cause to its peculiarities (relative reduced dimensions and open waters quite close to the coast) the Mediterranean Sea is very reactive to climatic and environmental changes so that is considered among the regions the most sensitive to climate change (IPCC 2007). Therefore, analysing chemical composition of aerosols collected in this area results very interesting in order to characterize natural and anthropogenic sources and their contribute to PM. In this thesis chemical composition of PM10 (particulate matter with AED <10 μm) sampled at daily resolution on the Island of Lampedusa (35.5°N, 12.6° E) over a ten years' time (from 2004 to 2014) is presented. Indeed, thanks to its position in the centre of Mediterranean sea, Lampedusa is an ideal remote sampling site for

studies on the background aerosol and is part of the regional World Meteorological Organization/ Global Atmospheric Watch network. Furthermore, this work is connected to several international multidisciplinary programs as MISTRALS (Mediterranean Integrated Studies At Local And Regional Scales) and ChArMEx (the Chemistry-Aerosol Mediterranean Experiment) which aim to better understanding the atmospheric chemistry and meteorology of the Mediterranean basin.

In particular Saharan dust inputs, Sea Salt aerosols an anthropic emissions from maritime traffic at Lampedusa are identified and characterized both from the chemical composition and from others parameters as optical properties and backward trajectories. Moreover studies on the solubility and the sizing of the main components of these aerosol sources are carried out. Finally the application of a statistical model (The Positive Matrix Factorization - PMF) to 2-year long data set (2007 and 2008) of PM10 mass concentration and chemical composition are presented: results confirmed the experimental data set and its interpretation illustrated in this thesis.

CHAPTER 1 - Atmospheric Aerosol

1.1. Atmospheric aerosol: definition and prominence

An aerosol is by definition a collection of solid or liquid particles suspended in a gas. Therefore atmospheric aerosol is defined as the whole of solid or liquid particles suspended in the atmosphere. Atmospheric aerosols have significant local, regional and global impacts. Local impacts include vehicular emissions, wood burning fires and industrial processes that can lead to urban air pollution (Fenger, 1999; Mayer, 1999) and possible adverse health effects (Harrison and Yin, 2000). Regionally, aerosols can be transported from areas of high emissions to relatively clean remote regions. Moreover atmospheric aerosols influence the global climate of the planet in a number of ways:

1. Through scattering and absorption of solar radiation. Backscattering of solar radiation towards space results in a reduction of incoming solar radiation at the Earth's surface, a loss of energy and a cooling of the climate system. Absorption of solar radiation is accompanied by a heating within the aerosol layer, but also by a reduction of incoming solar radiation at the Earth's surface.

2. The absorption of solar radiation by aerosols modifies the vertical temperature profile. This impacts the relative humidity, atmospheric stability, and therefore cloud formation.

3. Aerosols serve as cloud condensation nuclei in liquid water clouds, thus exerting a partial control of cloud microphysical and optical properties. An increase in the concentration of aerosols leads to an increase in the concentration of cloud condensation nuclei, and generally

to an increase in the concentration of cloud droplets. For a fixed cloud liquid water content, this is accompanied by a reduction in the cloud droplet size and an increase in the cloud reflectivity. Altogether this leads to less solar energy absorbed and a cooling of the climate system.

4. The modification of cloud microphysical properties is expected to have an impact on cloud evolution, in particular in terms of the ability of clouds to generate droplets that are large enough to initiate precipitation.

5. Aerosols can impact the properties of mixed-phased and ice clouds, in particular through their role as ice nuclei.

6. Absorbing aerosols may deposit onto snow and ice surfaces, thus making these surfaces less reflective (i.e. more absorbing). This contributes to warm the surface and thus the climate system.

7. Finally, aerosols also interact with vegetation through changes in incoming solar radiation, fraction of diffuse radiation and as a source of nutrients.

At present, the radiative effects of aerosols have the largest uncertainties in global climate predictions. In particular, the Fifth Assessment Report of IPCC has indicated that the radiative forcing from aerosols has a weaker cooling effect respect to the previous evaluations. In fact the aerosol radiative forcing over 1750–2011 is estimated as –0.9 [–1.9 to −0.1] W/m^2 and presents two competing components: a dominant cooling effect from most aerosols and their cloud adjustments and a partially offsetting warming contribution from black carbon absorption of solar radiation. Thus, aerosols continue to contribute the largest uncertainty to

the total radiative forcing estimate (IPCC 2014). In addition aerosols are expected to have negative effects on air quality an human health (IPCC 2007). A better understanding of the formation, composition and transformation of aerosols in the atmosphere is of critical importance in order to better quantify these effects.

1.2. Classifications and sources of atmospheric aerosol

Atmospheric aerosols can be classified in different types according to their properties and formation processes. In particular two great categories have been recognized: primary and secondary aerosols. Primary aerosols have been directly emitted into the atmosphere as particles. This is the case of aerosols produced by the effect of the wind friction on an oceanic or terrestrial surface (sea spray and soil dust) and aerosols produced during an incomplete combustion as black carbon, organic matter in exhaust fumes or volcanic ash. Secondary aerosols designate those particles that have not been emitted directly in the particulate phase but come instead from the condensation of atmospheric gas-phase species. These gas-phase species, which can undergo a number of chemical transformations before they condense, are called aerosol precursors. As explained before, atmospheric aerosol can have both natural and anthropic origin and can be classified on the basis of its source. Here is presented a brief description of the main types of aerosol sources.

Marine Aerosols

The wind friction at the ocean surface ejects fine particles of salty marine water into the atmosphere. A fraction of the water evaporates, so that

the concentration of salt in the particle increases. This gives rise to sea salt particles that are more or less hydrated according to the ambient humidity. Although these particles are often called sea salt aerosols, this is yet another misuse of language because these particles may also contain biological material and other impurities. It is therefore more appropriate to refer to sea spray aerosols. Sea spray aerosols cover sizes that range from typically 100 nanometres (nm) to several tens of micrometres (μm). The largest particles fall back fairly quickly to the ocean surface and are therefore of lesser climatic importance.

Desert Dust

The wind friction on continental surfaces can detach soil particles and suspend them in the atmosphere. This is particularly the case in desertic, arid, and semiarid regions where the wind is not slowed down by the vegetation that is either completely absent or fairly sparse. The emission of soil particles to the atmosphere also requires a reduced soil humidity so that cohesive forces between soil particles are also reduced. As for sea spray aerosols, desert dust particles span sizes that range from typically 100 nm to tens of μm. Larger particles can also be lifted but they fall down quickly. Desert dust aerosols are also called mineral dust or mineral aerosols. Emissions of desert dust depend very much on environmental and meteorological conditions.

Volcanic Aerosols

Volcanoes can emit fragments of pulverized rocks and minerals, usually called volcanic ash, during explosive eruptions. These particles have sizes typically ranging from a micrometre to millimetres. Volcanic ash can be

transported over distances of a few hundreds to a few thousand kilometres but being micronic particles they tend to fall down rapidly. Hence their climate effect is limited. Volcanoes also emit sulphur-rich gases (in the form of sulphur dioxide, SO_2, and hydrogen sulphide, H_2S) that get oxidized in the atmosphere to form submicronic sulphate aerosols. If these sulphur-containing gases are emitted in the troposphere, the residence time of the subsequent aerosols will be short, a few weeks at most. However, if the eruption is powerful enough to inject the sulphur gases in the stratosphere, then the volcanic aerosols have a much longer residence time, of the order of a few months to more than a year, depending on the region and altitude of injection.

Biogenic Aerosols

The terrestrial biosphere is a source of primary biogenic aerosol particles. They comprise plant and insect debris, pollen (a fine powder produced by seed plants that contains the male gametes that serve for reproduction), spores (a reproduction cell or organ from many plants and fungi), bacteria and viruses. Once airborne, these particles can be transported by the wind on varying distances depending on their size. Debris are usually larger than 100 µm, pollen, spores and large bacteria are generally in the range of 1–100 µm, while small bacteria and viruses are generally smaller than 1 µm. Seawater also can contain biological material, some of which is transferred to sea spray aerosols during the emission process (primary biogenic aerosols). Moreover, terrestrial and marine ecosystems are important sources of aerosol precursors. Some species of phytoplankton produce dimethylsulphide (DMS), a gaseous

compound that is oxidized in the atmosphere to form sulphur-containing aerosols (Becagli et al. 2013). Plants and algae emit volatile organic compounds (VOCs) that are oxidized in the atmosphere and condense and contribute organic material to the atmospheric aerosol. These aerosols are referred to as secondary biogenic aerosols.

Biomass Burning Aerosols

In biology, biomass refers to material produced by living organisms, but we adjust the definition here to mean all biological (organic) material that comes from the living world and can potentially burn (i.e. vegetation, dead wood, animal dung, peat) while excluding so-called fossil fuels (coal, gas, and oil) that are formed on geological timescales. The burning of biomass generates primary aerosols that stem from the incomplete combustion of the organic matter. Biomass burning aerosols include organic carbon, that is associated with hydrogen and oxygen atoms, and black carbon, where the carbon content is very high. These aerosols are generally submicronic and are clearly visible in smoke plumes. The sources of biomass burning aerosols are both natural and anthropogenic. The combustion of biomass also emits gaseous compounds, such as volatile organic compounds and sulphur dioxide, which are aerosol precursors (O. Boucher, 2015).

Aerosols from Fossil Fuel Combustion

The combustion of coal and oil derivatives also produces black carbon and organic carbon, as well as sulphur dioxide that converts into sulphate aerosols. These are essentially submicronic particles, that are also a source of air pollution in developing and industrialized countries. Air

pollution due to particles and gas-phase pollutants, such as ozone and nitrogen oxides, is responsible for a wide range of adverse health and environmental effects. Effects on human health include increased respiratory and cardio-vascular diseases and associated mortality. Furthermore, aerosols and acidic deposition are responsible for damages on historical buildings.

1.3. Properties of Atmospheric aerosols

1.3.1. Particle size

Particle size is one of the most important parameters for characterising the behaviour of aerosols. The diameters of atmospheric aerosols can span over four orders of magnitude, from a few nanometres to around 100 µm. Atmospheric particles are usually referred to as having a diameter, implying they are spherical. However, particles in the atmosphere have widely variable shapes for which geometrical diameters are often not meaningful. In practice, the size of such irregularly shaped particles is expressed in terms of an equivalent diameter that depends on a physical, rather than a geometrical, property. An equivalent diameter is defined as the diameter of the sphere that would have the same value of a particular physical property as that of the irregular particle (Hinds, 1999). There are different types of equivalent diameters. One of the most commonly used is the aerodynamic diameter, AED, which is defined as the diameter of a sphere of unit density (1 g cm^{-3}) that has the same settling velocity in air as the particle under consideration. Aerodynamic diameter standardizes particles of various shapes and densities to spheres having the same aerodynamic property, settling velocity.

Atmospheric aerosols are classified into separate modes according to their size, formation process and atmospheric age. Based on the number, surface, and volume distributions of aerosol particles shown in Figure 1.1, three distinct groups of atmospheric particles can be defined: ultrafine (Nucleation mode), fine (Aitken and Accumulation mode) and coarse particles (Coarse mode).

Particles with diameters larger than 1.0 μm are identified as the coarse mode. These particles are mainly produced by mechanical processes and are introduced directly into the atmosphere from both natural and anthropogenic sources. The most significant sources of these particles are marine, soil dust and anthropogenic ones that are introduced into the atmosphere through the abrasion of machinery, on the surface of roads, and in industrial and agricultural processes. Because of their relatively large size, coarse particles settle out of the atmosphere in a reasonably short time by sedimentation, except on windy days, where fallout is balanced by reentrainment. Particles with diameters between 0.1-1.0 μm are considered as the accumulation mode representing a region of particle growth mainly due to the coagulation of particles with diameters smaller than 0.1 μm and from condensation of vapours onto existing particles, causing them to grow into this size range. They can also be introduced directly into the atmosphere, mainly through the incomplete combustion of wood, oil, coal, gasoline and other fuels. Because of the nature of their sources, particles in the accumulation size range generally contain substantial amounts of organic material as well as soluble inorganics such as ammonium, nitrate and sulphate. The

accumulation mode is so named because particle removal mechanisms are least efficient in this regime, causing particles to accumulate there until they are ultimately lost through rain or other forms of precipitation (wet deposition).

The Aitken mode particles, extending from 0.01 to 0.1 μm diameter, are formed from ambient-temperature gas-to-particle conversion as well as condensation of hot vapours during combustion processes. These particles act as nuclei for the condensation of low-vapour pressure gaseous species, causing them to grow into the accumulation range. The lifetime of these particles is short, as they are lost principally by coagulation with larger particles. The Aitken and accumulation mode particles are referred to collectively as fine particles.

The final type of particles are those with diameters smaller than 0.01 μm (not shown in Figure 1.1) and are known as ultrafine particles. They are thought to be generated by gas-to-particle conversion processes but they are difficult to study because of their very small size and mass. Moreover these particles have a very short lifetime, sometimes on the order of seconds or minutes, due to their rapid coagulation or random impact onto surfaces.

The nucleation and Aitken mode particles account for the majority of atmospheric particles by number, but due to their small sizes, they rarely account for more than a few percent of the total mass of PM. Hence if the toxicological effects are determined primarily by the number of particles, rather than their mass, these small particles could ultimately prove to be of high importance. The Accumulation mode particles

account, generally, for a significant fraction of the total aerosol mass and have the greatest surface area. This makes these particles of significant importance to gas phase deposition and atmospheric heterogeneous chemistry. Most of the aerosol mass is found in the coarse mode, where large particles contribute significantly to the optical properties of atmospheric aerosols.

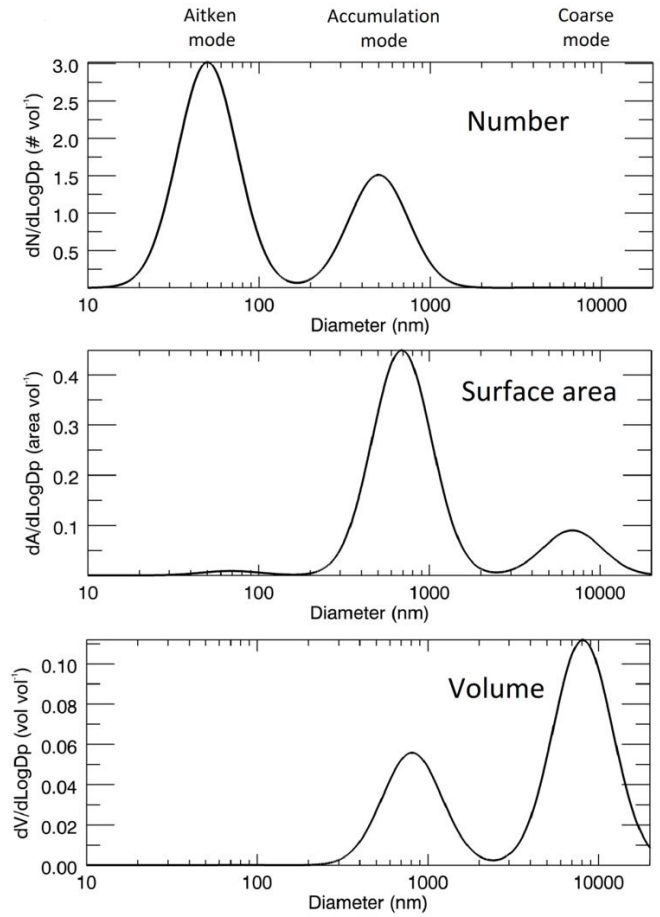

Figure 1.1 - *The hypothetical log-normal aerosol distribution plotted, from top to bottom, as a number vs. diameter distribution, a surface area vs. diameter distribution, and a volume vs. diameter distribution.*

Fig.1.2 shows the size distribution and the main mechanisms which lead to the formation of coarse, fine and ultrafine particles in the atmospheric aerosol. These modes, in general, originate separately, are transformed separately and removed from the atmosphere by different mechanisms, have different lifetimes, chemical composition and optical properties, and differ significantly in their deposition patterns in the respiratory tract. Therefore, the distinction between nucleation, Aitken, accumulation and coarse particles is fundamental in any discussion of the physics, chemistry, measurement, or health effects of aerosols.

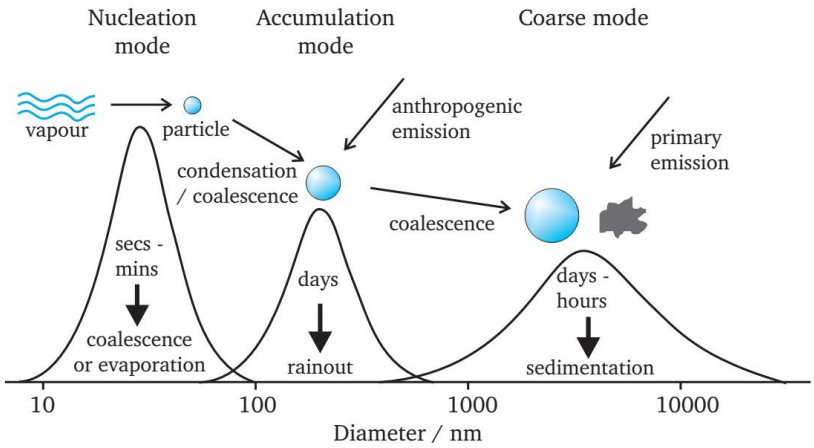

Figure 1.2 - *Schematic size distribution of atmospheric aerosol with the main formation processes of the particles.*

Finally, often in literature is used a similar classification based on the size of the particles suspended in the atmospheric aerosol (particulate matter - PM) and that are selected by the sampling instrumentations:

1) The coarse fraction contains the larger particles with a size ranging from 2.5 to 10 μm and correspond to the fraction from PM10 (PM with AED < 10 μm) to PM2.5 (PM with AED < 2.5 μm);
2) The fine fraction contains those particles with a size up to 2.5 μm and correspond to PM2.5.
3) The Ultrafine fraction contains particles smaller than 0.1 μm.

Most of the total mass of airborne particulate matter is usually made up of fine particles ranging from 0.1 to 2.5 μm. Ultrafine particles often contribute only a few percent to the total mass, though they are the most numerous, representing over 90% of the number of particles. In this thesis even this classification will be used since that results on the chemical composition of PM10 collected at Lampedusa will be presented.

1.3.2. Optical properties

As explained before aerosols interact strongly with solar and terrestrial radiation in several ways. The main optical variables used to quantify the impact of light-aerosol interaction on the environment are briefly descripted below. In particular in this thesis results about AOD (τ) and Aerosol Angstrom Exponent (α) values measured in PM10 samples will be illustrated in chapter 7.

Aerosol optical depth (AOD) is a measure of the amount of incident light either scattered or absorbed by airborne particles. Formally, aerosol optical depth is a dimensionless quantity, the integral of the product of particle number concentration and particle extinction cross-section (which accounts for individual In addition to AOD, particle size, composition, and structure, which are mediated both by source type and

subsequent atmospheric processing, determine how particles interact with radiant energy and influence the heat balance of the planet. Size and composition also determine the ability of particles to serve as nuclei upon which cloud droplets form. This provides an indirect means for aerosol to interact with radiant energy by modifying cloud properties.

Aerosol Angstrom Exponent (α) It is an exponent that expresses the spectral dependence of aerosol optical thickness (τ) with the wavelength of incident light (λ). The spectral dependence of aerosol optical thickness can be approximated (depending on size distribution) by,

$$\tau a = \beta \lambda^{\alpha}$$

where α is Angstrom exponent (β = aerosol optical thickness at 1 μm). The Angstrom exponent provides additional information on the particle size (larger the exponent, the smaller the particle size), aerosol phase function and the relative magnitude of aerosol radiances at different wavelengths.

Single scattering albedo (SSA) describes the fraction of light interacting with the particle that is scattered, compared to the total that is scattered and absorbed. Values range from 0 for totally absorbing (dark) particles to 1 for purely scattering ones; in nature, SSA is rarely lower than about 0.75.

Asymmetry parameter (g), reports the first moment of the cosine of the scattered radiation angular distribution. The parameter g ranges from -1 for entirely back-scattering particles, to 0 for isotropic (uniform) scattering, to +1 for entirely forward-scattering.

Surface albedo (A) is the a measure of reflectivity at the ground, and, like SSA, ranges from 0 for purely absorbing to 1 for purely reflecting. In practice, A can be near 0 for dark surfaces, and can reach values above 0.9 for visible light over snow.

AOD, α, SSA, g, and A are all dimensionless quantities, and are in general wavelength-dependent. Light-aerosol interaction is on the basis of which an important class of instruments, optical ones, is used to measure aerosol dimension and concentration. Their great advantage is that they are responsive, almost instantaneously responding time and they don't need a physical contact with particulate.

1.3.3. Aerosol chemical composition

Understanding the chemical composition of aerosol particles is crucial in order to better quantify their effects on human health and global climate. Atmospheric aerosols are generally composed of variable amounts of sulphate, ammonium, nitrate, sodium, chloride, trace metals, crustal elements, water and carbonaceous material. Here a summary report of those main components is given, a more detailed description of the aerosol chemical composition of the Mediterranean basin will be provide in the next chapters of this thesis.

The sulphate component is derived predominantly from the atmospheric oxidation of anthropogenic and natural sulphur-containing compounds such as sulphur dioxide (SO_2) and dimethyl sulphide (DMS), respectively. Nitrate is formed mainly from the oxidation of atmospheric nitrogen dioxide (NO_2). Sulphate and nitrate are initially formed as sulphuric (H_2SO_4) and nitric acids (HNO_3), but are progressively

neutralised by atmospheric ammonia (NH_3) forming the corresponding ammonium salts.

The main source of chlorides is sea spray even at locations hundreds of miles from the coast. Chloride is a typical primary aerosol component, but it is also possible to observe as a secondary aerosol, in the form of ammonium chloride (NH_4Cl), in ammonia and hydrochloric acid rich atmospheres. Exchange between H_2SO_4 HNO_3 and NaCl carries to gaseous HCl, that can be transported in the atmosphere (so aerosol Cl/Na ratio varies from seawater ratio).

Crustal materials include soil dust and windblown minerals. They vary in composition according to local geology and surface conditions and reside mainly in the coarse particle fraction.

The carbonaceous fraction of the aerosols consists of both elemental and organic carbon. Elemental carbon (EC), also called black carbon, graphitic carbon, or soot, is emitted directly into the atmosphere, predominantly from combustion processes. While particles containing organic carbon (OC) can be directly emitted into the atmosphere (i.e. from primary sources such as biomass burning and combustion processes), they can also be introduced by secondary organic aerosol (SOA) formation. The latter process occurs when volatile organic compounds undergo atmospheric oxidation reactions, forming products that have low enough volatilities to form aerosol via either nucleation or gas-to-particle conversion processes.

Volatile organic compounds (VOCs) are emitted into the atmosphere from anthropogenic and biogenic sources especially from vegetation and

farming. Anthropogenic VOC sources comprise organics such as alkanes, alkenes, aromatics and carbonyls, while biogenic sources include organics such as isoprene, monoterpenes and sesquiterpenes. Once in the atmosphere, such VOCs can react very complexly starting from ozone and nitrate and hydroxyl radicals.

Finally methane can be emitted in the atmosphere directly, moreover CH_4 can be formed by formaldehyde, terpens and isoprenes emitted from forests areas, after photolytically breakdown processes. Formaldehyde is an important intermediate of other short chain hydrocarbons oxidation; and other kinds of intermediate may be represented by short chain organic acids (acetic, formic, propionic, pyruvic), concurring to precipitations pH in remote areas.

In this thesis the attention will be focused on the main inorganic components of the aerosol even if some additional data about the carbonaceous fraction from EC-OC measurements will be given in chapter 9 and 10.

1.4. Formation processes and removal mechanisms of atmospheric aerosols

1.4.1. Aerosol formation: nucleation and particles growth

A significant fraction of the total number of particles present in the atmosphere is formed originally by nucleation from the gas phase. There are two types of nucleation processes. Gases preferentially condense onto surfaces of pre-existing aerosol particles, known as heterogeneous nucleation. With sufficiently high supersaturation and no suitable surfaces, particles may condense in the absence of a pre-existing surface,

known as homogeneous nucleation. This results in the addition of very small, rapidly growing particles to the particle-size distribution.

Favourable conditions for nucleation processes include a strong source of condensable vapour, high UV radiation intensity, low aerosol surface area, high relative humidity (RH), low temperature, presence of ions and atmospheric mixing processes. Binary nucleation of sulphuric acid and water, ternary nucleation of sulphuric acid, water and ammonia and ion-induced nucleation are thought to be the most important aerosol nucleation processes in the atmosphere. Nucleation has been observed at many different places in the atmosphere: in the boundary layer, in the free troposphere, in remote locations, in coastal areas, in boreal forests as well as urban areas and pollution plumes. In most cases gaseous sulphuric acid is assumed to be the key precursor gas. Indeed, the most prevalent trace gases do not generally nucleate new aerosols (or even condense onto existing ones), because they are too volatile (i.e. they have a high saturation vapor pressure and thus evaporate readily). They first have to be oxidized (usually under the influence of sunlight) to produce a compound with a lower vapour pressure. The prime example of this is the oxidation of sulphur dioxide (SO_2) into sulfuric acid (H_2SO_4), which has a very low vapour pressure. The H_2SO_4 can then condense together with water vapour (and perhaps organic compounds and/or ammonia) to form a stable cluster of molecules: a new particle is typically 1-2 nanometres in diameter. Ions can also play a role, by lowering the energy barrier that needs to be overcome: the attractive forces between the molecules are stronger when one of them is charged. Instead of

nucleating into a new particle, H_2SO_4 could also condense on an existing aerosol particle, making it grow in size. After nucleation, other supersaturated substances, especially low vapour pressure organics often take part in the subsequent aerosol growth. Condensation of more vapour onto the nucleated aerosol makes it grow in size. However, other processes hamper its possibility to grow: two aerosols can collide together, in a process called coagulation. Coagulation is particularly efficient between very small nano-particles and larger particles (of a few hundred nanometres). It causes the bigger one to grow in size, whereas the smaller (recently nucleated) one disappears.

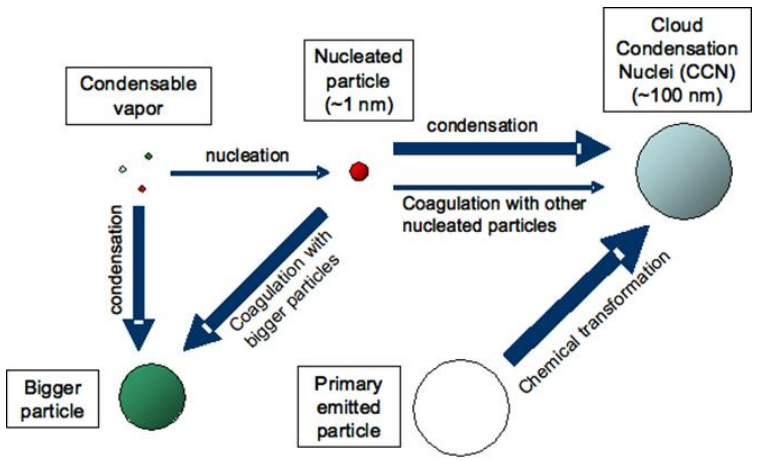

Figure 1.3 - *Main Gas-particle conversion processes with the formation of Cloud Condensation Nuclei (CCN).*

When there are a lot of very small aerosols around (i.e. after a nucleation event), they can also coagulate together. This causes them to grow in size, but decreases their number concentration. These Gas-particle conversion processes produce lower dimension (sub-

micrometric) particles than direct production of aerosol (primary aerosol). Such small particles (Aitken Nuclei) have an equivalent aerodynamic diameter lower than 0.08μm and they can act as condensation nuclei. Aitken nuclei exhibit a more global distribution than bigger ones because of their greater atmospheric residence times, and they play a key role on climatic cycles because a part of them acts as cloud condensation nuclei or fog formation nuclei (see fig.1.3).

1.4.2. Mechanisms of transport and removal processes of atmospheric aerosol particles

Once released into the atmosphere from primary production or formed via gas to particle conversion, aerosols are subjected to many processes that affect their global distribution and their chemical-physical properties. They are dispersed in the atmosphere through processes of advection, convection and turbulence. They are also transformed and removed by chemical and physical processes involving clouds, precipitations as well as processes occurring in cloud free air.

Different aerosol types can stay for very different times in the atmosphere. The time spent in the atmosphere by aerosol particles is influenced by various processes, such as wet and dry depositions and inside-cloud transformations. Moreover, it can be measured through different parameters: relaxation time, mean life time and residence time. Residence time is defined by the following equation:

$$\tau = M / S$$

where τ is residence time, M the reservoir content (e.g. the mass), S the source strength (or removal process strength) at the equilibrium (e.g.

mass / time). Particle mean life time comes from the ratio between release processes and removal ones. For a well distributed atmospheric substance, both the processes can be considered constant; in such case residence time is equal to mean life time. Instead, in the case of a particle emitted in the stratosphere, where removal times are quite long, residence time is longer than mean life time; for near soil emissions, where deposition times are extremely short, residence time is lower than mean life time. Till the aerosol particles are not removed by wet and dry deposition processes they could be subjected to different mechanisms of transport. The most important factor that determines aerosol diffusion in the atmosphere is the wind. Wind origins from atmospheric pressure difference between two areas and depends on the Earth low-high pressure areas. Between 0° and 40°/42° latitudes, solar radiation reaching the surface is not balanced by the subsequent nocturnal irradiance to the space. At higher latitudes, the received diurnal heath is lower than the one lost during the night. So there is a continuous low atmospheric exchange of matter and energy from equatorial regions to polar ones, by means of wind. In addition to wind there are other mechanisms of transport in which aerosol particles are involved: a brief description of those processes is given below.

Turbulent diffusion uses turbulent force to transport particulate matter along a concentration gradient. As long as particles are deposited, there is a concentration gradient between atmosphere and deposition surface. This transport mechanism is the most important one in free atmosphere, where turbulence is big.

Gravitational settling (sedimentation) larger particles are influenced more by gravity and fall back to the surface. This process becomes increasingly important for particle sizes above 1 μm.

Brownian diffusion is caused by air and particles thermal energy and it creates random mobility. It is less intense than turbulent diffusion and it becomes significant only when the latter is negligible, for instance in a low viscosity medium. Brownian diffusion coefficients increase as particle diameter decreases and this process dominates for particle sizes below 0.2 μm. Additionally, in a very thin (about 1 mm) layer over the surface, the Brownian diffusion becomes more important for larger particles too.

Interception and inertial forces can also transport big particles through a viscous medium. It may happen when the particle is transported by a current flowing through the radius of an obstacle. Inertial forces can carry to an impact or to a turbulent inertial deposition. The impact occurs when the particle leaves the current flow since it can no more follow rapid flux changes and it impacts with an obstacle. Instead, turbulent deposition occurs when inertial force coming from the current normal component (eddies) transports a particle. Negligible mechanisms of transport are both **migration**, due to electrostatic interactions between particles, and the **thermophoresis**, causing a motion from warm temperate to colder areas. The most important removal mechanisms of atmospheric aerosols are dry deposition at the surface and wet deposition from precipitations. In an annual global mean, about 80-90% of aerosol particles are removed from the atmosphere by in-cloud and

below-cloud scavenging (wet deposition). Remaining part of particles is removed by different ways of dry deposition.

Wet deposition processes

The expressions in-cloud and below-cloud scavenging mean the washing-out process in and under the clouds. Both liquid (fog, clouds and rain droplets) and solid (ice crystals, snow, hail) precipitations can be involved. As already described, aerosol cluster nucleation rises from gas-particle conversion and it can form CCNs, upon which water vapour can condense. In the clouds there could be an incorporation of smaller particles by water droplets and then everything can deposit after a precipitation (in-cloud scavenging). Coarse aerosol particles, not deposited by dry deposition, can be literally captured during precipitation processes; in this case we observe the so called below-cloud scavenging.

Dry deposition processes

Dry deposition consists on a direct particle deposition on a surface and is greatly influenced by atmospheric transport processes of such particles, in addition to other parameters depending on surface properties (chemical and biological reactivity, geometry, roughness). Once particles are deposited, they can also be re-suspended in the atmosphere in event of a force stronger than those holding them on the surfaces. Figure 1.4 shows typical aerosol sources distribution and removal processes.

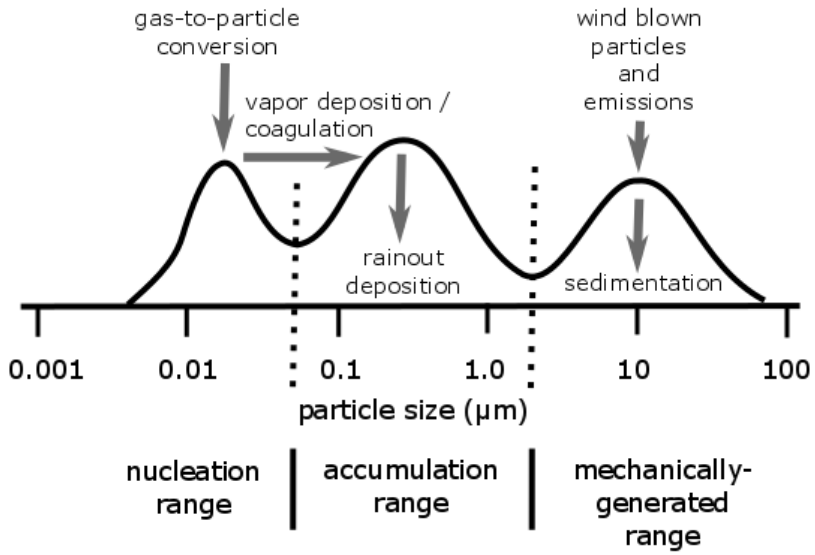

Figure 1.4 - *Typical aerosol size distributions sources and removal processes.*

CHAPTER 2 – The Mediterranean Basin

As exposed in the introduction of this thesis, The Mediterranean Basin atmosphere is heavily affected by aerosols cause to its vicinity both to African deserts and industrialized areas of European countries. Indeed, due to its relatively reduced dimensions (2.5106 km^2, i.e. only 1% of the world oceanic surface) and since this semi-enclosed basin is subjected to ever growing anthropogenic pressure and natural pulsed as Saharan dust events (Béthoux et al., 2002), it results to be one of the most polluted areas of the world. Moreover, cause to these peculiarities and because its open waters are never further than 300 km off the coasts, the interactions between land-based emission sources and offshore waters are particularly strong and they significantly affect the biogeochemistry of this basin. As a result, the Mediterranean Sea is very reactive to climatic and environmental changes so that is considered among the regions the most sensitive to climate variations in the 2007 IPCC report and can be used as an ocean model for climatic and environmental studies. Owing to its importance, in last decades Mediterranean atmospheric aerosol and meteorology have been intensively studied (e.g., Salvador et al., 2014; Pey et al., 2013; Pace et al., 2006; Kopanakis et al., 2012; Dayan et al., 1989) and several international programs have focused on the assessment of chemistry and climate and their interactions in this area.

Figure 2.1 – *The Mediterranean Basin.*

In particular this work of thesis is connected to the MISTRALS international program (Mediterranean Integrated STudies at Regional And Local Scales) that is a decennial program for systematic observations and researches dedicated to the understanding of the Mediterranean Basin environmental process under the planet global change. Its aim is to anticipate the behaviour of this system over a century, from an interdisciplinary analysis conducted over the 2010-2020 decade. At this purpose the data set presented in this thesis resulted to be very interesting since that cover a ten years period of sampling campaign (from June 2004 to December 2014) in the central Mediterranean sea.

Moreover, results from an intensive campaign carried out in summer 2013 within the framework of the Chemistry and Aerosol Mediterranean Experiment (ChArMEx) will be presented. As part of the international multidisciplinary MISTRALS project, ChArMEx is a research program that aims to improve the actual knowledge of the tropospheric chemistry and its impacts in the Mediterranean with a focus on air quality, regional climate, and biogeochemistry, and of their future evolution. In fact, despite the increasing scientific interest, the present knowledge of the

current and future state of the atmospheric environment and of its impacts on the Mediterranean basin, is still uncompleted. Indeed most of the previous studies performed in this area are based on sampling campaigns carried out at coastal sites, with strong influences from the continental meteorology and from anthropogenic sources; thus, regional background and remote sites are essential in order to study both natural and anthropogenic aerosol sources and to understand their effects on the Mediterranean basin climate (Querol et al., 2009; Koulouri et al., 2008; Pace et al., 2006).

In this context, the island of Lampedusa represents an ideal sampling site such as result to be a super-site of the ChArMEx international project. In fact, more than being a remote site Lampedusa is located in the central Mediterranean Sea, where few background sampling stations exist despite this position is very crucial in order to understand the Mediterranean atmospheric chemistry. In fact, as several studies have demonstrated, western and eastern Mediterranean Basin areas are known to be prone to different atmospheric dynamics and pollution conditions (Pey et al., 2013, Querol et al., 2009). For instance PM10 concentration is observed to increase from the north-western to south-eastern Mediterranean due to increasing contributions from both natural and anthropogenic sources (Pey et al., 2013). Moreover the western and eastern Mediterranean basins have been observed to be characterized by different atmospheric dynamical and chemical processes (e.g., neutralization of secondary aerosol; Querol et al., 2009). In this view the assessment of the chemical composition of atmospheric aerosol collected

in the centre of Mediterranean sea is crucial to obtain more information about this area and its interaction with the global climate.

2.1. The Mediterranean climate system and air masses circulation pattern.

The Mediterranean Sea is closed from all sides and is surrounded by high peninsulas and important mountain barriers. The gaps between these major mountainous regions act as channels for the air masses toward this basin (Kallos et al., 2006).

The climatic conditions in this area can be roughly divided into cold (cool and wet autumn and winters) and warm periods (hot and dry spring and summers) (Maheras et al. 1999). Due to the differential heating between the two land areas (southern Europe and North Africa) and the Mediterranean Sea during both the cold and the warm periods of the year, the general trend of the winds is from north to south across the Mediterranean region with significant variations in each area. Owing to these complicated flow patterns, the air pollutants released from various sources located in the surrounding areas (as both anthropic pollutants from southern Europe countries and Saharan dust input from North Africa) can be transferred long distances, in a complex scenario (Kallos et al. 1993, 1998a; Luria et al. 1996; Dayan and Levy 2002; Dayan and Lamb 2005). Landscape variability and, especially, land - water contrast result in the formation of thermal circulations that range from a few hundred meters to a few thousand kilometres (Millán et al. 1997, 2005).

The Mediterranean boundary layer has been observed to generally follow a clear annual behaviour, with minimum vertical extension during

summer and maximum altitudes in winter (with an opposite trend with respect to the one commonly observed in continental areas) (Pey et al., 2009; Dayan et al., 1989); therefore, stagnation of pollutants is favoured in summer over the Mediterranean basin. Moreover, the position of the ITCZ (Inter Tropical Convergence Zone) during summer is located over the northern part of the Saharan Desert (whereas during winter it is close to the equator). The height of the mixing layer over Europe is approximately 1-2 km during summer days and 100–1000 m during the winter and the transient seasons. The height of the mixing layer over North Africa varies between a few tens of meters during the night and 2–4 km or even deeper during the day, especially during summer (Kallos et al. 1998a). Thus, the mixing layer over the Mediterranean Sea is almost stable during the diurnal cycle (300 m) and varies slightly with the seasonal cycle (200-350 m) (Kallos et al. 2006).

An important feature of the coastal zones of the Mediterranean areas is the formation of the internal boundary layer. The islands and the peninsulas act as chimneys and obstacles, causing abrupt changes in the mixing depth (Kallos et al. 1997). The formation of relatively strong updrafts can inject polluted air masses from the boundary layer into the free troposphere. All these local meteorological features contribute to the formation of pollutant transport patterns with multifaceted spatial and temporal characteristics (Kallos et al., 2006). However the Mediterranean sea boundary layer behaviour will be discussed in the next chapters of this thesis regarding to each aerosol source identified and characterized.

CHAPTER 3 - Sampling and methodology

3.1. Sampling site

The island of Lampedusa (35.5°N, 12.6°E) is located in the Central Mediterranean and, as described above, is an ideal remote sampling site. In fact, Lampedusa's environment is poorly affected by anthropogenic pollution sources from local origin, due to its scarce population and industrialization, and from abroad, as it is more than 100 km far from the nearest coast. Thus, as described by Henne et al. 2010, Lampedusa is one of the most remote sites with respect to air quality measurements among 34 measurement stations throughout Europe and is part of the regional World Meteorological Organization/ Global Atmospheric Watch network as regional station.

The island covers a total area of about 20 km^2 with a coastal extension of 33 Km. It was formed prevalently by calcareous rocks and its soil is practically devoid of vegetation. About 6000 inhabitants live stably in Lampedusa, though during summer this number significantly grows due to its importance as tourism destination. As reported before, industrial activities are scarce (fish canning industry) so local anthropic aerosol sources are very low and the main contribute to them arise from ship crossing the Mediterranean Sea (about 100 km North respect to the sampling site). Instead natural source (as Sea spray aerosol and Saharan dust) significantly contribute to the aerosol concentrations affecting the air quality of this area.

Figure 3.1 – *Geographical location of Lampedusa Island.*

The aerosol sampling campaigns were carried out at the Station for Climate Observations “R. Sarao” maintained by ENEA (the national Agency for New Technologies, Energy, and Sustainable Economic Development of Italy) that is located at Capo Grecale, a 45m a.s.l. plateau on the North-Eastern coast of Lampedusa. At this site continuous observations of greenhouse gases concentration (Artuso et al., 2009, 2010), aerosol properties (di Sarra et al., 2011; Meloni et al., 2006; Pace et al., 2006), total ozone, ultraviolet irradiance (di Sarra et al., 2002; Meloni et al., 2004; Di Biagio et al., 2010), and other climatic parameters are carried out.

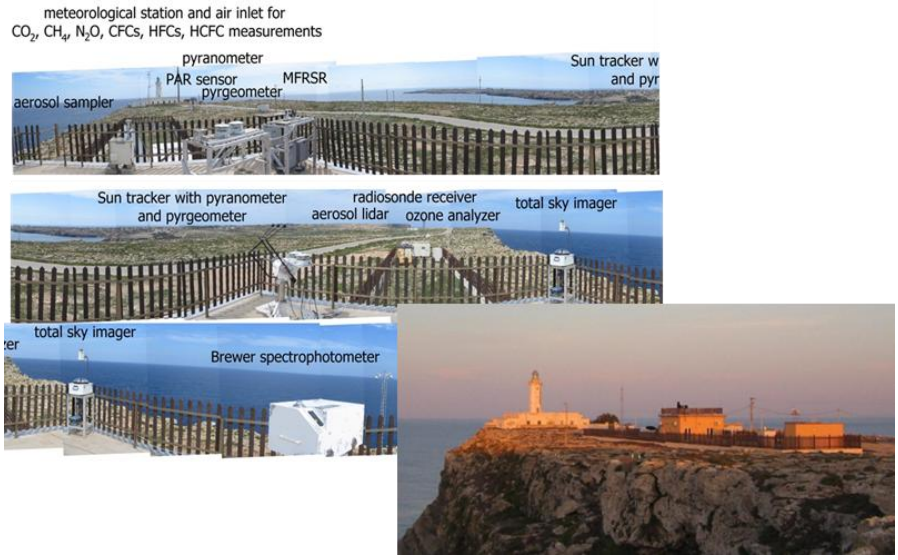

Figure 3.2 - *Instrumentations at the "R. Sarao" ENEA station for climate observations located at Capo Grecale.*

3.2. Aerosol sampling

The aerosol sampling started in June 2004 at daily resolution, alternating in sequence sampling of PM10 (particulate matter with AED < 10µm), PM2.5 (particulate matter with AED < 2.5µm), and PM1.0 (aerosol particles with AED < 1µm). Since 2007 only PM10 sampling at daily resolution was accomplished. The aerosol PMX daily sampling is carried out by using low volume sequential samplers (TECORA Skypost from 2004 to 2010 and FAI-Hydra dual sampler since 2011) equipped with sampling heads operating in accord with EN12341. Cut-off sampling heads worked on the basis of inertial impact and can select, upstream the filter, the dimension of particulate matter than will be collected on the filter. During the sampling period some interruptions occurred due to technical failures (for more details see Tab. 6.1).

The sample collection was carried out at constant flow of 2.3 m3/h over the time of 24 hours. 47-mm diameter 2 µm nominal porosity Pall-Gellman Teflon filters were used to collect the aerosol samples meant to the quantification of aerosol load, ion chromatographic analysis of soluble ions, atomic emission spectroscopy for soluble metals, and proton-induced X-ray emission (PIXE) for the total (soluble+insoluble) elemental composition.

Conversely, from 2010 to 2014 when the aerosol sampling was accomplished by a Fai Hydra dual channel, in addition to the Teflon filters 47 mm pre-fired, 2 µm nominal porosity, quartz filters are meant to the elemental (EC) and organic carbon (OC) determinations. Blank values were negligible with respect to the concentration in the samples for Teflon filters. Blank values for quartz filters were negligible for most of the analysed species, and when not negligible, anyway lower than 25^{th} percentile, they were subtracted from the measured concentrations.

The OC and EC measurements were carried out on a 1.5x1 cm punch of the quartz filters by means of a Sunset thermo-optical transmittance analyser, following the NIOSH protocol (Wu et al., 2016). More details about all the analytical technique used in this thesis (IC, ICP-AES, PIXE and SUNSET) will be given in chapter 4.

Additional 3 days resolution sampling with an Andersen 8 stage impactor working at constant flow of 1.7 m^3/h was performed at Lampedusa in summer 2006 and 2008. This type of sampler is designed to cut the PM into 8 fractions on the basis of the aerodynamic diameter of its particles (see fig. 3.3). The sampler was loaded with Teflon filters: half

of each filter was used to determine the ionic composition, while the other half was used to measure the metals soluble fraction content with the same methodology described below in the next section of this chapter (ICP-AES after extraction at pH1.5).

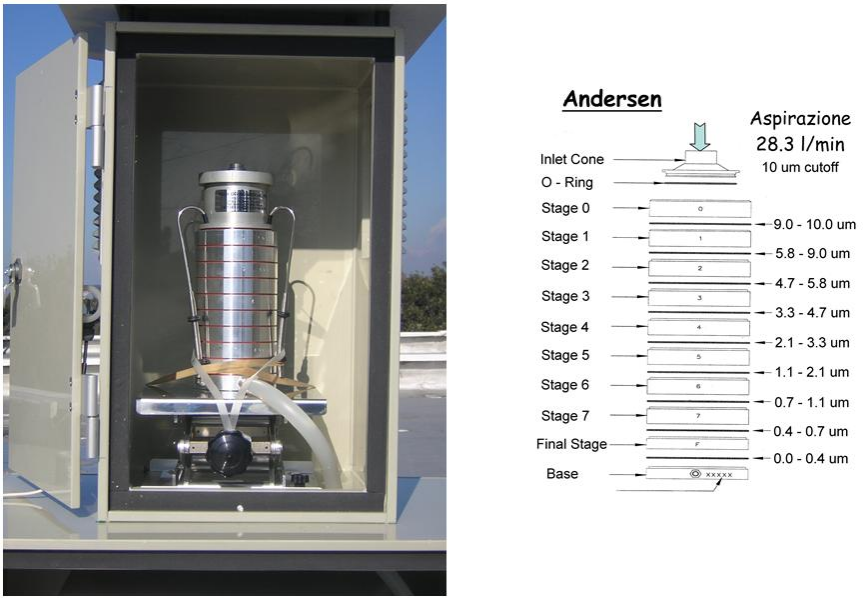

Figure 3.3 – *Picture and schematic representation of the Andersen 8 – stage impactor used in summer 2006 and 2008.*

3.3. Filters treatments

The mass of PMX was determined by weight the filters before and after the sampling with an analytical balance in controlled conditions of temperature (20±1 °C) and relative humidity (50±5 %). The estimated error on the basis of balance tolerance for the PMX mass is around 1% at 30 µg/m^3 of PMX in the applied sampling conditions. After weighing each filter was cut in three part using stainless steel tweezers and scissors

under a laminar flow hood that provides a clean work area shielding the samples from external contamination.

Figure 3.4 – *Filter's partition.*

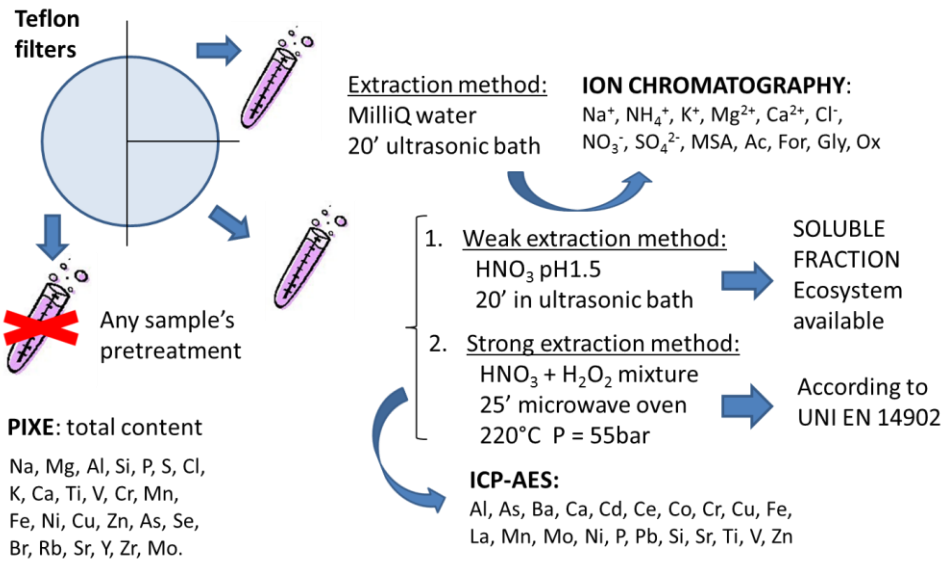

Figure 3.5 – *Schematic representation of both filters treatments and analytical techniques used in this thesis.*

After partitioning a quarter of each filter was destined to ion chromatography analysis for the ionic content determination, a quarter to ICP-AES analysis for the soluble metal content assessment and the remaining half to PIXE analysis for the total metal content (see figure 3.5). Before the ion chromatography analysis the quarter of filter was extracted using about 10 ml of MilliQ water in ultrasonic bath for 15 minutes.

Instead before performed ICP-AES analysis two extraction procedure were used in order to compare results with those obtained by PIXE measurements (see chapter 5):

1. Weak method (on the filter quarter): 0.1% sub-boiled distilled HNO_3 (pH 1.5) extraction in ultrasonic bath for 15 min at room temperature. In this way we derived the metal soluble fraction usually more available for the ecosystem.
2. Strong method (on the half filter previously analysed at PIXE and only for the 2013 PM10 samples): 30% Ultrapure H_2O_2 and concentrated sub-boiled distilled HNO_3 mixture in a microwave oven at 220°C for 25 min (P=55bar) according to the UNI EN 14902 (2005) methodology for As, Cd, Ni and Pb determination.

CHAPTER 4 - Chemical Analysis

4.1. Ion Chromatography

In this work, the soluble ionic fraction was determined by Ion Chromatography (IC). Ion Chromatography is an HPLC (High Performance Liquid Chromatography) chromatographic separation technique, that uses an ion exchange resin as stationary phase. The pseudo equilibrium establishing between stationary and mobile (eluent) phase allows the separation of ionic species in the analysed solution. The sample is injected in the separation column by an injection valve to whom a sampling loop or a pre-concentration column (loaded at a constant sample flow, for a reproducible and well known period of time) is connected. Separation system is made by a guard-column, that avoids not eluable (in the chosen analytical method conditions) ionic species to arrive in the separation column, and by an ion exchange column, that separates ions in the liquid sample on the function of competitive partition equilibria (based upon ion interactions) between the fixed resin and analyte and eluent ions. After the passage through a background conductivity (due to eluent) suppression system, component separated bands arrive to the conductivity detector. Since analytes are ionic species, a conductivity detector is used to reveal different components bands (chromatographic peaks). The analytical signal is given by the difference between the eluent conductivity (background conductivity) and the one of analysed ions. To gain signal/noise ratio, it is necessary to decrease, at most, eluent conductivity and, if possible, to increase analytes one. All

these processes take part within the suppression system (electrochemical suppressor). The same computerized system managing separation phases, acquires the signal, formerly converted in a digital format. Since high accuracy and reproducibility are requested, every chromatogram is optimized to obtain correct peak height through a specific software (Chromeleon™).

Figure 4.1 – *The three Thermo – Fisher - Dionex ion-chromatography systems.*

Aerosol ionic content of the samples is determined in the aqueous extracts prepared just before analysis. Cations, inorganic anions, methanesulphonic acid (MSA) and some short-chain organic anions were simultaneously measured using three Thermo- Fischer-Dionex ion-chromatography systems. The ion chromatography were contemporaneously feed by using a Gilson 222 XL autosampler. All samples were filtered using an on-line 0.45 µm filter before the injection in the ion chromatographic systems.

Cations (Na^+, $NH4^+$, K^+, Mg^{2+} and Ca^{2+}) were determined using a Dionex CG12A-4mm guard column and a CS12A-4mm analytical column with H2SO4 20 mM as eluent. The samples were injected through a 250 µL loop.

Inorganic anions (Cl^-, NO_3^-, SO_4^{2-} and $C_2O_4^{2-}$) were analysed using a Dionex AG4A-4mm guard column and an AS4A-4mm analytical column with a Na_2CO_3/$NaHCO_3$ (1.8 and 1.7 mM, respectively) buffer solution as eluent. The injected sample volume was 500 µL.

Organic anions (acetate, glycolate, formate and methanesulphonate MSA) and F^- were determined by using a Dionex AS11 separation column with $Na_2B_4O_7$ solution as eluent. The separation was performed by gradient elution. At the beginning of each analysis, a column cleaning step was carried out using a relatively high $Na_2B_4O_7$ concentration (45 mM). The separation was obtained increasing $Na_2B_4O_7$ concentration from 0.075 mM to 2.5 mM. 1 mL of sample is loaded by a peristaltic pump on Thermo-Ficher -Dionex TAC-2 pre-concentration column (50 µl dead-volume) than injected in the separation column.

The chromatographic systems were daily calibrated with 5-6 standard solutions, in the concentration range of the analysed samples, freshly prepared by dilution in MilliQ water of 1g/L Merck™ certified standards.

4.2. ICP-AES analysis

ICP-AES (Inductively Coupled Plasma - Atomic Emission Spectroscopy) technique is one of the most powerful analytical tools for the determination of trace elements in a great number of sample types. The technique is based upon the spontaneous emission of photons from

atoms and ions that have been excited in a radiofrequency discharge. Liquid and gas samples may be injected directly into the instrument, while solid samples require extraction or acid digestion so that the analytes will be present in a solution. The sample solution is converted to an aerosol and directed into the central channel of the plasma. At its core the inductively coupled plasma (ICP) sustains a temperature of approximately 10.000 K, so the aerosol is quickly vaporized. Analyte elements are liberated as free atoms in the gaseous state. Further collisional excitation within the plasma imparts additional energy to the atoms, promoting them to excited states. Sufficient energy is often available to convert the atoms to ions and subsequently promote the ions to excited states. Both the atomic and ionic excited state species may then relax to the ground state via the emission of a photon. These photons have characteristic energies that are determined by the quantized energy level structure for the atoms or ions. Thus the wavelength of the photons can be used to identify the elements from which they originated. The total number of photons is directly proportional to the concentration of the originating element in the sample.

Figure 4.2 – *ICP-AES Varian 720-ES used in this thesis.*

The main analytical advantages of the ICP over other excitation sources originate from its capability for efficient and reproducible vaporization, atomization, excitation, and ionization for a wide range of elements in various sample matrices. This is mainly due to the high temperature, 6000–7000 K, in the observation zones of the ICP. The higher atomization temperature and a more inert environment makes the ICP less susceptible to matrix interferences respect to the others analytical techniques as AAS and GFAAS. Furthermore, in cases where sample volume is not limited, ICP-AES provides detection limits as low as, or lower than its best competitor, GFAAS, for all but a few elements. Even for these elements, the simplicity with which the ICP-AES instrument is operated often outweighs the loss in sensitivity. Finally, ICP-AES technique can provide simultaneous determinations for up to 70 elements producing an high gain in terms of time (Hou and Jones, 2000).

In particular in this thesis an ICP-AES Varian 720-ES was used to determine Al, As, Ba, Ca, Cd, Ce, Co, Cr, Cu, Fe, La, Mn, Mo, Ni, P, Pb, Si, Sr, Ti, V and Zn atmospheric concentrations (see fig 4.2).

4.2.1. Sample introduction system

As shown in fig. 4.3, an introduction system is used to transport the sample into the central channel of the ICP: at this purpose nebulizers are the most commonly used devices in ICP-AES. With a nebulizer, the sample liquid is converted into an aerosol and transported to the plasma.

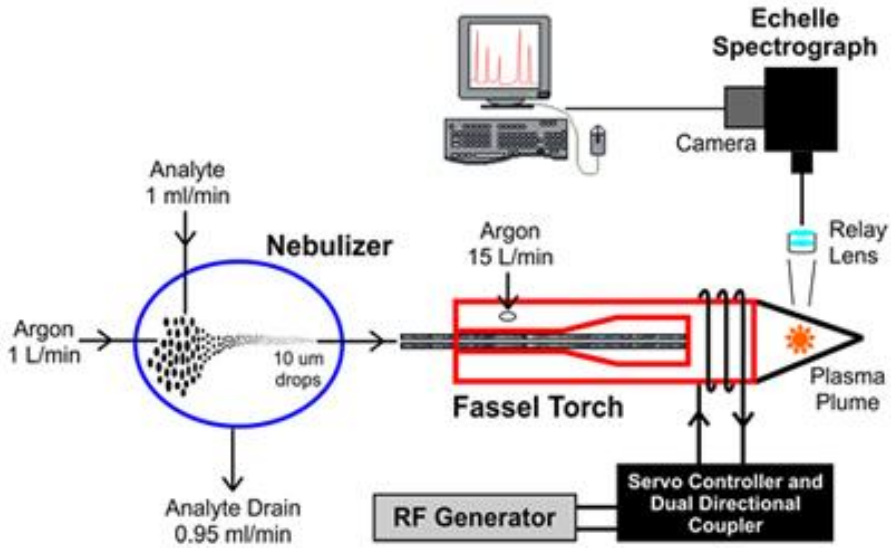

Figure 4.3 – *Block diagram of the ICP-AES operation mode.*

Both pneumatic and ultrasonic nebulizers have been successfully applied in ICP-AES technique (Hou and Jones, 2000) and even the Varian 720-ES used in this thesis is equipped by either these two types of devices. Pneumatic nebulizers make use of high-speed gas flows to create an aerosol, while the ultrasonic ones breaks liquid samples into a fine

aerosol by the ultrasonic oscillations of a piezoelectric crystal. Only very fine droplets (about 8 μm in diameter) in the aerosol are suitable for injection into the plasma. In the case of pneumatic type a spray chamber is placed between the nebulizer and the ICP torch to remove large droplets from the aerosol and to dampen pulses that may occur during nebulization. However pneumatic nebulization is very inefficient because only a very small fraction (less than 5%) of the aspirated sample solution really reaches the plasma. Most of the liquid is lost down the drain in the spray chamber.

Since that nebulizer efficiency is crucial when measurements must be performed at or near the detection limit as in our case, in this thesis the use of an ultrasonic nebulizer was chosen. In particular we used a CETAC U5000 AT+: in this device the sample solution is first introduced onto the surface of a piezoelectric transducer that is operated at a frequency of 10 MHz. The longitudinal wave, which is propagated in the direction perpendicular to the surface of the transducer towards the liquid–air interface, produces pressure that breaks the liquid into an aerosol (see fig. 4.4). The efficiency of an ultrasonic nebulizer is typically between 10 and 20%. As said before, this nebulizing efficiency is greater than that of a pneumatic nebulizer, and it is independent of argon flow rate. Therefore, a slower gas flow rate can be used to transport the aerosol to the plasma, thus prolonging the residence time of analyte in the plasma. However, a better nebulization efficiency, involves a greater load of water inside the plasma; to overcome this problem the ultrasonic nebulizer is equipped with a particular desolvation system consists of two units, an heating and

a refrigerant one, which allow the introduction of a dry aerosol in the torch. In particular, the nebulizer used in this thesis was provided with a Peltier cooling system (refrigeration at 3° C). All these characteristics result in improved sensitivity, and the detection limit (DL) for most elements is usually lowered by an order of magnitude respect to that of the pneumatic one.

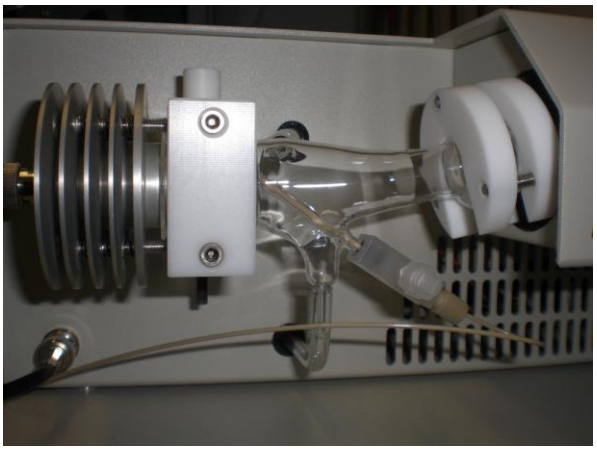

Figure 4.4 – *A particular of the CETAC U5000 AT+ ultrasonic nebulizer used in this thesis.*

4.2.2. Inductively Coupled Plasma operation

As shown in Figure 4.5, the ICP torch is formed by an assembly of three concentric fused-silica tubes. These are frequently referred to as the outer, intermediate, and inner gas tubes. A water-cooled, three-turn copper coil, called the load coil, surrounds the top section of the torch, and is connected to a radiofrequency generator. The outer argon flow (15 L/min) sustains the high temperature of plasma, and positions the plasma relative to the outer walls and the induction coil, preventing the walls from melting and facilitating the observation of emission signals.

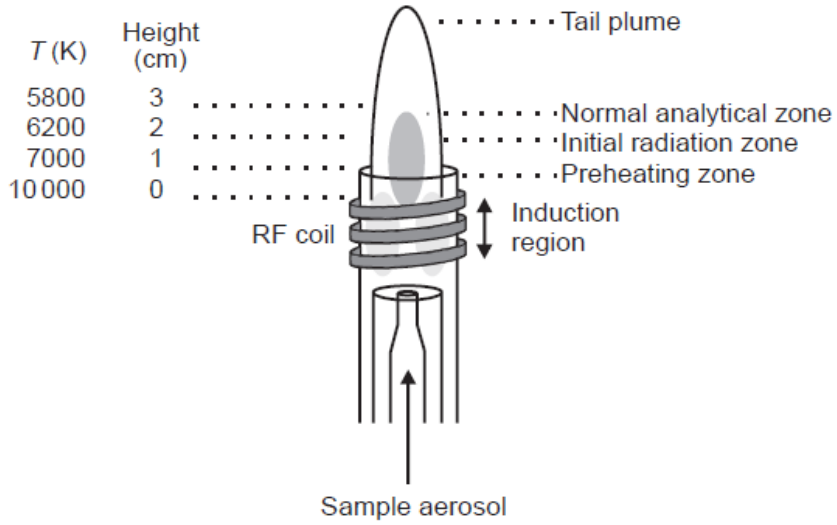

Figure 4.5 - *Schematic diagram of an ICP assembly showing the three concentric tubes composing the torch, the RF coil, the different plasma regions, and the temperature as a function of height above the load coil.*

The sample aerosol carried by the inner argon flow (0.75 L/min) enters the central channel of the plasma and helps to sustain the shape. The intermediate argon flow (1.5 L/min) has the function of lifting the plasma slightly and diluting the inner gas flow in the presence of organic solvents. The ICP is generated as follows. RF power, 1200 W in our case, is applied to the load coil and an alternating current oscillates inside the coil at a rate corresponding to the frequency of the RF generator. For ICP-AES Varian 720-ES used in this thesis the frequency of the RF generator was 40 MHz. The oscillation of the current at this high frequency causes the same high-frequency oscillation of electric and magnetic fields to be set up inside the top of the torch. With argon gas flowing through the torch, a spark from a Tesla is used to produce some electrons and ions in

the argon gas inside the load coil region. These ions and electrons are then accelerated by the magnetic field, and collide with other argon atoms, causing further ionization in a chain reaction manner. This process continues until a very intense, brilliant white, teardrop shaped, high-temperature plasma is formed. Adding energy to the plasma via RF-induced collision is known as inductive coupling, and thus the plasma is called an ICP. The ICP is sustained within the torch as long as sufficient RF energy is applied. In a cruder sense, the coupling of RF power to the plasma can be visualized as positively charged Ar ions in the plasma gas attempting to follow the negatively charged electrons flowing in the load coil as the flow changes direction 27 million times per second. Figure 4.5 shows the temperature gradient within the ICP with respect to height above the load coil. It also gives the nomenclature for the different zones of the plasma as suggested by Koirtyohann et al. 1981.

The induction region (IR) at the base of the plasma is ‘‘doughnut-shaped’’ and it is the region where the inductive energy transfer occurs. This is also the region of highest temperature and it is characterized by a bright continuum emission. From the IR upward towards to the tail plume, the temperature decreases. The aerosol is carried into the centre of the plasma by the argon gas flow through the IR. Upon entering the plasma, the droplets undergo three processes. The first step is desolvation, or the removal of the solvent from the droplets, resulting in microscopic solid particulates, or a dry aerosol. The second step is vaporization, or the decomposition of the particles into gaseous state molecules. The third step is atomization, or the breaking of the gaseous

molecules into atoms. These steps occur predominantly in the preheating zone (PHZ). Finally, excitation and ionization of the atoms occur, followed by the emission of radiation from these excited species. These excitation and ionization processes occur predominantly in the initial radiation zone (IRZ), and the normal analytical zone (NAZ) from which analytical emission is usually collected (Hou and Jones, 2000).

4.2.3. Optical system (Echelle grating)

The optical system is composed both from the transfer optic system, that from the electromagnetic radiation selection system. In our case the torch configuration was axial (the plasma is rotated in the horizontal position) and the radiation emitted from the normal analytical zone is observed at the final extremity of the plasma. The axial view imply a greater optical path and, consequently, better sensitivity with a factor of 5-10 with respect to the radial gain vision (plasma in vertical position). In this thesis, to reduce the interference phenomena which occur in the cold tail of the plasma (such as self-absorption and recombination), the instrument was equipped with a nickel cone interface system with an 8 mm hole that allows the vision of the central part of the plasma cutting off the undesired area from the transfer optics (see fig. 4.6).

Figure 4.6 – *The ICP-AES Varian 720-ES torch and the nickel conic interface system .*

ICP-AES technique is characterized by remarkably rich spectra. For example, the 70 elements most commonly determined by the technique give rise to at least 70 000 total emission lines in the 200 -600 nm wavelength range. A consequence of this high density of spectral information is the need for high resolving power. In our case, the separation of the spectral lines is carried out via the "Echelle" configuration, a device that provides the use of a diffraction grating, which separates the light into different wavelengths, and a prism, able to separate each wavelength in the different orders of diffraction.

The Echelle spectra emerging from this configuration system, is a two-dimensional picture in which wavelengths and diffraction orders are resolved in a plane and focused on a solid-state detector (CCD – Charge Coupled Device). The bi-dimensional Echelle image striking the entire surface of the detector constitute by 904 x 1280 pixels. The coupling of those systems (the Echelle configuration with the CCD detector) allows simultaneous multi-elemental analysis with high resolution (see Fig. 4.7).

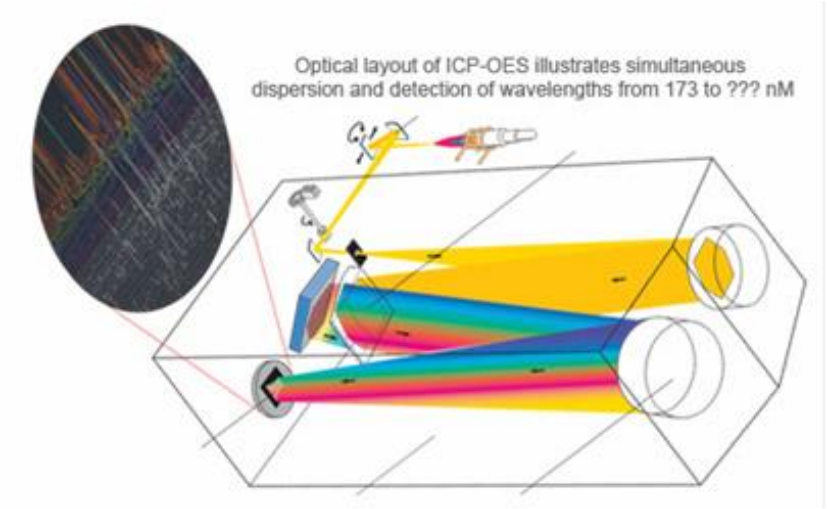

Figure 4.7 – *Schematic representation of the Echelle configuration.*

The software used to operate the instrument is the ICP-Expert: this program permits to choose operating parameters, elements to be analysed and the analytical wavelengths relative to each element. Generally for each element one analytical wavelength is chosen: this operation is crucial and it requires to take into account the interference from other nearby lines (two lines must be distant for more than 7 pm to be discriminated), the intensity of each line and the relative abundance of the elements within the sample. For this reason In this thesis it was chosen to analyse three different lines for each element, in order to exclude possible interferences on a particular wavelength. As regards to the choice of the best calibration method in our case it was selected the use of an internal standard methodology. Indeed, since the heterogeneity of the aerosol samples, this method is the most fast and reliable in order to minimize possible interferences due to the complexity of the matrix. In

particular Ge was chosen as internal standard since its rarity in the earth's crust.

4.3. PIXE technique

Half of each Teflon filters was analysed by proton induced X-ray emission (PIXE) technique in order to obtain the total elemental composition (soluble + insoluble).

Particle-induced X-ray emission (PIXE) belongs to the Ion Beam Analysis (IBA) techniques. In particular, when a material is exposed to an ion beam, atomic interactions occur giving off electromagnetic radiation of wavelengths in the x-ray part of the electromagnetic spectrum specific to an element. Indeed, bombardment with ions of sufficient energy (usually MeV protons) produced by an ion accelerator, will cause inner shell ionization of atoms in a sample. Outer shell electrons drop down to replace inner shell vacancies, however only certain transitions are allowed and so X-rays of a characteristic energy of the element are emitted. An energy dispersive detector is used to record and measure these X-rays. Only elements heavier than fluorine can be detected.

The lower detection limit for a PIXE beam is given by the ability of the X-rays to pass through the window between the chamber and the X-ray detector. The upper limit is given by the ionisation cross section, the probability of the K electron shell ionisation, this is maximal when the velocity of the proton matches the velocity of the electron (10% of the speed of light), therefore 3 MeV proton beams are optimal.

Particle Induced X-ray Emission (PIXE) technique is excellently applied to the aerosol chemical composition determination due to its capability to detect with high efficiency in a single measurement all the elements with Z > 10. Furthermore, as will be explained in chapter 5 and 7, PIXE is an important technique for the study of the dust component of aerosol, due to its high sensitivity to crustal markers (in particular Si, which is difficult to detect with other chemical techniques since that it requires the use of HF to solubilize the silica matrix and even in this way the quantification might be poor due to the volatility of SiH_6) (Calzolai et al. 2014). PIXE measurements showed in this thesis were performed at the aerosol-dedicated experimental set-up (Calzolai et al., 2006) available at the LABEC laboratory of the National Institute of Nuclear Physics (INFN) in Florence, equipped with a 3 MV Tandetron Acceleretor.

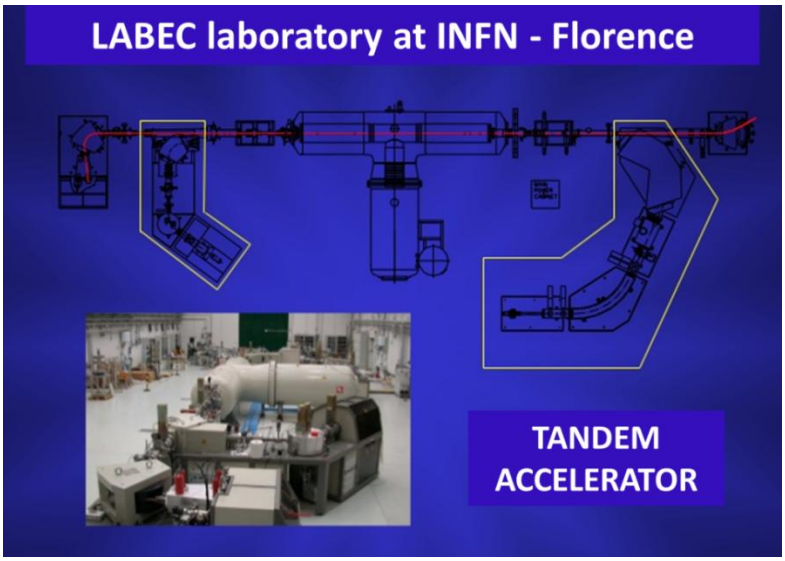

Figure 4.8 – *Schematic illustration of the Tandetron Accelerator at the LABEC laboratory of the INFN Florence section.*

Briefly, the proton beam is extracted in air through a 500 nm thick Si_3N_4 window; aerosol samples are positioned at a distance of about 1 cm from the extraction window, with the volume of atmosphere between them saturated with helium, to reduce the absorption of the emitted radiation. A collimator located in the end of the in-vacuum beam line sets the beam size (usually to 1.0 - 2.0 mm^2). The use of two X-ray detectors (Silicon Drift Detectors, SDDs) optimized for low and medium–high Xray energies, respectively, allows an effective simultaneous detection of all the elements of interest (Calzolai et al. 2014, Lucarelli et al. 2014).

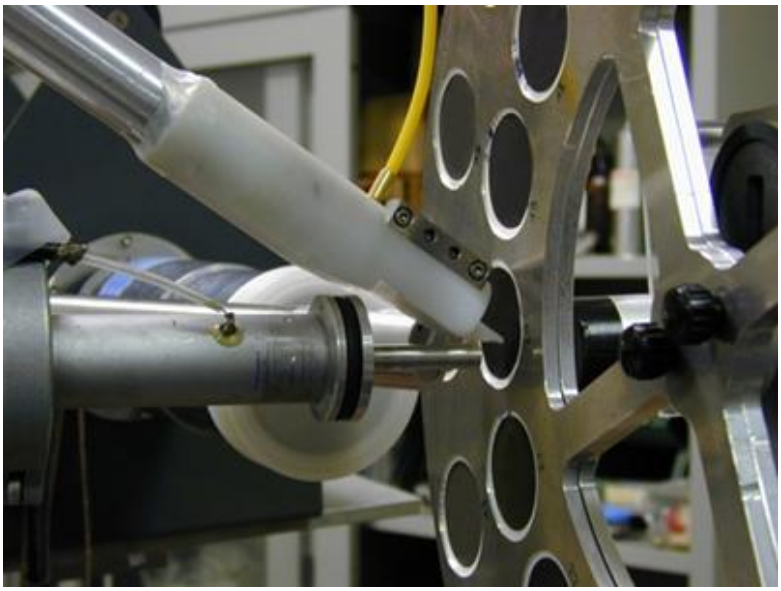

Figure 4.9 – *A particular of the PIXE set-up used in this thesis.*

Aerosol samples present a non-uniform deposit, with many point-like spots enclosed in 8 mm diameter area. Therefore, for the analysis of these samples, the beam is defocused and collimated to obtain a homogeneous spot on the target and the area enclosing the aerosol spots

is uniformly scanned thanks to suitable movements of the sample holder with respect to the beam (see fig. 4.9).

Samples were irradiated with a 2.9 MeV proton beam with currents and durations ranging from 70 nA to 100 nA and from 650 to 1070 s, respectively, depending on the sample aerosol load. X-ray spectra were fitted using the GUPIX code (Campbell et al. 2010, Calzolai et al. 2014).

4.4. Thermal-optical transmittance analysis (SUNSET)

In this work, a thermal-optical transmittance (TOT) analyser by the Sunset Laboratory was used to quantify EC, OC, and TC in aerosol samples. As PIXE analysis also these types of measurements were carried out at in the INFN laboratories in Florence. The EC-OC determination was carried out on the quartz filters collected starting from 2010 following the NIOSH protocol. A brief description of the SUNSET instrument operation mode is given below.

In general thermal methods offer a measurement of the carbon (C) that leaves the filter as the temperature increases, following a specific thermal evolution in different atmospheres (oxidising or inert). The Total Carbon (TC) content obtained correspond to the sum of Elemental Carbon and Organic Carbon. However during charring reactions some of the OC may turn into EC due to pyrolysis in an oxygen-deficient atmosphere leading to an ambiguous separation. This limit can be overcome through the optical properties monitoring as in the Sunset Thermo-Optical-Transmittance analyser.

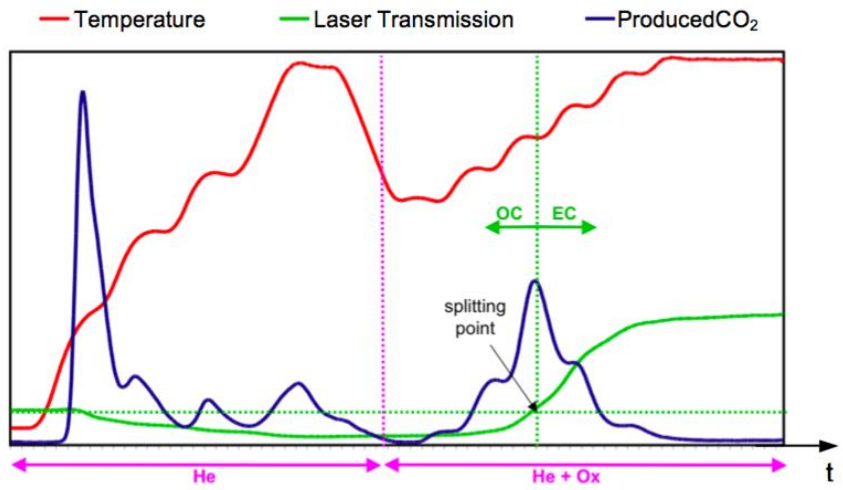

Figure 4.10 – *The graph shows temperature, laser transmission and produced CO2 vs time in a typical Sunset analysis.*

Figure 4.10 shows the various steps of a typical Sunset analysis. In the first part the sample is heated in an inert atmosphere (He) using a thermal ramp depending on the protocol chosen. Then, the second part of the analysis is carried out in an oxidising atmosphere (He/O_2 mixture, 90/10 %) (Birch and Cary, 1996). The carbon evolving during heating is completely oxidised to CO_2 by a MnO_2 catalyst and then reduced to CH_4 to be quantified by a flame ionisation detector (FID). In order to take into account the formation of pyrolytic carbon, the transmission of a laser beam through the sample is constantly monitored during the analysis. Transmittance usually decreases throughout the He-step, indicating the formation of light-absorbing pyrolytic carbon. In the He/O_2 phase, an increase of the laser signal is registered and the pyrolytic carbon evolution is conventionally assumed completed when the transmittance reaches its initial value. Carbon evolving after this point (called split-

point, see fig. 4.8) is then considered as EC (Piazzalunga et al., 2011). Regarding to the choose of the thermal ramp, after an inter-comparison among the most used measurements protocols (V. Bernardoni et al. 2011), NIOSH, that is indeed among the most selective and flexible protocols, was chosen (for the operating conditions see fig. . Indeed, for this kind of samples, with a very low amount of EC, the problem of discrimination between the two fraction of carbon is not a critical point and it was preferable to choose the fastest protocol, as NIOSH is, to be able to analyse a large quantity of samples in the shortest time possible.

NIOSH

NIOSH 5040 protocol

	time (s)	temperature (°C)
He1	60	250
He2	60	500
He3	60	650
He4	90	870
He/$O_2$1	30	650
He/$O_2$2	30	750
He/$O_2$3	30	850
He/$O_2$4	120	940

Figure 4.11 – *Thermal ramp used in the NIOSH protocol.*

CHAPTER 5 – Comparison between PIXE and ICP-AES measurements

Analysing chemical composition of aerosols results very interesting in order to characterize natural (as Sea Spray and Saharan dust emissions) and anthropogenic sources at Lampedusa. In this chapter the attention is focused on the metal content: in particular results obtained by two of the most largely used techniques in the analysis of the atmospheric aerosol composition as Particulate Induced X-ray emission (PIXE) and Inductively Coupled Plasma Atomic Emission Spectroscopy (ICP-AES) were compared. Metals are very important markers for natural (mineral dust) and anthropic sources. While PIXE provides total metal content, metal concentration by ICP-AES depends on the extraction procedure. In fact PIXE technique is able to perform a multi-elemental analysis of the aerosol collected on the filter surface without any pre-treatment of the samples, whereas ICP-AES requires solubilisation and metal extraction procedure.

As the easily soluble fraction of the metals is directly available for the environment and organism, to evaluate the impact of metals on the environment and human health, the two analytical technique are compared. The metal fractions solubilised were calculated considering PIXE result as 100% of the metal content. Since PIXE is a non-destructive technique after the analysis this part of the Teflon filter was used for the determination of metals by ICP-AES through the strong solubilisation procedure. Thus, as the ICP-AES values depends on the extraction conditions (i.e. extracting solution composition, pH, temperature,

pressure, contact time), two different solubilisation method were performed: a weak procedure (HNO_3 at pH 1.5) on a quarter of each Teflon filters and a strong procedure (HNO_3 and H_2O_2 solution in microwave oven following the EU rule EN14902) on the half of the filters previously analysed by PIXE (see chapter 3.3). The chosen value of pH used in the weaker method is the lowest found in rainwater (Li and Aneja, 1992, R. Traversi et al., 2014) and for this reason represents the metals fraction available to biological organisms. Conversely, we will verify how is the percentage of recovery obtained by following the European rules EN14902.

Besides the extracted fraction can depend on the aerosol sources. In fact, metals emitted by anthropic sources are usually in more soluble form because of the chemical speciation and their occurrence in the finest particle fraction. Thus, as will be illustrate in next sections, the efficiency of the extraction resulted to be strongly dependent on the PM main sources (crustal or anthropic).

As PIXE analysis results are not available over all the ten years from 2004 to 2014, in this chapter only data obtained during the 2013 sampling campaign (where the PM10 year sampling coverage percentage correspond to 83% as reported in table 6.1 and both PIXE and ICP-AES measurements were carried out on each filters) were used.

5.1. Metals emitted by natural sources

Due to its position natural aerosol sources result very significant at Lampedusa: indeed, beside marine emission, this site is strongly subjected to Saharan dust input. As well as the sum of crustal oxides (as will be illustrated in chapter 7), alternatively crustal content can be estimated from a single tracer: in literature the most common used marker is Al concentration (e.g. Rodriguez et al., 2012 and references therein) considering that it represents 8.2% of the upper continental crust (Henderson and Henderson, 2009). Comparing the crustal content obtained in this way (using [Al] content results from PIXE measurements) with that obtained as the sum of the crustal oxides, we found a good correspondence between the two data sets (R=0.96, n= 347, Slope= 1.09). Indeed anthropic emissions have a negligible impact on Al and on the others main crustal metals content, as shown by their low enrichment factor (E.F): in particular the mean Fe/Al experimental ratio (0.92 w/w) is very close to the value ofthe earth's crust ratio (0.68 w/w) (Henderson and Henderson, 2009). Thus, since their prominence in the crustal matrix, in fig. 5.1 temporal evolutions of Al and Fe content obtained through the three different type of measurements carried out (ICP-AES analysis after weak and strong extraction method and PIXE results) are reported.

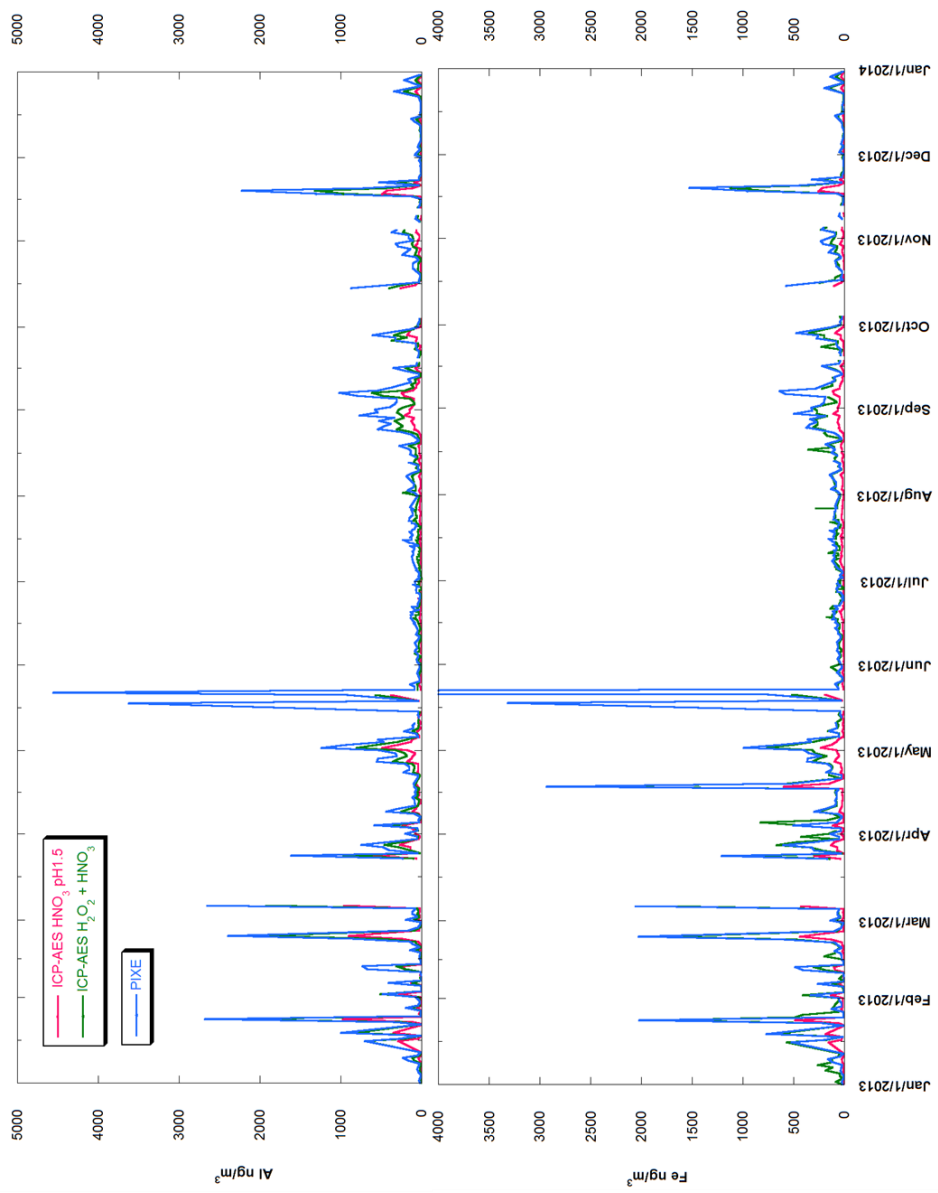

Figure 5.1- Temporal evolution of Al and Fe atmospheric concentration obtained with three different type of analysis: ICP-AES measurements after extraction with HNO3 at pH1.5 in ultrasonic bath and after solubilisation in microwave oven with HNO_3 and H_2O_2 mixture, and PIXE analysis.

It has to be notice that the trend is the same in all the three types of analysis: indeed values from weaker extraction conditions represent the metal soluble fraction available for the ecosystem, while levels obtained after digestion in microwave oven with HNO_3 and H_2O_2 mixture are close to the results obtained from PIXE analysis that represent the total metal content. Moreover, in Table 5.1 mean solubility percentage of the two different extraction methods and the correspondence between the data sets obtained with PIXE analysis are reported.

	slope HNO_3 pH1.5 vs PIXE	R^2 HNO_3 pH1.5 vs PIXE	slope HNO_3-H_2O_2 vs PIXE	R^2 HNO_3-H_2O_2 vs PIXE
Al	0.33	0.93	0.71	0.94
Fe	0.21	0.98	0.87	0.98
Cu	0.78	0.82	0.81	0.87
Mn	0.69	0.97	0.92	0.96
Cr	0.20	0.85	0.65	0.80
Ni	0.79	0.96	0.88	0.93
V	0.85	0.94	0.87	0.98
Pb	0.77	0.93	0.91	0.86
Ti	0.12	0.94	0.17	0.96
Sr	0.72	0.96	0.85	0.97
As	0.31	0.69	0.34	0.66
Si	0.12	0.93	0.22	0.85

Table 5.1- *Slope and R^2 obtained by the comparison between ICP-AES values after weak and strong extraction method and PIXE analysis for all the aerosol samples collected during the 2013 sampling campaign.*

As said before, metal's solubility is affected by various processes, such as chemical speciation, mixing of different types of particles, size distribution, and ageing processes. In general crustal elements (such as Al, Fe, Mn, Ti and Si) have a lower solubility respect to anthropic elements. However mean solubility percentage of all the elements analysed sensibly increase when stronger extraction conditions were carried out indicating the high recovery efficiency of the EU rule method. In the case of Fe and Al, that are mainly contained in crustal matrices, the solubility at pH1.5 is low (the slope values are 0.33 and 0.22 respectively – see table 5.1): these values increase to 0.38 and 0.31 if the days with strong Saharan dust input are excluded. Indeed usually the solubility is lower in Saharan dust samples than in non-Saharan dust events, because, after the weaker extraction method only free metals, carbonates, oxides hydrates, or complexes of the elements with organic compounds are solubilized while elements present as oxides or taking part to the silica matrices are not solubilized (Marconi et al. 2014).

Moreover, if we compared the values obtained from ICP-AES analysis after solubilisation under stronger conditions with that obtained from PIXE analysis, the solubility of main crustal metals as Fe and Al considerably increase: indeed the slope of the linear regression obtained is higher than the slope of the comparison between ICP-AES values after weaker extraction and PIXE.

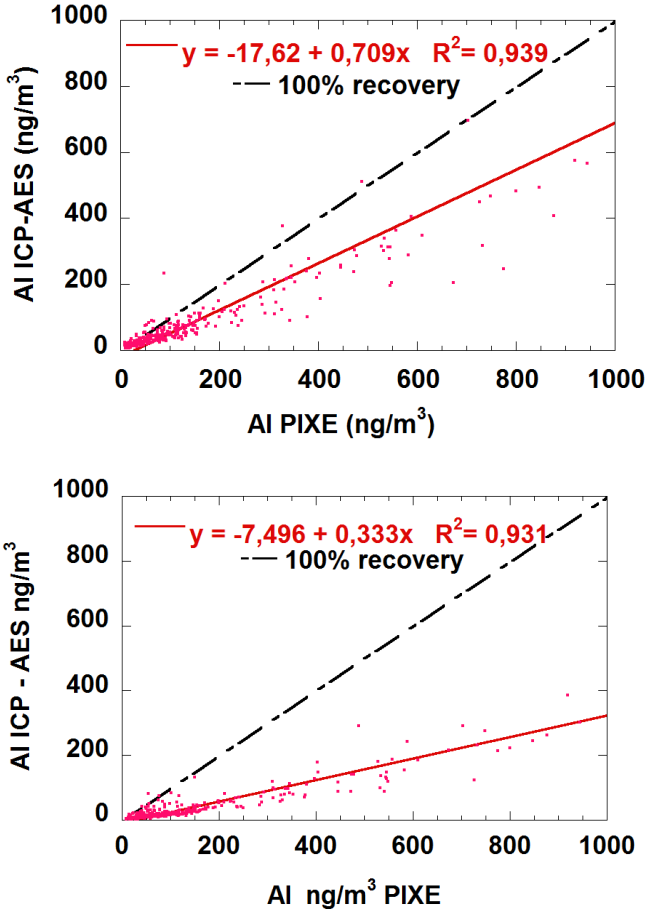

Figure 5.2 - *Correlation between atmospheric concentrations as determined by ICP-AES after the two different extraction methods and by PIXE for Al.*

In particular in the case of Al we found a very good correspondence between the two data set (R^2= 0.96 and n= 347) and 0.71 as slope value indicating that with the strong extraction method based on the EU rule EN14902 up to the 70% of Al was solubilised despite it was strongly linked to the crustal matrices. This experimental evidence is very interesting in order to quantify the crustal content: indeed as said before, Al is a commonly used marker for this source and the strong extraction

method grants its high recovery percentage. Thus, this information allows the use of ICP-AES technique (that is more easy respect to the complexity of instrumentation for PIXE measurements and in general for the total chemical analysis since it requires Si determination) even for a reliable estimate of crustal content.

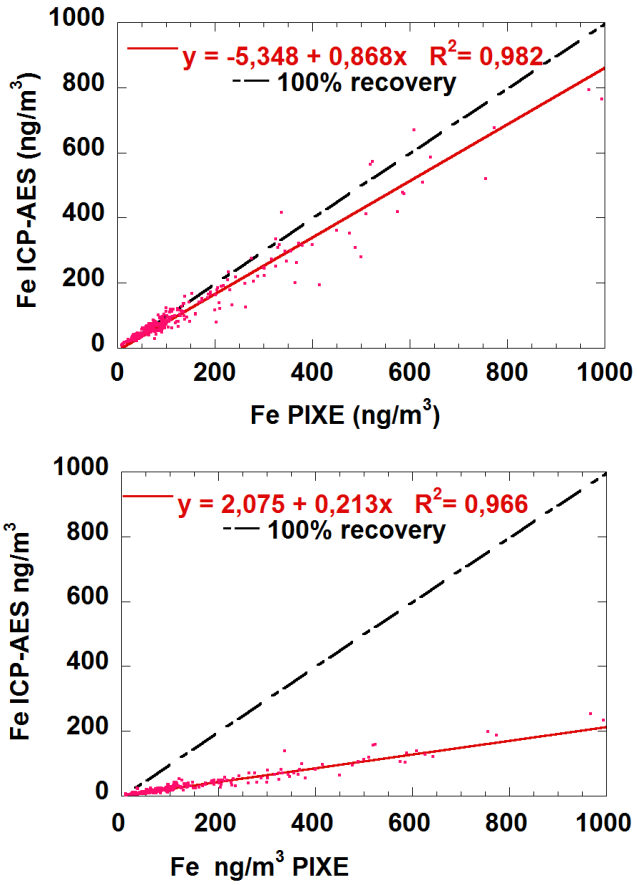

Figure 5.3 - *Correlation between atmospheric concentrations as determined by ICP-AES after the two different extraction methods and by PIXE for Fe.*

Moreover, it must be notice that the correlation coefficients for both the linear regressions between PIXE and ICP-AES values after the strong

and the weak extraction procedures for both Al and Fe are very high confirming the reproducibility of both the two extraction methods used (see fig. 5.2 and 5.3).

The solubility of Fe after the acidic digestion in microwave oven is higher than the values found for Al probably because it was present in crustal matrix mainly as more soluble compounds (such as oxides or carbonates) than as silicates, which are insoluble even in these stronger conditions. Indeed Si recovery percentage is low even after the application of the strong solubilisation method (the slope of the linear correlation between PIXE and ICP-AES values after the extraction with HNO_3 at pH 1.5 is 0.12 and 0.22 for the values obtained after digestion with HNO_3 and H_2O_2 mixture – see table 5.1).

Fe atmospheric concentration measured at pH 1.5 deserve a particular attention in order to evaluate the soluble fraction available as nutrient for marine organism. Indeed the evaluation of the role that Fe could play as fertilizing agent is actually debated and depends on its soluble content not on its total content. Moreover it has to be considered that in this site the frequent occurrence of Sharan dust events could deliver on sea surface a not negligible amount of Fe and others nutrients (as Al, Mn, Zn and Pb): in literature there are several authors that assume an important role of this metal in the fertilization of high nutrient low chlorophyll areas (HNLC) as the Mediterranean Sea (S.Bonnet an C. Guieu 2006).

5.2. Metals from anthropic sources

Although the remoteness of this site, anthropic emissions of heavy metals (in particular Pb, V and Ni) are not negligible at Lampedusa. Moreover metals emitted by anthropic sources are usually in more soluble form because of the chemical speciation and their occurrence in the finest particle fraction: indeed as shown in Tab. 5.1 the solubility of Pb, V and Ni is higher than the others metals even at pH 1.5 (the measured slope values are 0.79. 0.85 and 0.77 respectively). In the case of Pb the high solubility can be explained by the emissions of fuel combustion that contain this metal in weak complexes such as organometallic compounds (R. Traversi 2014, M.P. Pavageu 2004). Besides V and Ni are markers for heavy fuels oil (HFO) combustion: in particular at Lampedusa their presence in the atmosphere is principally caused by maritime traffic. Previous work demonstrate that the V and Ni soluble fractions at pH1.5 are better tracer of anthropogenic emission than the total content, as the total content account both for anthropic and crustal contribution. Thus, also in this case even the determination after the weak extraction method is very interesting. Fig.5.4 shows the linear regressions between PIXE and ICP-AES values after the strong and the weak extraction procedures both for Ni and V: even in these cases the correlation coefficients are very high confirming the reproducibility of both the UNIEN14902 and pH1.5 extraction procedures.

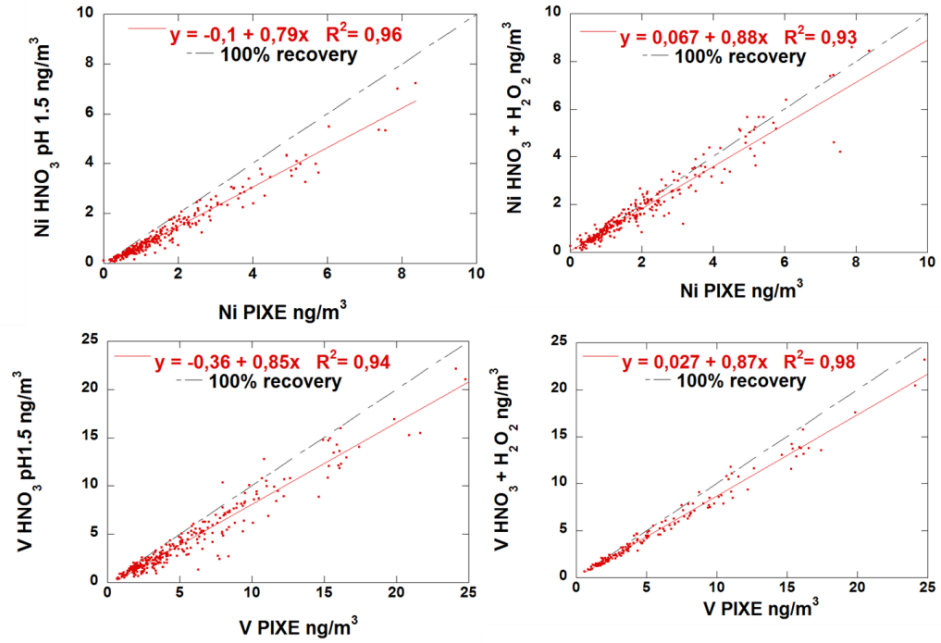

Figure 5.4 - *Correlation between atmospheric concentrations as determined by ICP-AES after the two different extraction methods and by PIXE for Ni and V.*

Temporal evolution of Ni and V atmospheric concentrations obtained with the three different types of analysis carried out were shown in fig. 5.5. The reader must notice that V and Ni content is higher in later spring and summer: this evidence is mainly due to the ship traffic that increase in this period. However a more detailed study of this important anthropic source will be illustrated in chapter 9.

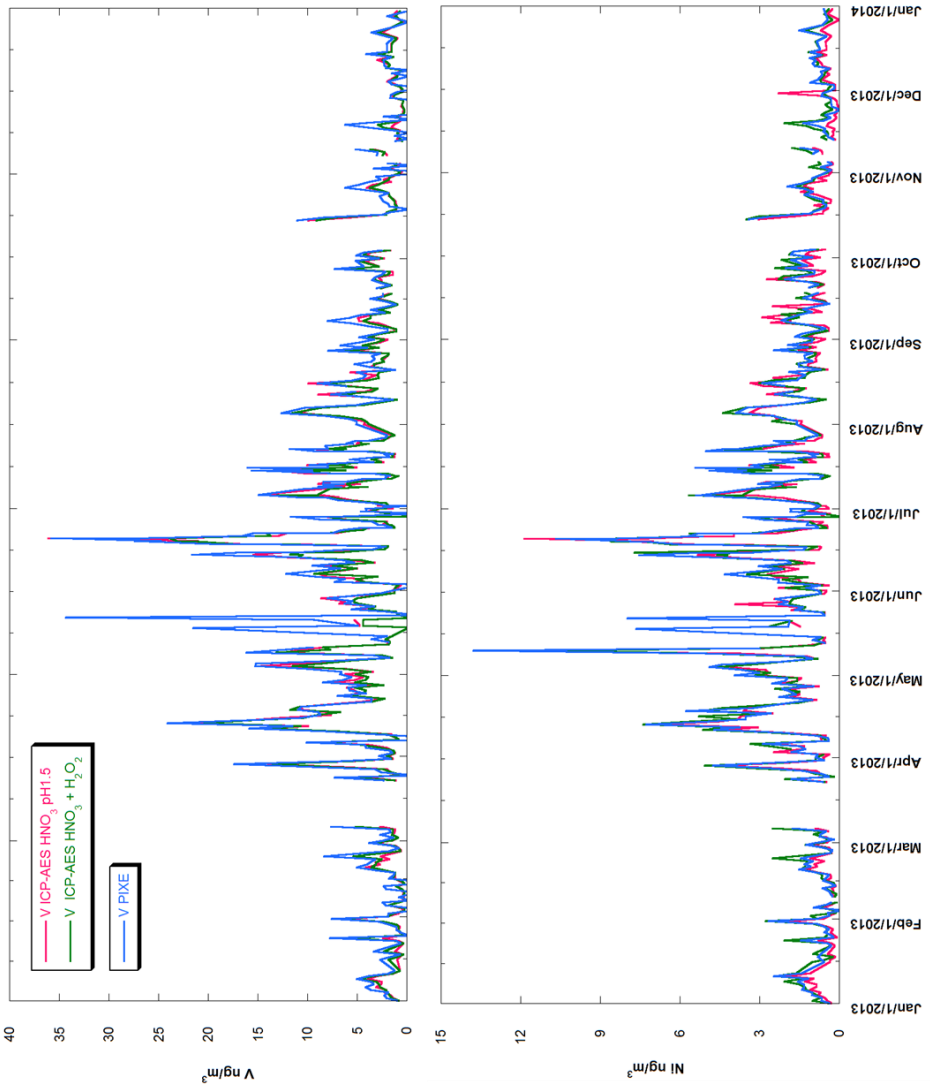

Figure 5.5 - *Temporal evolution of V and Ni atmospheric concentration obtained with three different type of analysis: ICP-AES measurements after extraction with HNO3 at pH1.5 in ultrasonic bath and after solubilisation in microwave oven with HNO_3 and H_2O_2 mixture, and PIXE analysis.*

Figure 5.6 shows the enrichment factors for several metals with mixed anthropic and crustal sources. The E.F. are calculated as the ratio between the soluble content of each metals (obtained by ICP-AES analysis after strong extraction method) respect to Al total content (obtained from PIXE): indeed, Al is to be considered the more reliable marker for the crustal source. Characteristic crustal ratios of each metals (black dashed lines) are calculated from their abundance in the upper continental crust (Henderson and Henderson, 2009). As reported by several previous studies (Becagli et al., 2012; Chester et al., 2000), samples with an enrichment factor <10 represent cases influenced by the crustal source, while E.F. values >10 identify events dominated by anthropic sources (anomalously enriched elements) such as heavy oil combustion. As regards to V and Ni the 50.4% and 58.2% of the samples present E.F. values >10. These percentages are much higher if the days identified as crustal events (>75th crustal oxides content) are excluded: in fact those samples result to be enriched in V and Ni in the 74.1% and 75.5% of the cases respectively. As expected since their prevalent anthropic origin, Pb, Cd, Cu and As are enriched respect to the crustal source: in particular Pb/Al, Cd/Al, Cu/Al and As/Al ratios result to be 10 times higher than the earth's crust characteristic values in the 90.2%, 93.1%, 76.6% and 85.88% of the samples respectively. Conversely, Cr and Sr result to be dominated by the crustal source.

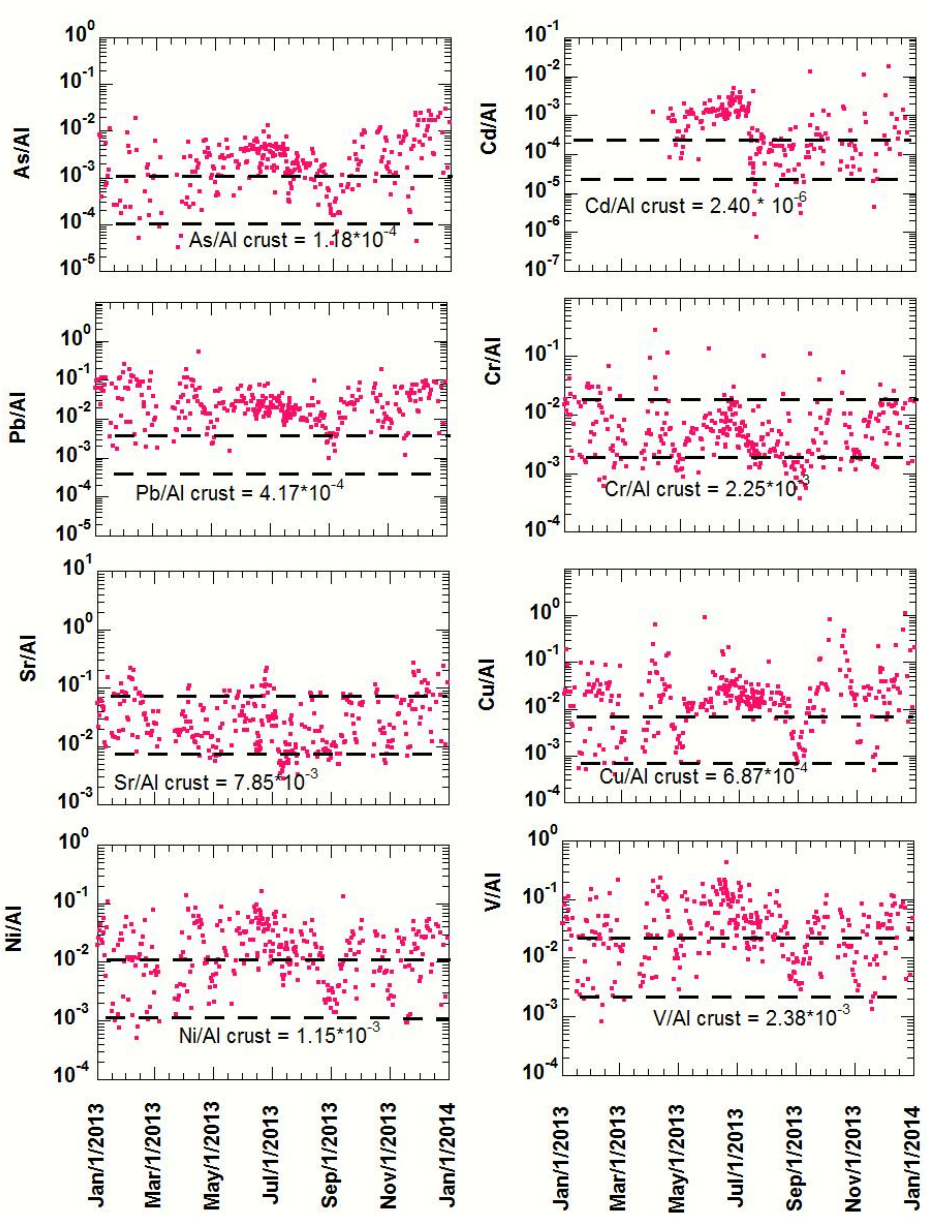

Figure 5.6 - *E.F. temporal evolution of As, Cd, Pb, Cu, Sr, Cr, Ni and V.*

CHAPTER 6 –Atmospheric aerosol load at Lampedusa

6.1. PM10 aerosol content over ten years of sampling

As explained in chapter 3.2 the aerosol sampling campaign was started on June 2004 and is still going on. In this thesis results from June 2004 to December 2014 are presented. In figure 6.1 PM10 daily concentrations ($\mu g/m^3$) obtained over all this period with gravimetric method (filters were weighted before and after sampling and the sampling volume was provided by the sampler as illustrated in section 3.2) is illustrated. At the beginning the aerosol sampler worked at daily resolution alternating in sequence sampling of PM10, PM2.5 and PM1.0 but since 2007 only PM10 sampling at daily resolution was accomplished. On a theoretical total samples number of 2857, 2157 filters were actually collected and analysed, with a sampling efficiency percentage of 82%. The most interruptions occurred during the sampling campaign were caused to technical failures, however such sampling effectiveness on a time period of ten years is high enough to consider the results obtained very representative of the atmospheric aerosol load and of its chemical composition in this area.

The average PM10 concentration over all the sampling period is 27.6 $\mu g/m^3$. In spite of the large variability in daily values the PM10 mean is quite to those measured at various regional background sites in the Mediterranean basin: in particular Querol et al. (2009) reported values similar to Lampedusa at Montseny (26 $\mu g/m^3$ - NE Spain), Finokalia (31 $\mu g/m^3$ Crete Island, Southern Greece) and Erdemli (36 $\mu g/m^3$ Southern Turkey) during the period 2001–2007.

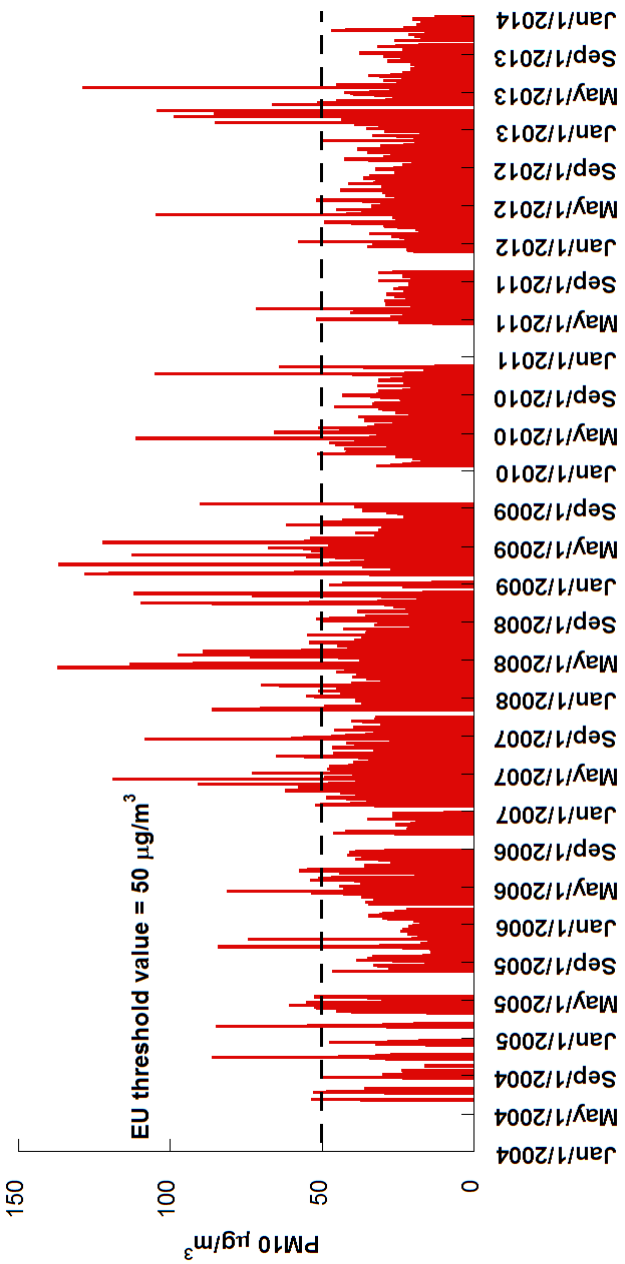

Figure 6.1 – *PM10 daily values from June 2004 to December 2014. Black dashed line represent the threshold value indicates by EU rule.*

Conversely, these values are slightly more than those reported by Pey et al. (2013) for a series of rural background sites across the Mediterranean region with the highest concentrations registered in eastern-basin areas (values ranging from 21 to 24 μg/m^3). This fact is likely due to the different elevation of the sampled sites and the different dust impact. Anyway, the mean PM10 value at Lampedusa is in accord with the increasing PM gradient from the NW to the SE of the Mediterranean Basin. This augment coincides both with that of African dust occurrence (that is particularly true at Lampedusa since the Sahara desert vicinity), and both with the increase of the regional pollution towards the eastern part of the Basin. As explained in chapter 2 this increment was largely studied and reported by several authors (Querol et al. 2009, Koulouri et al. 2008, Gerasopoulos et al.2007): these experimental evidences point out the importance of a remote site as Lampedusa in the central of Mediterranean sea.

The PM10 annual mean, even if calculated on different numbers of values, shows a certain interannual variability, ranging from 20.6 μg/m^3 in 2011 to 33.9 μg/m^3 in 2010. It has to be considered that in those two years the year sampling coverage percentage correspond to 31 and 36% respectively (see table 6.1), though if we considered the PM10 annual mean content for the years with the same percentage major to the 80% these values range from 22 μg/m^3 in 2012 to 32.5 μg/m^3 in 2007. In spite of the mean annual PM10 are quite high, they are below the EU annual standard for PM10 (40 μg/m^3). 147 days (corresponding to 6.8% of the total number of the data) exceed the daily threshold value established by

the European Commission for PM (50 μg/m^3, European Community, EC/30/1999). The percentage of the exceedances is lower than admitted by the EU law: 35 days/year, corresponding to 9.6%. However, it has to be noticed that the annual mean values and the number of exceedances have to be calculated over the 90% of the year in order to be compared with the limit imposed by the EU rules, but in our data set, although the whole year is cover by the sampling, only for 2007, 2008, 2012 and 2013 more than 90% of the day in the year is sampled. At this purposed table 6.1 reports the year sampling coverage percentage for PM10 from June 2004 to December 2014. Although the days in which PM10 content exceeds the EU threshold value of 50 μg/m^3 do not show a marked seasonality, however their occurrence over all the sampling period is much higher in spring with the 36% of the cases measured in April and May (33 and 20 exceedances respectively). Conversely, the minimum of exceedances occurrence is recorded in summer (in particular July show the lower percentage with only 2% of the days in which PM10 overcomes the threshold value). This fact is in accord with several studies which report an higher stability of the marine boundary layer in summer than in the other season over the Mediterranean Sea (U. Dayan et al. 1989). The importance of the marine boundary layer behaviour for the atmospheric aerosol content and composition in this region will be more explained in chapter 7, 8 and 9 where the contribute of natural and anthropic source to PM10 will be discussed. Indeed, as reported in chapter 1, atmospheric aerosols can be classified in different types according to their chemical composition, properties and formation processes. Ascertain the

principles aerosol sources and quantify their impact on PM is crucial to understand the air quality of this area and the role that those can play in global climate change. At this purpose next chapters of this thesis will be focused on the study of Sharan dust events, sea Spray contribute and anthropic emissions at Lampedusa.

	PM10 1 day every three sampling			PM10 daily resolution			PM 10 1 day every three sampling	PM10 daily resolution			
Months of the year	**2004**	**2005**	**2006**	**2007**	**2008**	**2009**	**2010**	**2011**	**2012**	**2013**	**2014**
	n	n	n	n	n	n	n	n	n	n	n
Jan		14[+]	9[+]	12	30	27	5	-	27	26	11
Feb		4[+]	6[+]	26	28	16	10	-	29	27	12
Mar		9[+]	8[+]	30	27	29	10	-	28	15	15
Apr		5[+]	10[+]	25	25	25	11	4	30	29	15
May		9[+]	13*[+]	31	23*	30	11	16	21	28	21
Jun	4[+]	9[+]	10*[+]	30	29*	26	8	13	24	27	30
Jul	15[+]	9[+]	10*[+]	26	27	30	13	18	31	25	31
Aug	8[+]	9[+]	9[+]	30	21	31	11	29	31	30	31
Sep	8[+]	9[+]	1[+]	27	28	15	11	26	23	27	30
Oct	8[+]	9[+]	5[+]	17	27	-	9	3	30	20	15
Nov	8[+]	9[+]	8[+]	8	27	-	13	-	30	26	15
Dec	15[+]	10[+]	8[+]	30	22	-	2	23	27	22	15
TOT	66[+]	105	97	292	314	229	114	132	331	302	241
Year Sampling Coverage %	18	29	27	80	86	63	31	36	90	83	66

[+] PM1.0 and PM2.5 alternating sampling.

* Andersen 8-stage impactor 3-day resolution sampling campaign (3rd June - 20th October 2006 and 17th May - 23th June 2008)

Table 6.1 – *Numbers of days covered by PM10 sampling during every month of the year from June 2004 to December 2014.*

CHAPTER 7 – Saharan dust aerosol

Mineral aerosol is produced by wind erosion and resuspension in arid and semiarid regions and contribute by about 45% to the total atmospheric aerosol load (Duce at al., 1991). In particular, the Sahara desert is the largest source of soil-derived aerosols, with an annual emission estimated to be about 600 Tg yr-1 (D'Almeida, 1986; Marticorena et al, 1997). By comparison, estimates of global dust emission range from 1000 to 3000 Tg yr-1 (Zender et al., 2004). Mineral aerosols affect the atmospheric radiative balance through scattering, absorption, and emission of radiation (IPCC 2007; di Sarra et al., 2011), and by acting as cloud condensation nuclei (Levin et al. 1996). The investigation of the role that dust plays on climate is among the main priorities to reduce uncertainties in future climate projections (Engelstaedter et al. 2006). Dust may also greatly increase the atmospheric levels of PM, adversely affecting air quality. This effect is especially relevant in Southern and Eastern Europe (Escudero et al., 2005, 2007, Pederzoli et al., 2010, Gerasopoulos et al., 2006, Dayan et al. 1991) due to the transport processes from Africa and the Arabian peninsula and to the relatively low precipitation, which causes a long residence time of PM in the Mediterranean atmosphere (Querol et al., 2009). Intense dust transport episodes may cause health impacts due to the high levels of PM, to which may be associated transport of anthropogenic pollutants (Erel et al., 2006). In addition, dust particles frequently act as reaction surfaces for reactive gases (Dentener et al., 1996; Levin et al. 1996), affecting atmospheric chemical processes. Dust influences atmospheric

chemistry also through modulation of the solar radiation, particularly in the ultraviolet spectral range, thus influencing photochemical processes (Casasanta et al., 2011; Meloni et al., 2003). Furthermore, observations in southern Europe show that the atmospheric deposition of specific nutrients is enhanced by dust input from Northern Africa (Avila and Rodà 2002). Mediterranean marine regions are highly influenced by crustal dust deposition, which may provide large amounts of nutrients for phytoplankton (Béthoux et al., 1996, Guerzoni et al., 1999). However, the processes that control the speciation and cycling of micronutrient in the surface ocean after dust deposition are scarcely known (Baker and Croot, 2010) and the hypotheses about biogeochemical responses to sporadic input of dust are controversial (Wagener et al., 2010). At this purpose, the study of the micro-nutrient solubility in the aerosol is particularly useful in determining their bio-availability and to understand the bio-chemical processes at the ocean-atmosphere interface.

Thus, many recent studies have focused on the estimation of the African dust influence on air quality in southern European countries, and especially in Spain and Italy (Rodriguez et al., 2001; Escudero et al., 2007; Perrino et al., 2008, Nava et al., 2012, Evan et al., 2016). Due to the range of mechanisms in which dust is involved, the characterization of its evolution and chemical composition is very important, especially in the Central Mediterranean Sea, where, as explained before, experimental studies are scarce.

7.1. Mineral aerosols characterization at Lampedusa

It is known that PM10 concentrations are strongly influenced by the occurrence of African dust events over the Mediterranean region: in this chapter the evolution of dust markers in aerosol samples collected at Lampedusa throughout the ten years period of sampling campaigns is presented. The aim was to quantify the Saharan dust contribute to PM10 and assessing its seasonal evolution. In addition such ground level measurements were compared with spectral aerosol optical depth (used as an indicator of columnar aerosol burden) aiming to understand the atmospheric behaviour of the air masses from North Africa.

In order to quantify the impact of Saharan dust intrusion episodes on PM10 concentrations, the mineral content was estimated as the sum of the contributions of all the main crustal element oxides (SiO_2, Al_2O_3, Fe_2O_3, CaO, Na_2O, MgO, K_2O, TiO_2), following the approach reported in literature by several authors (Eldred et al., 1987; Malm et al., 1994; Miranda et al., 1994; Marcazzan et al., 2001; Nava et al., 2012):

$$[\text{crustal content}] = 2.14\,[Si] + 1.89\,[Al] + 1.43\,[Fe] + 1.40\,[Ca] + 1.35\,[Na] + 1.66\,[Mg] + 1.21\,[K] + 1.67\,[Ti]$$

Some corrections were however applied to this formula to take into account the sea salt contributions to Na, Mg, K, and Ca, which may be relevant at Lampedusa, and possible anthropogenic sources to the other elements. In particular, the non-sea salt (nss) Na^+, $nssCa^{2+}$, $nssMg^{2+}$, and $nssK^+$ fractions were calculated by the 5 equation system reported below:

$nssNa = nssCa * (Na/Ca)_{crust}$

$nssCa = Ca - ssCa = Ca - ssNa * (Ca/Na)_{seawater}$

$nssMg = Mg - ssMg = Mg - ssNa * (Mg/Na)_{seawater}$

$nssK = K - ssK = K - ssNa * (K/Na)_{seawater}$

where

$ssNa = Na - nssNa = Na - nssCa * (Na/Ca)_{crust}$

and where Ca, K, and Mg represent the concentrations of these elements actually measured by PIXE in the samples. Na represents the concentration measured by ion chromatography in each samples. The concentration by ion chromatographic determination was chosen for Na because of the high error in PIXE measurements for this element, besides all Na salts are water soluble then the soluble fraction can be considered the total concentration. “Ss” and “nss” stand for “sea salt” and “non-sea salt”, respectively. For $(Na/Ca)_{crust}$ we used the value of 0.56, which is the mean ratio in the Earth crust (Henderson and Henderson, 2009); for $(Ca/Na)_{seawater}$, $(Mg/Na)_{seawater}$, and $(K/Na)_{seawater}$ the values 0.038, 0.119, and 0.037 were assumed, respectively (Henderson and Henderson, 2009), as they represent the mean ratios in bulk seawater ((Kisha et al., 2012, Marconi et al. 2014). Ratios are expressed as weight to weight [w/w]. In the Lampedusa aerosol, the calculated non sea salt fraction mean percentage on the whole sampling period for Na, Ca, Mg, and K are 7.39%, 81.04%, 29.87%, and 39.93%, respectively (see figure 8.1 in chapter 8). Possible anthropogenic contributions to Al, nssK, and Fe were

estimated by the use of aerosol-crust Enrichment Factors (EFs), which were calculated with respect to Si using the upper continental crust composition in EF calculation (Henderson and Henderson, 2009). Only few samples present EF higher than 10 for Fe and about 10% of the samples for nssK. However, since the nssK concentration is very low with respect to the other crustal markers, we used also nssK for the crustal content calculation, instead of recalculating its contribution from another oxide.

A criterion based on the crustal content was defined with the aim of identifying Saharan dust events. Cases with crustal content exceeding the 75th percentile of the crustal oxides content distribution (corresponding to 5.44 µg m-3) were identified as dust events (Marconi et al., 2014). Using this threshold for 2007 and 2008 samples (in those two years continuous daily sampling and PIXE analyses were performed) we identified 174 samples characterized by a strong crustal contribution; in the average, for these samples dust constitutes 34% of the PM10. The average crustal content over those two years is 5.8 µg m^{-3} (corresponding to 18% of the total PM10 mass), and reaches values as high as 67.9 µg m^{-3} during intense Saharan dust events. Figure 7.1 shows the temporal evolution of PM10 mass concentration and crustal oxides content from January 2007 December 2008: the black dashed line represent the 75^{th} percentile of crustal oxides content threshold value used to select Sharan dust events.

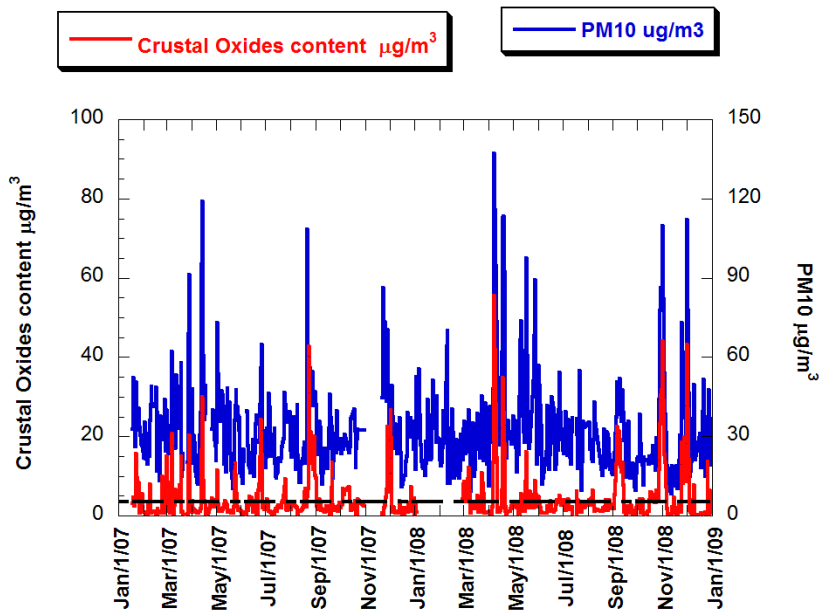

Figure 7.1- *Crustal oxides and PM10 content from January 2007 to December 2008.*

The average non-crustal PM10 concentration, obtained by subtracting the crustal content from the total PM10 concentration, is 26.9 µg m^{-3} (average over 698 samples measured during 2007 and 2008 where PIXE data are available), it has to be considered that the mean of PM10 content found for those two year was 32.4 µg/m^3. Over this data set 68 PM10 values are higher than 50 µg m^{-3} (9.7% of the total) and 29 values (4.2% of the total) of non-crustal PM10 exceeded the threshold. In order to understand the causes of such exceedances, it has to be consider that sea spray is the second most important aerosol source at Lampedusa island. In the considered data set (January 2007-December 2008) Sea spray account as average for 8.6 µg m^{-3} (28% of the PM10) and for 18.7 µg m^{-3} in day when the non-crustal PM10 is higher than 50 µg m^{-3}.

Anyway, a more detailed discussion of this important aerosol source at this site and for the whole period of sampling will be given in the next chapter.

Due to the complexity of instrumentation for the total chemical analysis and in particular for Si determination, in literature other methods have been proposed for the quantification of Saharan dust content. In particular, Escudero et al. (2007), by using only PM10 measurements, estimated the daily net dust load in PM10 attributable to an African episode in a given region by subtracting the daily regional background level from the PM10 concentration. Such method was accepted by the European Commission to establish guidelines for demonstration and subtraction of exceedances attributable to natural sources under the Directive 2008/50/EC on ambient air quality and cleaner air for Europe. By applying this procedure to our data set we obtain a good correlation whit crustal content calculation by oxides for Saharan dust events (R=0.852 n= 174), but the crustal content obtained following the method from EU guidelines is 1.79 times higher than the one obtained from the sum of the metal oxides. Thus, it appears that the method proposed in the EC guidelines for the determination of the Saharan dust contribution to PM10 is not properly applicable to a site like Lampedusa (Marconi et al. 2014). Alternatively, the crustal content has been estimated from a single tracer, the most common used marker is Al concentration (e.g. Rodriguez et al., 2012 and references therein), and considering that it represents 8.2% of the upper continental crust (Henderson and Henderson, 2009). Comparing the crustal content

obtained in this way with that obtained as the sum of the crustal oxides for 2007 and 2008, we found a very good correspondence between the two data set: R=0.984, n= 698, Slope= 1.0.

7.2. Saharan dust event identification: comparison between ground level measurements and optical properties.

Since PIXE analyses are available over limited time intervals, a different criterion applicable to the whole dataset, was defined to identify Saharan dust events; this criterion is based on the amount of nssCa measured with ion chromatography (Marconi et al. 2014).

We classify as dust events all cases with $nssCa^{2+}$ exceeding the 75th percentile of the nssCa distribution (483 ng m^{-3}). Although nssCa is only one of the elements used for the determination of the crustal content, and the Ca determined by ion chromatography is about 75% of the total Ca during Saharan dust events, it displays a good correlation with the crustal content (R=0.869 n= 698 $p<0.01$) and proves to be a reliable marker of Saharan dust events. The selection based on this threshold results to be slightly more restrictive than the one based on the total crustal content.

Indeed, by using the two criteria when both measurements are performed, we found that the samples which exceed the nssCa concentration threshold are 85% of those found on the basis of the total crustal content. Anyway, back trajectories analysis shows that all the selected events by nssCa are characterised by air masses at almost one altitude (500, 1000 or 3000 m a.s.l.) arising from Sahara desert. By comparison, we use other identification methods based on ground-based

measurements of column aerosol optical properties (Meloni et al., 2008) and air mass back trajectory analysis (Pace et al., 2006; Pederzoli et al., 2010). Aerosol optical properties are measured with a multi-filter rotating shadow band radiometer (MFRSR; Harrison et al., 1994) from June 2004 to December 2010. The measurement details and data retrieval is described by Pace et al. (2006). The data set obtained and here presented was accomplished by the ENEA agency. In fact a characterization of the aerosol types present over the atmospheric column can be based on measurements of the aerosol optical depth at 495.7 nm (τ) and Ångström exponent (α) calculated from the aerosol optical depth at 415.6 nm and 868.7 nm. While τ is directly proportional to the aerosol column density (number of particles), α mainly depends on the particle size distribution (low values of α indicate a prevailing role of coarse particles). The combined use of τ and α allows the identification of different aerosol types, including dust: usually, high values of τ associated with low values of α are typical of Saharan dust (Pace et al. 2006).

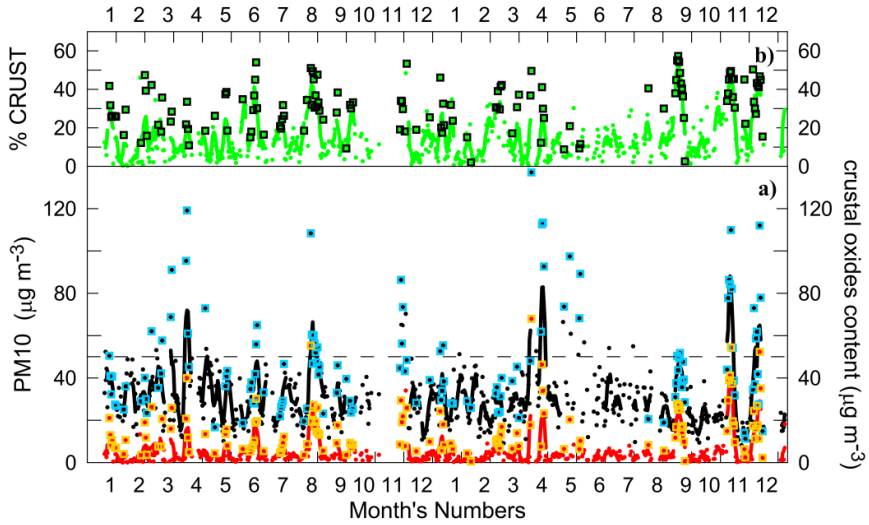

Figure 7.2 - a) *Temporal evolution of the PM10 mass concentration and of the crustal oxides content for the period January 2007 to December 2008. Daily measurements and 5 day's running means are plotted respectively as black (red) dots and lines for PM10 (crustal content). Measurements having nssCa > 483 ng m-3 are evidenced by cyan and yellow open square for PM10 and crustal oxides content.* ***b)*** *Temporal evolution of the mass ratio between crustal oxides content and PM10 for the same period. Daily measurements and 5 day's running means are plotted respectively as green dots and lines, measurements having nssCa > 483 ng m-3 are evidenced by black open squares.*

Figure 7.3 shows the behaviour of average values of α versus τ for cloud-free conditions for those days in which ionic composition measurements are available in the time period between June 2004 and September 2010. The average values are calculated for the duration of each daily sampling. A total of 776 values are used. Red markers identify the 193 (i.e. 24.9% of the total), days with large dust amount selected on the basis of the nssCa content (i.e., $nssCa^{2+}$ > 483 ng m-3). As suggested by Pace et al. (2006), the combined thresholds of $\tau > 0.15$ and $\alpha < 0.5$ are used to identify Saharan dust events from the column optical properties.

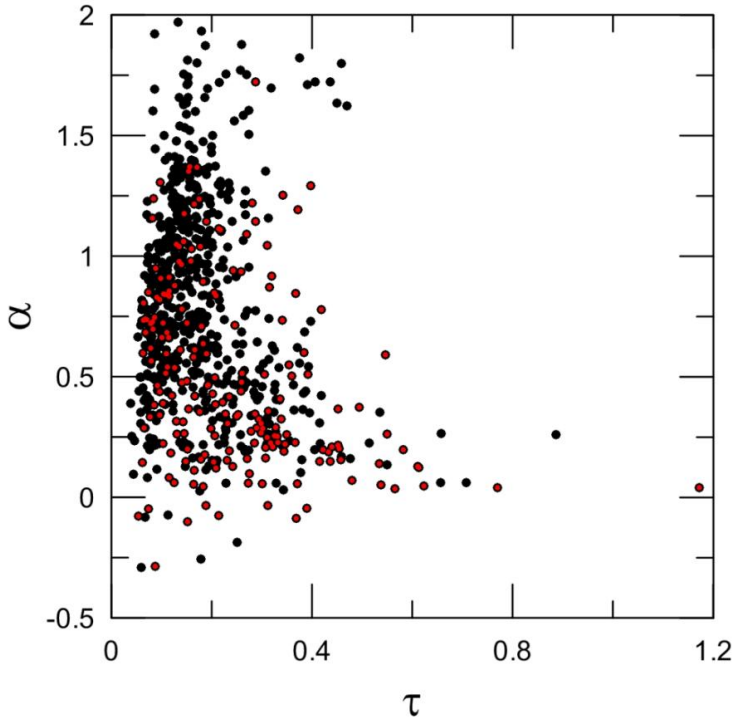

Figure 7.3- *Averages of aerosol Ångström exponent versus aerosol optical depth at 495.7 nm during the period June 2004–September 2010 for the days with PM10 ion analyses and for cloud-free periods, when aerosol optical depths measurements are possible. The red dots represent days characterized by elevated dust at the surface (nssCa > 483 ng/m^3).*

We found that 71.3% (129 episodes) of the events identified using the optical properties (181, i.e. 23,3% of the total) display a high nssCa, while 28.7% of the dust events selected by τ and α present low concentrations of nssCa. A plausible reason for these results is that Saharan dust transport frequently occurs above the marine boundary layer, with small impact on the surface aerosol properties. Considering the dust events selected on the basis of nssCa 55.4% (i.e. 107 episodes) of the cases

present τ and α outside of the expected range for dust events. In these cases the Saharan dust intrusion occurs only in the lower atmospheric layers. In order to identify cases in which Saharan dust is largely dominant over the column, we used more restrictive threshold values for τ and α (τ > 0.25 and α < 0.35). The number of events complying with this limits decreases dramatically from 181 to 80 (i.e. 10.3% of the total). About 62.5% of these 80 events displays nssCa >483 ng m^{-3}. However, no significant correlation between τ and PM10 or nssCa is found, suggesting that, even when the dust is very likely present in the lower and mid troposphere simultaneously, the behaviour observed at the surface is generally decoupled from what takes place above.

A statistical analysis is carried out separately for each season and reported in Table 7.1. In order to establish the seasonal occurrence of different dust transport scenarios at Lampedusa the number of cases and the percent with respect to the total number of PM10 measurements are reported for each season. Four criteria (1 through 4) to detect dust presence in the column and at surface are established, while their combination is used to identify six possible scenarios (a through f) of dust transport. Surface and large surface desert dust episodes correspond to values of $nssCa^{2+}$ respectively larger than 483 and 2*483 ng m^{-3}. Episodes characterized by the dominant presence of desert dust aerosol on the atmospheric column are identified when τ>0.15 and α<0.5, while intense transport episodes are defined when τ>0.25 and α<0.35. Please note that the percentages in 1-4 refer to the number of occurrences in each season, while those in a-f refer to the number of cases in 1-4.

Periods	DGF	MAM	JJA	SON
Number and frequency of cases	133 (17.1%)	229 (29.5%)	271 (34.9%)	143 (18.4%)
1) Surface episode	37 (27.8%)	68 (29.7%)	46 (17%)	42 (29.4%)
a) Columnar Episode	*7 (18.9%)*	*39 (57.4%)*	*21 (45.6%)*	*19 (45.2%)*
2) Large surface episode	23 (17.3%)	36 (16%)	13 (4.8%)	24 (16.9%)
b) Columnar Episode	*7 (30.4%)*	*24 (66.6%)*	*9 (69.2%)*	*15 (62.5%)*
c) Large column Episode	1 (4.3%)	13 (36.1%)	9 (69.2%)	7 (29.2%)
3) Columnar Episode	8 (6%)	66 (28.8%)	77 (28.4%)	30 (21%)
d) Surface episode	*8 (100%)*	*49 (74.2%)*	*43 (55.9%)*	*29 (96%)*
4) Large Columnar Episode	1 (0.75%)	33 (14.4%)	36 (13.3%)	10 (7%)
e) Surface episode	*1 (100%)*	*23 (69.7%)*	*18 (50.0%)*	*8 (80%)*
f) Large surface episode	1 (100%)	13 (39.4%)	9 (25%)	7 (70%)

Table 7.1 - *Seasonal occurrence of different transport scenarios identified on the base of $nssCa^{2+}$ on PM10 and τ and α from optical measurements.*

During the winter trimester, surface and columnar episodes appear decoupled also when large surface or columnar episodes are taken into account. On the other hand the few large observed columnar episodes always correspond to events of dust at the surface, suggesting that the aerosol flow at low altitudes and that a strong separation between marine boundary layer and free atmosphere does not exist. The reader should note that during this season cloudiness represents an important limiting factor for the detection of desert dust from optical measurements.

Spring and fall present quite similar behaviours. Surface episodes occur in the 29% of observations and appear to be independent from columnar episodes which are detected respectively in the 57% and 45% of cases; larger correspondences appear when intense columnar episode are taken into account (66.6% and 62.5% respectively), although a large number of cases are still observed only at the surface. As in winter, in spring and fall season columnar episodes strongly influence the surface presence of dust particularly in autumn (96% of correspondence). Considering intense columnar episodes, they do not increase the occurrence of a simultaneous event at surface, indicating that the columnar amount of dust does not play the main role in determining the presence of dust at surface in this seasons.

In summer, surface episodes present almost the same frequency of occurrence with (45.6%) or without (54.4%) simultaneous columnar episodes. These results change if cases of intense surface episodes are considered, presenting a 70% frequency that the event takes place during

a columnar episode. This suggests that when large amounts of dust are present on the column, the penetration in the marine boundary layer may be favoured, especially for long-lasting episodes. Differently from the other seasons, in summer columnar events do not necessary correspond to surface events, the frequency being of 55.9%, and the correspondence further decreases when intense columnar episode are taken into account.

In summer the presence of dust at surface and on the whole column shows the minimum correspondence, supporting the idea that the strength of the summer convection over the Sahara injects desert dust at high altitudes and that particles, advected over the stable marine boundary layer, seldom influence the surface aerosol amount.

Figure 7.4 shows two different scenarios of Saharan dust event: the typical summer situation with low nssCa Saharan dust passes over the marine boundary layer (Backward trajectories ending at Lampedusa on 29th June 2007) and the typical winter situation with very high nssCa at ground level (Backward trajectories calculated the 7 March 2008). In this case Saharan dust affects only the lowest atmospheric layers because the boundary layer over the Sahara in this season is low, and air masses located over the boundary layer are not affected by dust.

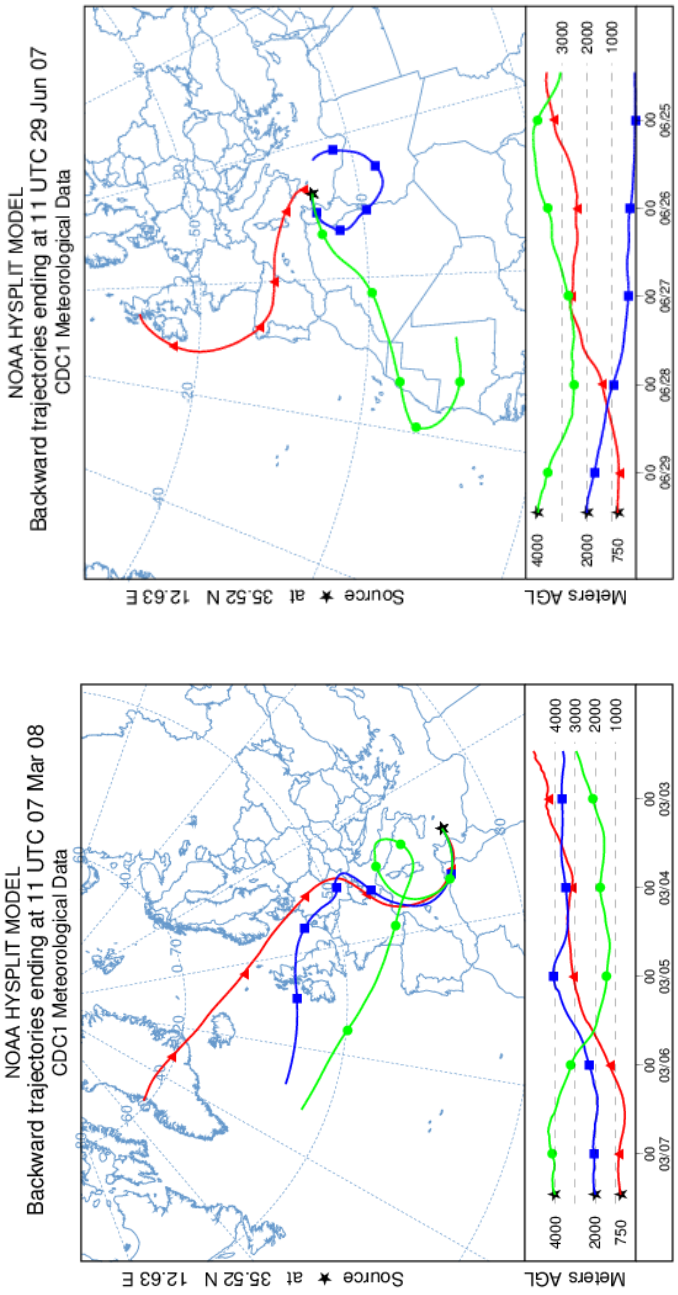

Figure 7.4- *Backward trajectories calculated from NOOA Hysplit Model and ending at Lampedusa on 29th June 2007 and 7th 2008.*

7.3. Seasonality of PM10 and Saharan dust events

In this section the seasonality of PM10 and Saharan dust event is discussed on the base of both optical properties and ground level measurements. Figure 7.5 shows the monthly distribution of PM10, nssCa, and τ for the period June 2004 - December 2010. The aerosol optical depth shows a marked seasonal pattern with spring-summer maxima. Previous studies reported that the dust optical depth and vertical distribution show a large seasonal cycle, with elevated τ and a wider vertical extension in spring and summer; the seasonal change is mainly controlled by dust transport occurring over the boundary layer (Di Iorio et al., 2009). On the contrary, PM10 and nssCa show no evident seasonal pattern, both in median values and in variability, which is however lower during summertime.

PM10 appears marginally higher during spring. Since τ provides information on the entire air column, high values of τ in spring and summer do not necessarily imply that a high aerosol load is present close to the surface, where PM10 and nssCa are measured. Nevertheless peaks in the 95th percentile occur in the same months for both PM10 and nssCa, confirming that very high PM10 values are associated with dust, when the marine boundary layer shows a weaker separation from upper atmosphere.

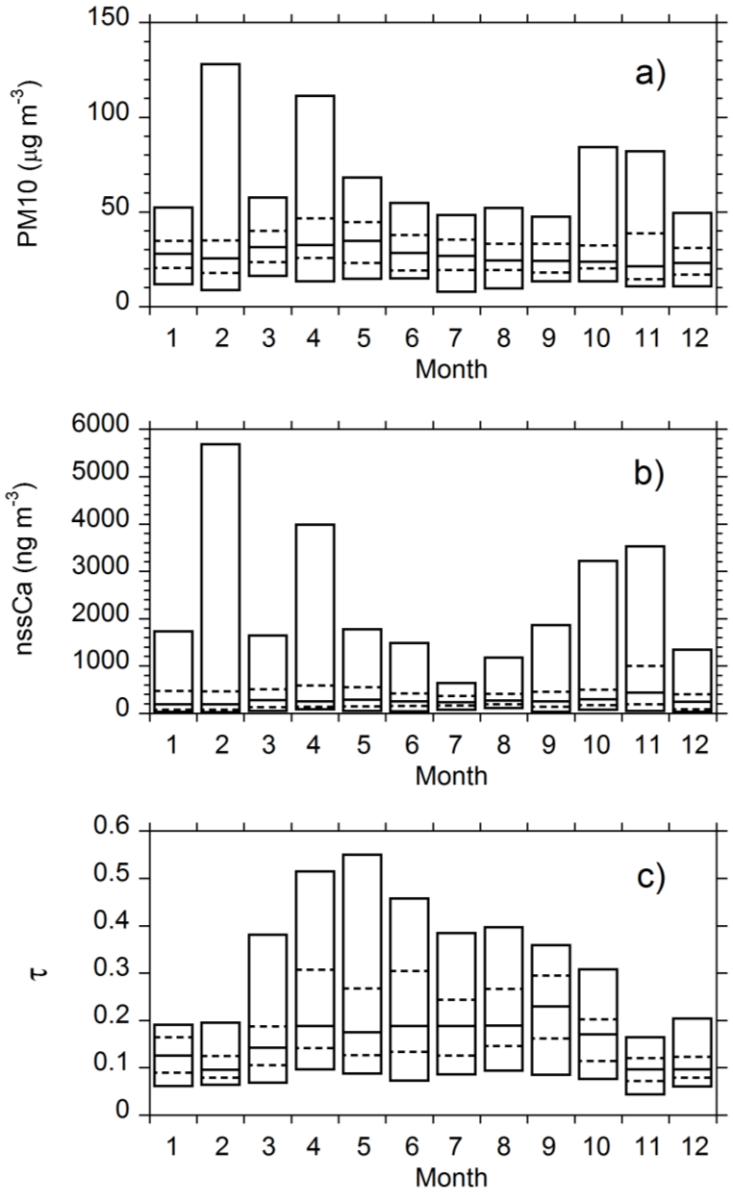

Figure 7.5 - *Monthly distribution of PM10 a), nssCa b), and τ c) for the period June 2004 - December 2010. The top and bottom of each box show the 5th and 95th percentiles. The middle line shows the median value, and the dashed lines show the 25th and 75th percentiles.*

Figure 7.6 reports the percentage of days of Saharan dust events occurring in each month as estimated from the column optical properties and from the threshold on nssCa, and the number of days with PM10 > 50 µg m^{-3} expressed in percent. The figure shows a very different annual pattern of the percentage of Saharan dust days identified from chemical and optical properties. The seasonal pattern of Saharan dust events identified by optical properties shows a well-defined summer maximum, as also reported by several authors over the central Mediterranean region; conversely, the Saharan dust days at the ground level show a very different pattern, with a high occurrence of events in March-April and October-November and minimum occurrence in summer. Besides, the intensity of Saharan dust surface events in February, April and October-November are more intense than those of other months. The mean percentage of events at ground level and their intensity pattern agree with results found by Pey et al. 2013 for central Mediterranean sea. Conversely, the minimum in percentage of Saharan dust event is summer was not detected by Pey et al. 2013 in the analysed site in Central Mediterranean. Besides, the difference between the results of the two methods (optical and chemical) is maximum in summer.

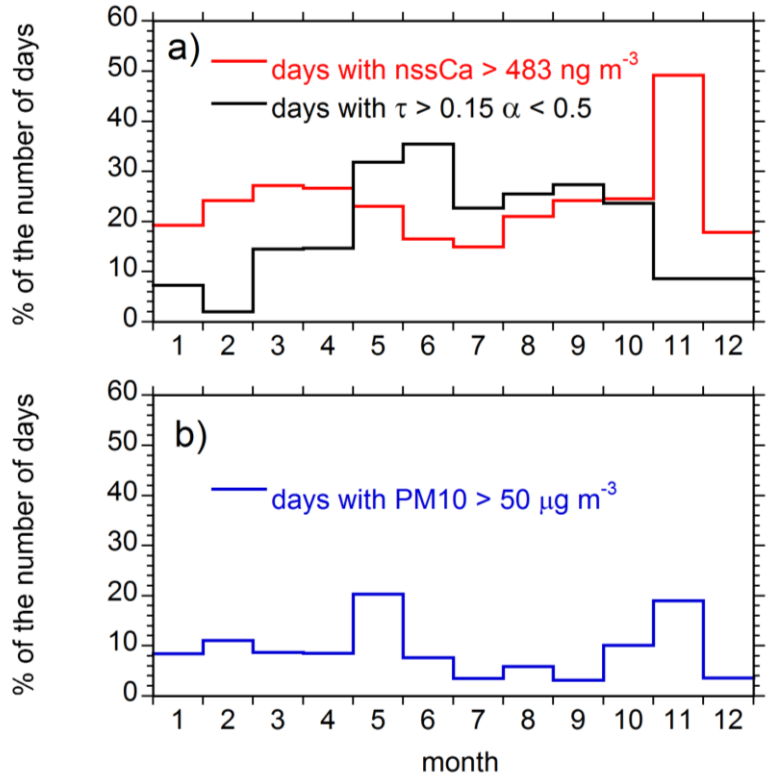

Figure 7.6 - *a) Percentage of Saharan dust events observed in each month identified from the aerosol optical properties (black line) and from the nssCa amount (red line) and, b) percent number of days with PM10 > 50 μg m^{-3}.*

These evidences suggest that in summer air masses coming from Saharan desert overpass the boundary layer over this area, and no significant mixing between inside and above the boundary layer occurs. Previous study showed that in summer African dust episodes over the western and central part of the Mediterranean basin have lower intensity than other season and occurs at high attitude, this is due to the presence of the Atlas mountainous barrier (2500 km extension and peak altitudes up to more than 4000 m a.s.l) that plays a dominant role in local and

mesoscale atmospheric circulation patterns (Pey et al., 2013). Besides, higher stability of the marine boundary layer in summer than in the other season over the Mediterranean Sea (Dayan et al., 1989) prevent the mixing between low and high atmospheric layers.

In spring and autumn the occurrence of Saharan dust days at the ground level is higher than those over the column. As discussed previously, this is related to seasonal changes in the convection intensity over the Sahara. This situation is typical of Saharan dust events determined by transport processes affecting the eastern part of Mediterranean basin in spring and autumn. They are induced by cyclones moving eastwards across the Mediterranean and/or north Africa, transporting dust at surface levels (Pey et al., 2013).

The percentage of PM10 exceedances shows two maxima, in May and November; only the latter corresponds to a higher occurrence of Saharan dust events as revealed by nssCa. Other sources, have to be considered to explain the high percentage of exceedances in May.

7.4. Size distribution and solubility of Saharan dust aerosol marker

In this section solubility of the different markers is discussed with respect to size distribution and aerosol sources, with the objective to quantify the fraction of each analysed element able to interact with the biological system (fertilization processes by Fe or environmental toxicity by heavy metals).

The deposition of atmospheric particles to surface waters may provide nutrients to marine biological systems, and affect the marine productivity

(Duce et al., 1991, Gallisai et al., 2012). These processes may be particularly relevant for oligotrophic oceans and for semi-enclosed seas, such as the Mediterranean. Most of the deposition in the Mediterranean is associated with Saharan dust events. Bioavailability of nutrients depends on several factors, and in particular on the size of the deposited particles and on the solubility of the various elements. Thus, the determination of the main dust components size distribution and of their solubility is crucial to understand the potential impact of dust events on biogeochemical processes.

	Saharan dust event				**Non Saharan dust events**			
	Median	**Mean**	**Std dev of the mean**	**N. valid data**	**Median**	**Mean**	**Std dev of the mean**	**N. valid data**
Al	10.7	12.5	0.8	159	14.8	18.6	0.6	497
Fe	5.9	7.5	0.4	158	13.0	15.3	0.5	499
Ca	75.8	75.2	1.5	163	76.8	76.4	1.0	495
Mg	75.4	73.4	2.5	147	91.7	87.1	1.4	395
K	39.5	40.5	1.3	166	63.7	63.0	0.9	510
Mn	54.6	53.9	1.2	153	54.9	55.2	1.1	330
V	46.6	46.7	2.1	104	66.7	65.1	1.5	295
Ni	50.9	50.7	2.1	136	63.0	61.3	1.3	400
Cr	6.2	6.9	0.5	94	6.0	7.6	0.7	71
Cu	45.7	47.3	1.8	143	53.1	53.6	1.4	397
Pb	62.7	64.8	2.8	84	56.3	56.8	2.0	177

Table 7.2 - *Median, mean, standard deviation of the mean and number of valid data for the percentage of metals solubility in samples classified as Saharan dust events and non-Saharan dust.*

The solubility of several elements in HNO_3 pH1.5 was calculated for PM10 samples corresponding to Saharan dust and non-Saharan dust events. Median, mean, and standard deviations of the percent solubility are reported in Table 7.2. The solubility of each element presents a large variability. The solubility is in general affected by various processes, such as chemical speciation, mixing of different types of particles, size distribution, and ageing processes. The large variability of the measured solubility is attributed to the influence of these processes. In spite of this large variability, usually the solubility is lower in Saharan dust samples than in non-Saharan dust events, because, in the used extraction condition, only free metals, carbonates, oxides hydrates, or complexes of the elements with organic compounds are solubilized. Conversely, elements present as oxides or taking part to the silica matrices (i.e. the 66.6 % main constituent of the upper continental crust) are not solubilized with this extraction condition.

As already said in chapter 5, metals emitted by anthropic sources are usually in more soluble form because of the chemical speciation and their occurrence in the finest particle fraction. The size distribution of various elements was determined from multi-stage impactor samples. Data from three days integrated sample characterised by high Saharan dust content (23, 24, and 25 June 2006) are reported in figure 7.7. The sampled event represent a large columnar episode (τ = 0.39 and α= -0.05 ±0.09) with high aerosol load and nssCa at the surface (PM10 = 57.4 µg m^{-3} and nssCa = 2050 ng m^{-3} measured on 23th June 2006). The concentration of each marker for each impactor stage is obtained using different extraction

procedures applied on different portions of the filter: HNO_3+H_2O_2 in microwave oven and HNO_3 pH1.5 were used for all the elements (see section 3.3); in addition, extraction in ultrapure water was also used for Mg, Ca, and K. The three different extractions give information on the bioavailability of each elements also as a function of the size of the particle in which they are present. Figure 7.7 shows that the typical crustal markers (Si, Al, Fe, Ca, Ti, Mn) but also elements having others sources (Mg, K, Ba) or present as trace in the crust (Li, Sc) characterized by two relative maxima in the concentration, respectively in the size ranges 2.1-3.3 μm and 5.8-9 μm. Others trace elements taking part in the mineral matrix (Sr, Rb, La,Y, Yb, Co) present only one large maxima in the range 2.1-5.8 μm. In the examined event all the elements excluding Ca, Mg, Ba, Mn, Sr present in these coarse modes solubility lower than 15%.

The finest mode is related to anthropic source mixed to crustal one, in fact, elements having only anthropic source or both (Fe, K, Co, Pb, V, Ni, Cd) present a maximum in the finest fraction, which is characterised by relatively high solubility. For instance, Fe present in the coarse fraction displays a very low solubility (8 % in the size range 2.1-3.3 μm). A maximum of Fe concentration in the finest particles fraction appears only when the soluble fraction is considered (fig. 7.7), as a result of a strong increase of solubility (69 % in the size range 0.4-0.7 μm) for decreasing size. The solubility of various crustal markers (Si, Al, Fe, Ti, Li, La, Y, Sc, Rb, and Co) in the 1-5 micron range, is generally low, because they are present mainly as oxides or as silicates, which are not soluble in HNO_3 pH1.5.

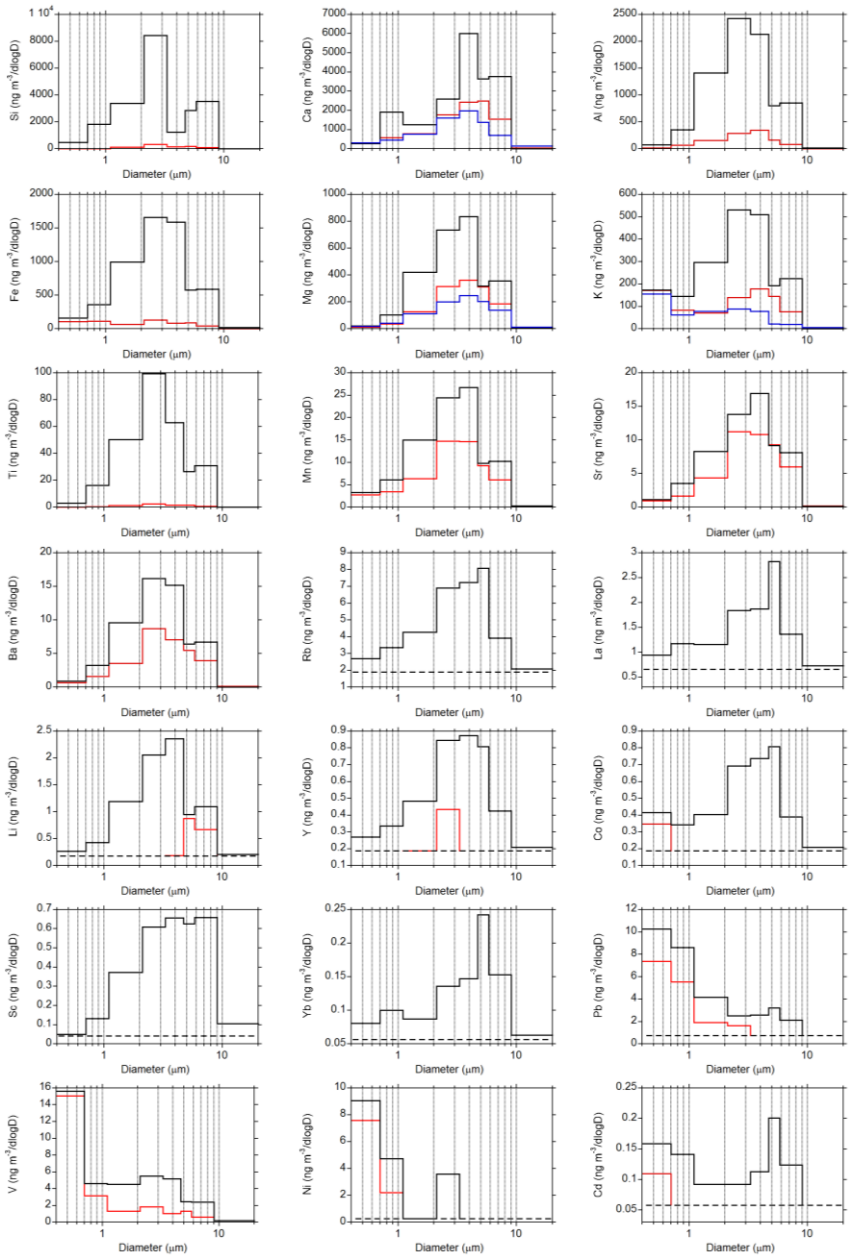

Figure 7.7 - *Size distributions of main and trace elements during a Saharan dust event (June 23rd - 26th, 2006) by using different solubilisation methods: HNO_3-H_2O_2 in microwave oven (black line), HNO_3 in ultrasonic bath (red line), and MilliQ water in ultrasonic bath (blue line). The dashed lines represent the instrumental detection limit for each element.*

On the other hand Ca, Mg, K, Ba, Mn, and Sr present a higher solubility in the same size range, suggesting that part of this elements is present as chloride, nitrate, sulphates and carbonates in crustal aerosols. The presence of carbonate can be estimate for Ca and Mg from the difference between the solubility in HNO_3 pH1.5 (red line in fig. 7.7) and in H_2O (blue line in fig. 7.7). Indeed, Ca and Mg sulphate, chloride, and nitrate salts are soluble in H_2O, conversely carbonate are soluble in acid condition (HNO_3 pH1.5). In this event the fraction of Ca and Mg present as carbonates are 20% and 18% respectively in the 1-10 micron size range.

Figure 7.8 shows the ionic balance calculated for each of the 7 stages of the impactor on the water extract: anions and cations are summed separately in each stage.

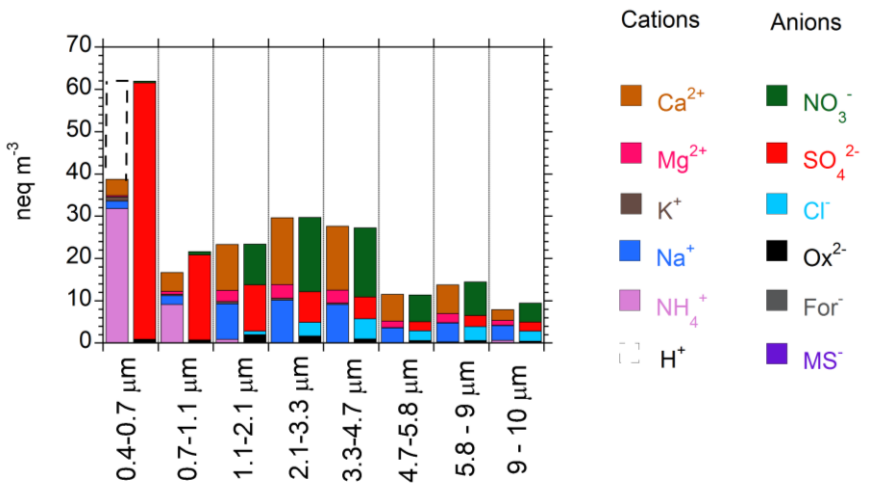

Figure 7.8 - *Ionic balance in each of the 7 stages of the multi-stage impactor for the sampling of June 23rd - 26th, 2006, characterized by a high crustal content.*

It can be noticed that nitrate, which is mainly due to the oxidation of anthropic NO_x (then expected to appear in the finest fraction) is mainly

present in particles larger than 1 micron, similarly to the main crustal marker (Ca). It is known that HNO_3 formed in the gas phase in the atmosphere undergoes exchange reactions with NaCl from sea spray, or with $CaCO_3$ from crustal aerosols (e.g. Fairlie et al., 2010 and references therein and chapter 8 of this thesis). The impactor data suggest that the exchange reactions with $CaCO_3$ is an important process in Saharan dust samples mixed with anthropic aerosols. This process may lead to an increase in the solubility of $CaCO_3$ and other carbonates.

The solubility of Ca, Mg, Fe, and Al is plotted versus the sum of NO_3^- and SO_4^{2-} content in figure 7.9. The sum of NO_3^- and SO_4^{2-} is used to give an indication of the anthropic acidic species capable of dissolving carbonate when they are absorbed over crustal particles. Sulphate is mainly present in the finest fraction of aerosol but its concentration in the size range of crustal markers is not negligible (red area in the ionic balances in figure 7.8), then it can contribute, together to NO_3^-, to dissolving carbonate. Although several other factors may play a role (for instance the time of contact between the air masses enriched in anthropic acidic species with those of crustal origin), an increase of anthropic acidic species should produce an enhancement of solubility. In fact, in spite of the uncertainties and the variability is large, an increase in solubility appears to be associated with elevated amounts of nitrate and sulphate, better evident for Ca and Mg. Thus, aging processes and mixing of crustal and anthropic aerosols during transport from source areas to the sampling site are able to change the aerosol chemical properties, and may affect solubility and, in turn, the bioavailability of crustal elements.

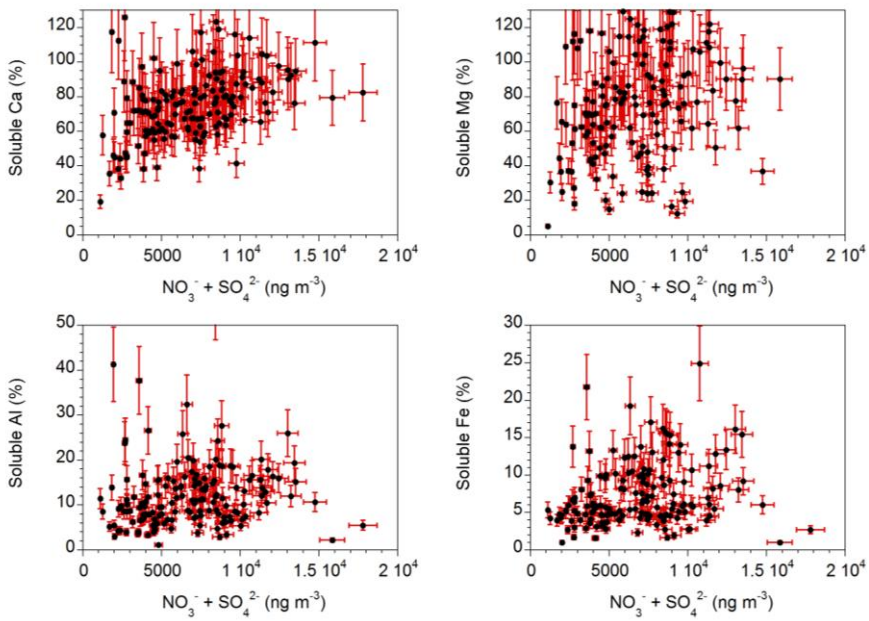

Figure 7.9 - *Scatter plot of solubility in HNO3 pH1.5, calculated with respect to the total elemental content determined by PIXE, for Ca, Mg, Al and Fe as a function of the sum of nitrate and sulphate for days characterized by high crustal content (nssCa > 483 ng m-3).*

7.5. Source areas of Saharan dust aerosol

In this section back ward trajectories were used to identify source regions of the collected dust. The Hybrid Single-Particle Lagragian Integrated Trajectory (HYSPLIT) modelling system (Draxler and Rolph, 2012) was used for the trajectory analysis. The National Centres for Environmental Prediction (NCEP) reanalysis database was used as meteorological input, with a 2.5x2.5 degrees horizontal resolution. The HYSPLIT model was run to compute 72 hours back-trajectories ending at Lampedusa at 50 m a.g.l. at the centre of the time interval of the filter samples. Trajectories were calculated for the days in which the measured nssCa exceeded 483 ng m^{-3}. Given the distribution of the

calculated trajectories, two sectors were selected as the main source regions for surface dust episodes. The two sectors are shown in Figure 7.10 and correspond to the Algeria-Tunisia region, and to the Libyan area. Each sector includes an important distinct dust source area, as identified by previous studies (Israelevich et al., 2002; Scheuvens et al., 2013). A sector was classified as main source region for each trajectory, and thus for the dust collected at Lampedusa on the arrival day of the trajectory, if the air mass spent more than 50% of the trajectory time over that sector (50% permanence criterion). Given the difficulty in associating a specific source area along a trajectory especially if the air mass is consistently travelling within the boundary layer, as it is often the case, and the distribution of the trajectory patterns, no information can be derived for other important source areas from this dataset. Out of the total number of samples on with PIXE analysis was carried out, and with nssCa>483 ng m^{-3}, 34% were associated with a source region in Northern Africa: in particular, 21% of the trajectories were classified as originating from Algeria-Tunisia, and 13% as coming from Libya. Trajectories spending most of their time over other areas, such as the Mediterranean Sea or Europe, were also found. These were disregarded in this analysis because, as discussed above, it was not possible to identify a specific source region. Trajectories originating from the two source regions are mainly found in autumn and winter (76% of the cases). The Algeria-Tunisia region is the predominant source (26%) with respect to Libya (9%) in winter, while the contribution from both regions is comparable (24% for Algeria-Tunisia and 19% for Libya) in autumn.

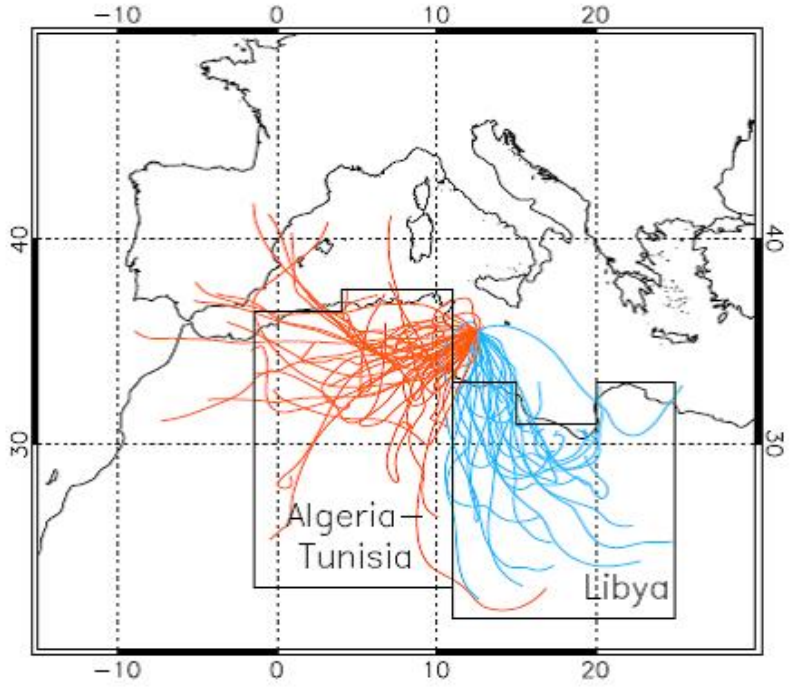

Figure 7.10 - *Dust source regions and back-trajectories fulfilling the 50% permanence criterion for each source region (orange for Algeria-Tunisia and blue for Libya).*

Different ratios between the elements could be considered to identify regional differences in the dust elemental composition: here we prefer to normalize the element abundances to Al in order to compare our data with recent literature data (Scheuvens et al., 2013). Si and Al are the dominant elements (e.g. Scheuvens et al., 2013) in north African dust and sediments. The median Si/Al ratio of the Saharan dust events detected from our measurements is 2.33 ± 0.17, and presents a low variability. Such ratio is characteristic for a mixture of quartz and alumosilicates (feldspar, clay minerals), typical of the Saharan desert. The average northern African dust composition exhibits Si, Fe, and Mg relative

contents comparable to those of the upper continental crust. Northern Sahara dust is slightly depleted in the alkali metals K and Na, and enriched in Ti and P with respect to the upper continental crust, but the ratios between these element and Al do not show significant variations over the Sahara region. Thus, the most useful ratios to discriminate the dust source areas are Ca/Al, Mg/Al, Fe/Al, and especially the elemental ratio (Ca+Mg)/Fe, which shows a pronounced North–South gradient with highest ratios in North-Western Africa (Scheuvens et al., 2013).

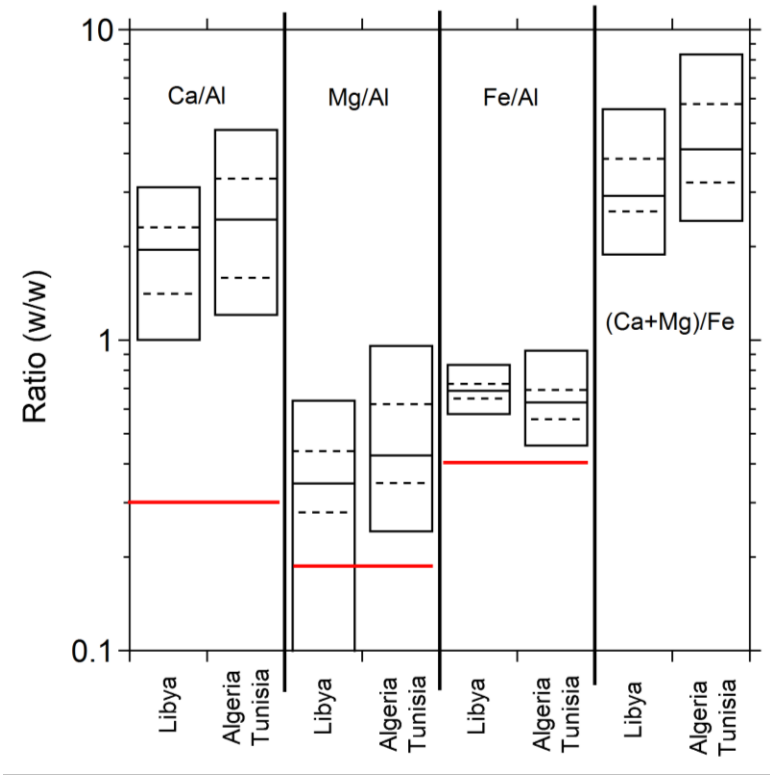

Figure 7.11 - *Percentile distribution of Ca/Al, Mg/Al, Fe/Al and (Ca+Mg)/Fe ratio for the two dust source region evidenced in fig 7. The top and bottom of each box show the 5th and 95th percentiles. The middle line shows the median value, and the dashed lines show the 25th and 75th percentiles.*

Figure 7.11 reports the percentile distributions of the above mentioned ratios for the Saharan dust episodes divided for the two source areas derived from the trajectory analysis.

The Ca/Al, Mg/Al and (Ca+Mg)/Fe ratios are calculated using the non-sea salt fractions of Ca and Mg, because the uptake of sea-salt during transport could produce an increase in the total concentration of these elements, which would not be due to the different Saharan source areas. Figure 7.11 shows that both source areas display Ca/Al and Mg/Al ratios higher than the mean crustal composition. The high Ca/Al are related to the elevated carbonate contents in the Sahara sediments, found in north-western (Morocco and Atlas region; Criado and Dorta, 2003; Khiri et al., 2004; Linke et al., 2006; Moreno et al., 2006; Castillo et al., 2008) and north-eastern Africa (Egypt, Libya; Linke et al., 2006). Intermediate values were reported for southern Egypt and northern Sudan (Tomadin et al., 1989; Sharif, 1995), while lower Ca contents (Ca/Al<0.5) were found in samples from central and southern Algeria and the Sahel zone. The amount of calcite within the silt fraction (Desboeufs and Cautenet, 2005) increases from <5% in the Sub-Saharan region to more than 10% in the northernmost part of northern Africa, with maxima in northern Libya (>15%). The other Ca mineral (Gypsum) generally exhibits a lower abundance (<2%) with respect to carbonate, with some local exceptions (northern Libya, central Algeria; Scheuvens et al., 2013).

The Mg content in dust and soil generally correlates with the Ca content. Thus, higher Mg/Al ratios and higher Mg enrichment factors were also reported for the Atlas region (Mg/Al>0.3) and for the eastern

Mediterranean (Mg/Al>0.3). The correlation of Ca and Mg most likely results from the association of the carbonates calcite and dolomite in source sediments, but may also be due to the preferential occurrence of additional palygorskite (a Mg-bearing clay mineral) in areas with higher carbonate contents.

Thus, the northern regions of Sahara are expected to be enriched in Ca and Mg, although data of bulk composition from Tunisia are missing (Scheuvens et al., 2013). Figure 7.11 shows that, in spite of the very large variability, the Tunisia-Algeria dust source area presents Ca/Al and Mg/Al ratios somewhat higher than the Libyan source. (Ca+Mg)/Al or (Ca+Mg)/Fe are also relevant ratios to discriminate between different source areas. As shown by Scheuvens et al. (2013), the mean values of (Ca+Mg)/Fe is higher (equal to 4.8) for Algeria-Tunisia than for southern Algeria (values of 0.6–1.2), and for the regions of Mali and Mauritania (Escudero et al., 2011). The areas in the sub-Saharan region present a still lower (Ca+Mg)/Fe ratio (<0.85). Therefore, due to the Fe content differences between north-western and north-eastern Sahara source regions, the ratio (Ca+Mg)/Fe may help to assign northern African dusts to a specific source region. Indeed, quite different median values for Algeria-Tunisia (4.1) and Libya (2.9) source areas are found in our dataset, as shown in figure 7.11.

It must however be pointed out that the retrieved results are characterized by a very large variability, and the distributions of the ratios we used are in most cases overlapping. This very high variability may depend on the uncertainties implied in the attribution of the air mass

trajectories to the source areas. Here we applied the permanence criterion to increase the probability that the sampled dust was produced in the identified region. However, uncertainties in the trajectories are expected to be large, due to the low resolution of the meteorological data, the lack of meteorological measurements over the Sahara, and the possible role of temporal variations in the trajectories during the sampling time, which are not taken into account. In addition, long range transport of dust over the Sahara may contribute to mix particles of different origin.

CHAPTER 8 – SEA SPRAY AEROSOL

The Marine aerosol is one of the most important natural aerosol system. It is produced by the action of the wind on the sea surface and is the main primary aerosol source. It has a significant role on the earth's radiative balance by scattering light and acting as cloud condensation nuclei: in particular it can contribute from 5% to 90% of CCN in the marine boundary layer (Clarke et al., 2006, Rosenfeld et al., 2002) affecting the regional and global climate (Lewis and Schwartz, 2004). In addition it takes place to biogeochemical cycles and impacts on ecosystems and air quality. For these reasons, recently the interest on sea spray aerosol is increased and focused on its role in climate change (IPCC 2001). Indeed, sea salt dominates the marine boundary layer (MBL) particulate mass concentration and is the principle sub micrometre scatterer in marine and ocean regions (IPCC 2001, O'Dowd et al. 2007). Sea salt contributes 44% to the global aerosol optical depths and estimates of global annual radiative forcing due to sea salt are -1.51 and -5.03 W/m^2 for low and high emission values respectively (IPCC 2001). Sea salt has also been linked to the MBL cycle from the activation of halogens leading to ozone depletion (Vogt et al., 1996, McFiggens et al. 2000).

The marine aerosol comprises primary and secondary aerosol components. While the secondary marine aerosol results from gas to particle conversion processes, its primary production occurs from the interaction of wind stress at the waves surface and results in the mechanical production of sea spray aerosol (O'Dowd et al. 2007). In

particular, sea-salt aerosol (SeaSA) is generated by the direct injection of sea-spray particles into the atmosphere through breaking waves during whitecap formation, resulting in a strong dependence of the SeaSA production flux on wind speed (G. De Leeuw et al. 2011). Many publications have discussed the observed relationship between SeaSA concentration and sea surface wind (P. Kishcha et al. 2011, P. Kishcha et al. 2012 and reference therein): accord to these studies wind speed is the dominant factor controlling wave generation and subsequent breaking.

Due to the range of mechanisms in which SeaSA is involved and its relevant contribution to the aerosol budget in the MBL, the study of its evolution and chemical composition is very important, especially in the Central Mediterranean Sea where experimental studies are scarce. Moreover Lampedusa is a marine remote site and ascertain SeaSA contribute to PM10 in this type of station is crucial to assess the regional background of this source and its influence on the atmospheric aerosol load even in others type of sites. Moreover characterizing SeaSA and its variation during field campaigns will be essential to validating large-scale models (Calzolai et al. 2015).

8.1. SeaSA contribution to the PMx at Lampedusa

In this section we present the evolution of SeaSA markers in aerosol samples collected on the island of Lampedusa throughout the period June 2004 - December 2014 (see fig. 8.2).

The sea salt aerosol fraction was calculated as the sum of the main components of sea water: Na^+, Mg^{2+}, Ca^{2+}, K^+, sulphate and chloride. Since that these ions can have also other sources than primary sea spray

as the crustal one (Na^+, Mg^{2+}, Ca^{2+} and K^+) and others secondary sources both anthropic and natural (SO_4^{2-}) as, for example, biomass burning (K), in this thesis for these components the sea salt (ss) and the non-sea salt (nss) fractions were calculated. As yet illustrated for the crustal oxides content quantification in chapter 6, the ss and nss fraction of Na^+, Mg^{2+}, Ca^{2+}, K^+ and SO_4^{2-} are obtained by the following equations:

$$ssNa = Na - nssNa = Na - nssCa * (Na/Ca)_{crust}$$

$$ssCa = ssNa * (Ca/Na)_{seawater}$$

$$ssMg = ssNa * (Mg/Na)_{seawater} \; ; \; nssMg = Mg - ssMg$$

$$ssSO_4^{2-} = ssNa * (SO_4^{2-}/Na)_{seawater} \; ; \; nssSO_4^{2-} = SO_4^{2-} - ssSO_4^{2-}$$

$$ssK = ssNa * (K/Na)_{seawater} \; ; \; nssK = K - ssK$$

Na^+, Mg^{2+}, Ca^{2+}, and K^+ represent the concentration measured by ion chromatography in each samples. For $(Na/Ca)_{crust}$, $(Ca/Na)_{seawater}$, $(Mg/Na)_{seawater}$, $(SO_4/Na)_{seawater}$ and $(K/Na)_{seawater}$ we used the value of 0.56, 0.038, 0.129, 0.253 and 0.036 respectively (Henderson and Henderson, 2009), as they represent the mean ratios in the earth crust and bulk seawater (for more details see chapter 7.1).

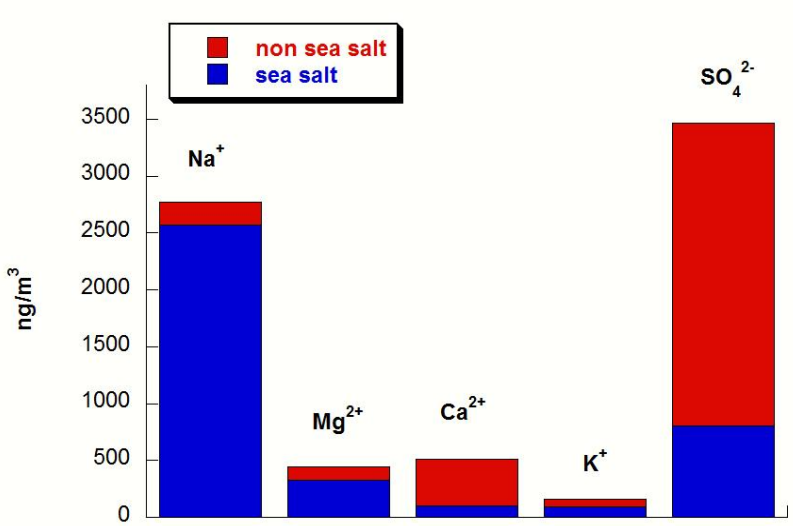

	Sea Salt %	Non Sea Salt %
Na	92.61	7.39
Ca	18.96	81.04
Mg	80.26	19.74
K	60.07	39.93
SO4	20.19	79.81

Figure 8.1 – *Ss and nss fractions contribution percentage to the absolute content of the main SeaSA compounds.*

Figure 8.1 shows the absolute content and the percentage contribution of the ss and nss fractions for the considered ions. It is interesting to notice that the ssNa percentage is dominant, but the contribution of nssNa is not negligible for a marine site as Lampedusa accounting for 7.39% of the total budget of Na. This is due to the input of crustal aerosol which is high especially during Saharan dust intrusion as illustrated in chapter 7. The same consideration can be applied to Mg. Instead, regarding to the nss- fraction percentage of Ca, K, and SO_4 it has to be considered the dominance of other sources than sea spray: the crustal

one in the case of Ca as discussed before (see chapter 7.2) and biogenic emissions in the case of sulphates. Concerning the nssK fraction it can be impute both to the crustal and the biogenic source since that this ion is also a product of the marine biologic activity.

Finally, for chloride we used the measured concentration instead of the calculation from ssNa, because during the aging of sea spray it undergoes to depletion processes, mainly due to exchange reactions with anthropic H_2SO_4 and HNO_3 (see section 8.2). Thus, in this thesis SeaSA amount was calculated as follow:

$$SeaSA = 1.46 * [ssNa^+] + [Cl^-]$$

In the ten years data set here presented, the SeaSA average contribution percentage to PM10 is 27.53% and the mean level of sea spray content calculated on the whole sampling period is 7.38 μg/m3. These values are close to those found in the Eastern Mediterranean sea at Erdemli on the coastline of South Turkey (SeaSA contribution to PM10 24% and sea spray content 8,9 μg/m3) (Querol 2009). However the daily SeaSA content can reach the level of 42.74 μg/m3 (up to the 70% of PM10 content) during an intense sea spray event (see section 7.2).

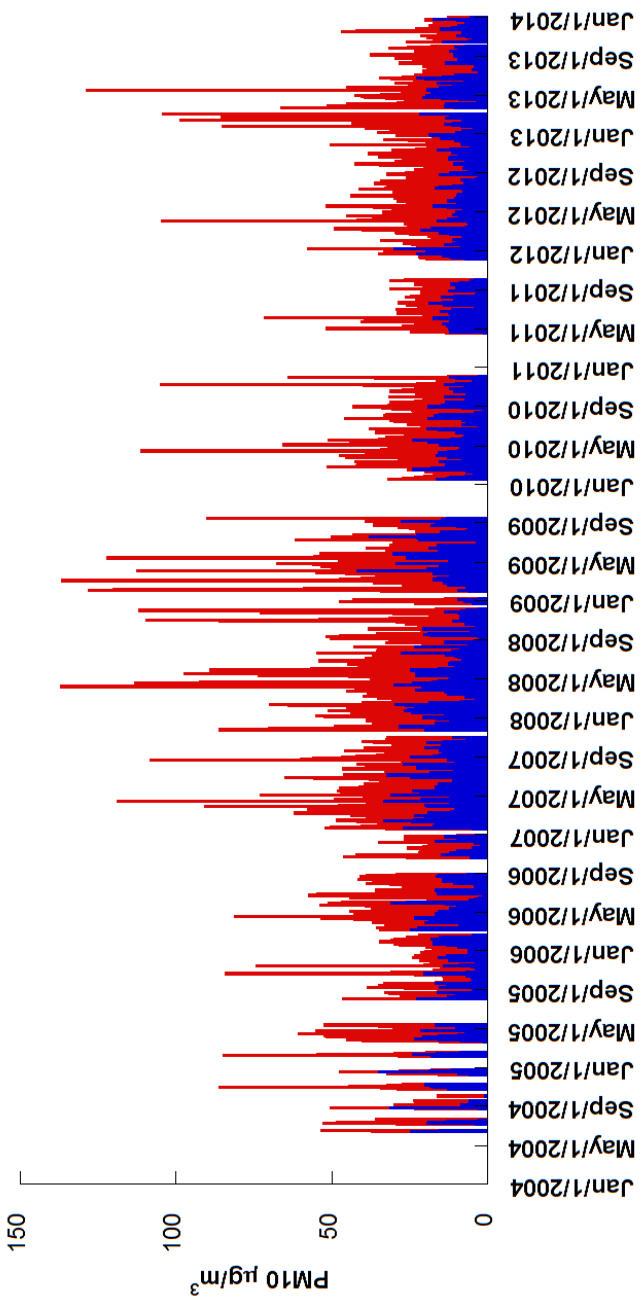

Figure 8.2 - *SeaSA and PM10 temporal trends (blue and red bars respectively) from June 2004 to December 2014.*

Since that SeaSA production mainly depends on wind speed (Kisha et al., 2012) the occurrence of strong marine aerosol inputs do not have a seasonal trend, as shown in figure 8.2. Nevertheless the days interested by percentage of SeaSA higher than 50% represent the 23,6% of the total samples collected. In particular if we subtract the SeaSA content to the PM10 level in those days characterized by an exceedance of the law threshold of 50 μg/m3 only in the 52.3% of the cases the PM10 value continue to overcome the EU limit (77 days respect to the total 147 days). This fact demonstrates the importance of quantify the contribution of natural input in the air quality assurance and policy.

Regarding SeaSA contribution to PM2.5 and PM1 here we presents the results about two years data (1 sample every three days from June 2004 to December 2006): indeed, as reported before from January 2007 only PM10 daily sampling was carried out.

As expected, since that SeaSA particles are mainly distributed in the coarse fraction (C. D. O'Dowd et al. 1997), their contribution to PM decreases with decreasing of particles size. In particular SeaSA average contribution percentage to PM2.5 results to be 13.85% and its mean level content is 1.77 μg/m3, those values register an even bigger decrease in PM1 rising 4.20% and 0.20 μg/m3 respectively (see Table 8.1). Very similar results were found at the Mediterranean sites of Finokalia and Erdemli (Querol 2009).

	SeaSA mean content	SeaSA average contribution percentage to PM
PM10	7.38 μg/m^3	27.53%
PM2.5	1.77 μg/m^3	13.85%
PM1	0.20 μg/m^3	4.20%

Table 8.1 - *SeaSA mean content and average percentage contribution to PM10, PM 2.5, and PM1.*

Thus, sea spray is one of the most important aerosol source at Lampedusa and, as said before, become predominant during marine storms. In particular, in this data set were found several days interested by sea spray input of very high intensity in correspondence of Mistral occurring.

A Mistral event can be defined as a marine storm characterized by high wind velocity at ground level and air masses coming from high altitudes over in the Atlantic Ocean (Jiang, Q. et al., 2003). The days interested by such meteorological conditions present high levels of aerosol load and in particular of fresh SeaSA (a more detailed discussion about fresh and aged sea salt particles will be given in the next paragraphs of this chapter). As an example in figure 8.3 the PM10 and SeaSA content during the Mistral event registered on the 25th and 26th June 2013 are reported (since the importance of mineral dust at this site, even the crustal aerosol content is shown). The identification of this event was accomplished through the backward trajectories obtained with the NOAA HYbrid Single-Particle Lagrangian Integrated Trajectory Model

(HYSPLIT; Stein et al. 2015) and reported in figure 8.4 that clearly shows how the air masses ending at Lampedusa in those two days were coming from the North Atlantic Ocean. Indeed, It has to be noticed that the high levels of PM10 registered in both these days (32.7 µg/m^3 on the 25th and 33.3 µg/m^{3}on the 26th June) were mainly due to the marine source: in particular SeaSA values measured at ground level were 22.8 and 19.9 µg/m^3 corresponding to 69.7% and 59.7% of PM10 total content respectively.

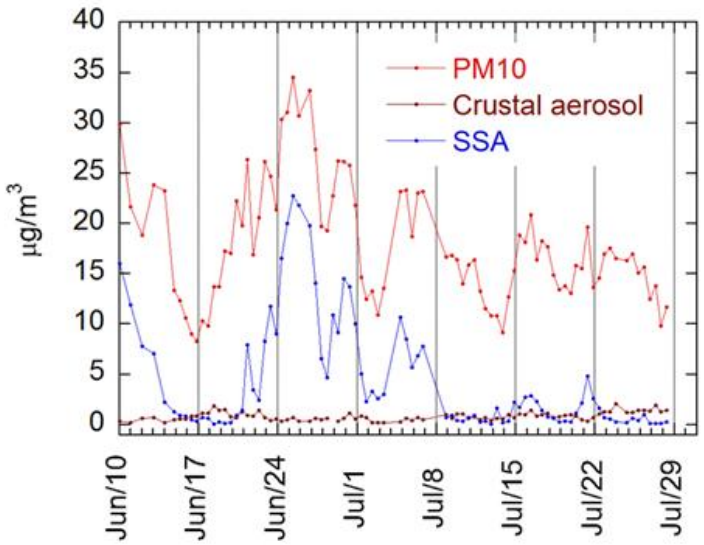

Figure 8.3 – *PM10, SeaSA and crustal oxides content measured during the 25th-26th June 2013 mistral event.*

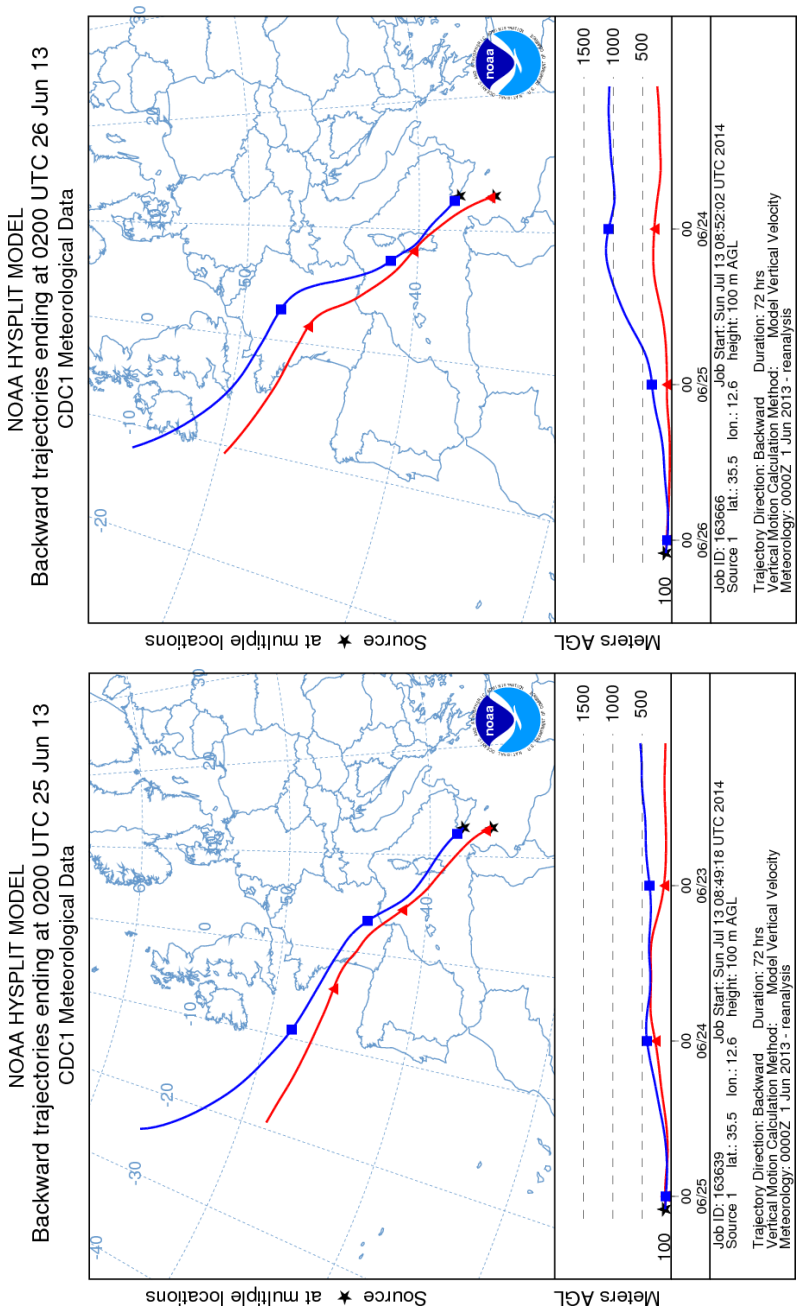

Figure 8.4 - *NOAA Hysplit Model Backward trajectories of 25th and 26th June 2013.*

8.2. Chloride depletion processes

Chloride depletion refers to the processes of chloride removal from sea salt aerosol through reactions with acidic species or their precursors (Zhao et Gao, 2008). This process results in changes in the deliquescence point and optical properties of coarse aerosol particles (Finlayson-Pitts and Pitts, 2000) and may also effects atmospheric acidic deposition caused by particles involving chloride and nitrate (Evans et al. 2014). Moreover, during these reactions chlorine atoms can be generated and can react rapidly with ozone and with organics species affecting the atmospheric oxidation capacity. This process starts when the sea-salt aerosols become acidic allowing multiphase reactions to proceed and displace Cl-. The most important process dechlorinating the SeaSA is due to the following reactions with H_2SO_4 and HNO_3 (Murphy et al., 1998a):

$H_2SO_4(g) + 2NaCl(a) \rightarrow 2HCl(g) + Na_2SO_4(a)$

$HNO_3(g) + NaCl(a) \rightarrow HCl(g) + NaNO_3(a)$

where (a) represents the aerosol phase and (g) the gas phase. Other processes for losing Cl^- involve reactions with NOx or with free radicals. Finally, heterogeneous reactions with metals on dust particles enhances Cl^- deficit in the presence of windblown continental dust.

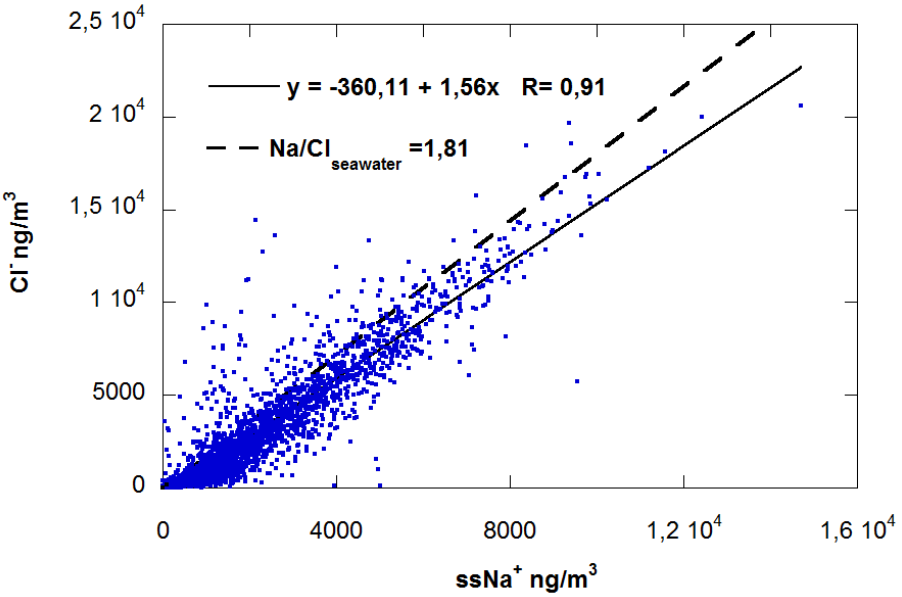

Figure 8.5 - *Correlation between [Cl-] and [ssNa$^+$] in PM10 sampled at Lampedusa from June 2004 to December 2014.*

As shown in fig. 8.5 the chloride depletion process is not negligible at Lampedusa even if it is a marine remote site. Indeed the slope of the linear correlation between Na^+ and Cl^- content is lower than that of sea water ratio (1.56 versus 1.81) and the intercept is negative confirming the presence of those processes. Moreover, the [Cl^-/Na^+] mass ratio temporal variation over all the sampling period shows a marked seasonal trend: chloride depletion principally occurs in later spring-summer as shown in Fig. 8.6.

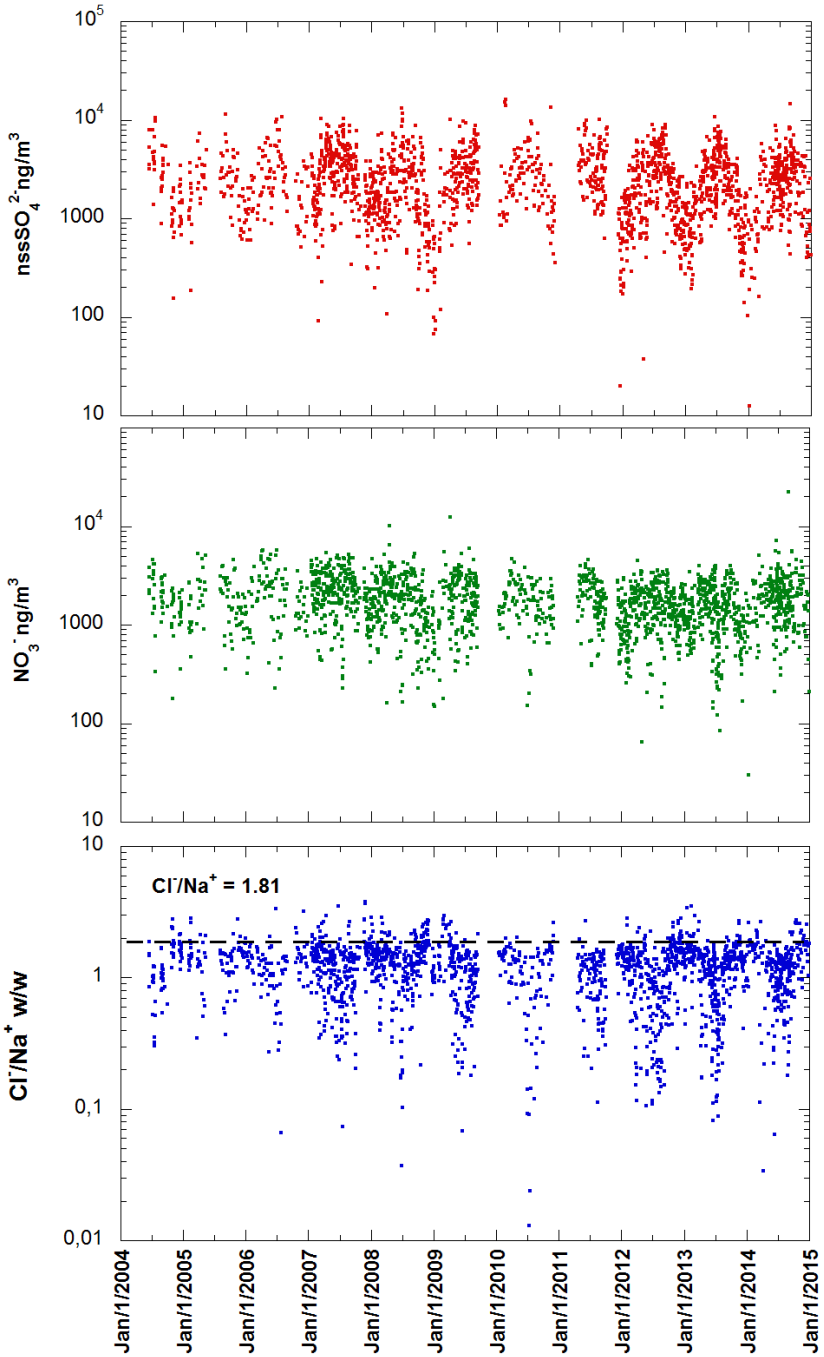

Figure 8.6 - *Temporal evolution of $[Cl^-]/[Na^+]$ w/w ratio, NO_3^- and $nssSO_4^{2-}$ atmospheric content from June 2004 to December 2014.*

This evidence is mainly due to the higher atmospheric acidity that is found at this site during these seasons respect to the others periods of the year. In fact it is known that at Lampedusa in these periods $nssSO_4^{2-}$ production is improved by the higher biological and anthropic activity. In particular, in later spring-summer the Sicily channel region is interested by an intense ship traffic that caused heavy fuel oil combustion emissions which are responsible for elevated levels of $nssSO_4^{2-}$ (the influence of this source at Lampedusa will be discussed in chapter 9). Moreover, in summer photochemical activity is higher than the others periods leading to a faster production of secondary aerosols, mainly $nssSO_4^{2-}$ from the oxidation of SO_2. Finally, even the emissions of DMS (derived from phytoplankton activity) which lead to methanesulphonate (MS) and sulphate production after atmospheric oxidation processes, are higher in later spring-summer (Bates et al., 1992).

Also nitric acid can contribute to the chloride depletion. The photochemical processes leading to the formation and decomposition of HNO3 is very complex and the seasonal pattern of nitrate in the aerosol present different behaviour in remote and anthropic regions. In urban environment nitrate present maxima concentration in winter, conversely remote region present maxima in summer.

Based on the typical $[Na^+]/[Cl^-]$ mass ratio in sea water 1.81, and assuming that all the sodium determined by Ion Chromatography is from sea salt, the percentages of chloride depletion are calculated by the equation:

%Chloride depletion = (1.81* [ssNa+] – [Cl-])/(1.81*[ssNa+])*100

The mean level of chloride depletion percentage in the ten years covered by sampling is 39.03%, instead in later spring-summer this value increases and reaches the 50.16%.

To estimate the potential maximum contribution of each acidic species to chloride depletion the concentration of NO3- and nssSO42- was normalized by the amount of chloride replaced in each sample. Nitrate has been observed as the dominant anion compensating chloride depletion (Zhao et Ghao 2008, Anlauf at al. 2006, Keminen et al. 1997): as reported in Lee et al. 2007 we have estimated the contribution of nitrate to chloride loss assuming that nitrate react with soil derived particles after they react with ammonium (the fraction of ammonium after neutralized sulphate) and sea salt. Indeed, in order to test the impact of ammonium, we observed that the equivalent ratios of sulphate to ammonium were greater than unity in all samples (the arithmetic mean of the equivalent ratios is 2.75) indicating that there was no excess ammonium to neutralizing nitrate if ammonium and sulphate were present as (NH4)2SO4. Thus in this thesis the ratios of nitrate to chloride depletion were calculated without considering the impact of ammonium by the following equation in equivalents:

$$[NO_3^-]/[Cl^-]loss = [NO_3^-]/(1.18*[Na^+]-[Cl^-])$$

As expected the results show that nitrate accounted almost for the total chloride depletion for all samples (the [NO3-]/[Cl-] loss average percentage over all the sampling period is 96.56%). Indeed the equivalent

ratios of nitrate to replaced chloride were around unity, suggesting that the chloride loss was mainly compensated by nitrate.

However, as observed in previous studies (Zhao et Ghao 2008, Zhuang et al. 1999, Wu and Okada 1994) even the $nssSO_4^{2-}$ accumulation could cause chloride depletion in sea salt particles. This is particularly true at Lampedusa where sulphates PM10 content is characterized by highest values in summer when chloride depletion mainly occurs. In fact, as explained before and according to Lee et al. 2007, even if $nssSO_4^{2-}$ reacts with sea salt aerosol after neutralizing ammonium, since the complex nature of aerosol components that could be mixed is difficult to established which species between nitrate and sulphates are responsible for chloride depletion process. Moreover, the equivalent ratios of ammonium to $nssSO_4^{2-}$ are resulted to be near the unity (the average ratio is 0.99) but the median value is 0.59 confirming the complexity of the atmospheric acidity neutralizing process. Thus, if we considered the nss-sulphate after neutralizing ammonium we found that this anion accounts for 1.90-42.02% of chloride depletion. For this reason we analysed the size distribution of both nitrates and sulphates in comparison with the chloride one using the 8-stage impactor data. Indeed, as said in chapter 3 two sampling campaign with this instrument were accomplished during the spring-summer seasons of 2006 and 2008.

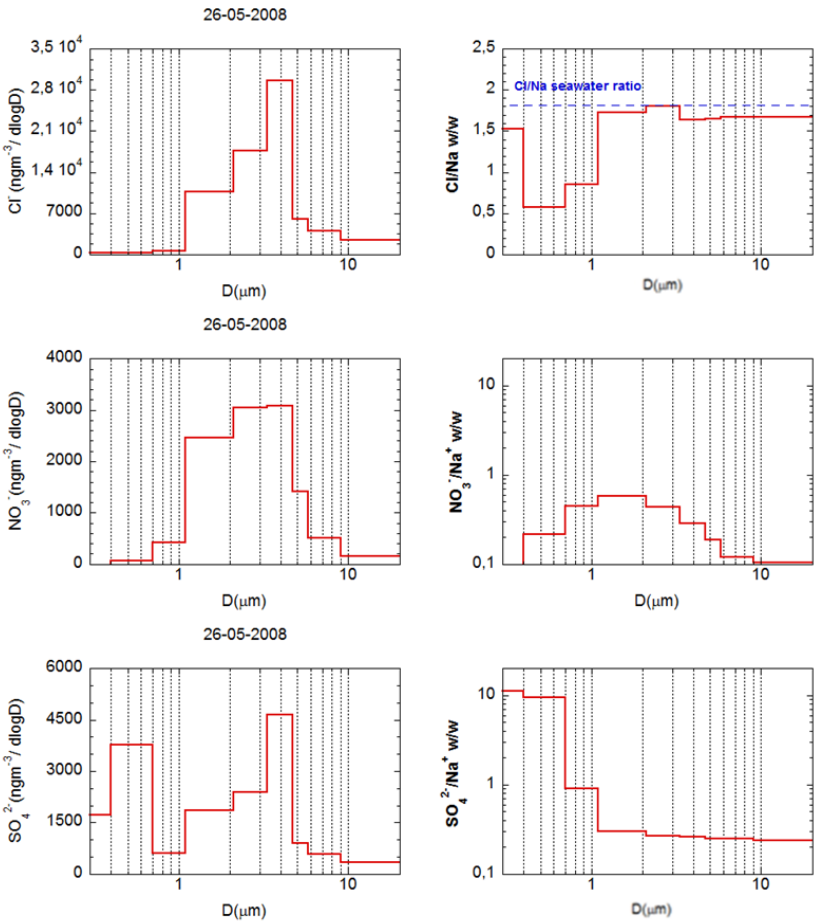

Figure 8.7- *Size distribution of Cl^- NO_3^- SO_4^{2-} and $[Cl^-/Na^+]$ $[NO_3^-/Na^+]$ $[SO_4^{2-}/Na^+]$ mass ratio in the SeaSA sampled on 26th May 2008.*

Figure 8.7 shows the size distribution of Cl^-, SO_4^{2-} and NO_3^- measured the 26th may 2008. Chloride ions are mainly distributed in the coarse mode (particles with AED ranging from 1 µm to 10 µm) with the highest content registered in the stages up to 5 µm. It has to be noticed that this distribution is quite similar to the NO_3^- one, that results distributed in the same size range confirming the relevance of this ion in chloride depletion processes.

Indeed, In fig. 8.7 is reported also the ratio between Cl^-, NO_3^- and SO_4^{2-} and Na^+ for each stage of the impactor is reported and it can be notice that in the range from 1 to 10 µm nitrate is the unique ion compensating the chloride loss. Instead sulphates are characterized by a bimodal behaviour with similar level content both in coarse, fine and in ultrafine range. It is known that the finest fraction of sulphates is constitute by secondary aerosol particles, in particular derived from biogenic and anthropic emissions: $nssSO_4^{2-}$ belong to these aerosols type (E. Vignati et al., 2009). In fact as it can see by SO_4^{2-}/Na ratio profile this fraction is the mainly responsible for chloride depletion occurred in the finest particles classes.

8.3. Fresh and aged sea salt aerosol

Since that SeaSA is originated from the sea surface, its chemical composition is very close to that of the sea water: the most ionic species present are Cl^- (55,0%), Na^+ (30,7%), SO_4^{2-} (7,7%), Mg^{2+} (3,6%), Ca^{2+} (1,2%), K^+ (1,1%), HCO_3^- (0,4%) e Br^- (0,2%). This composition can change due to acid-base exchange reactions that occur in the atmosphere causing the enrichment of sea salt particles in SO_4^{2-} and NO_3^- together with depleting Cl^- and Br^- content. As reported before, these processes gradually change the chemical composition of fresh sea-salt aerosols from a mixture of sulphates and chlorides to a mixture of sulphates and nitrates. Aged sea-salt particles are still quite soluble and potentially important as CCN, since both SO_4^{2-} and NO_3^- ions form soluble species with Ca^{2+} and Mg^{2+} within the aerosols (Table 7-6 in Warneck, 1988; Murphy et al., 1998a).

Thus, the newly sea salt particles formed from the wind stress on the sea surface have chemical composition and pH close to that of seawater; therefore even the ratios of the major seawater ions are preserved. Conversely, because of multiphase and heterogeneous reactions occurring in the atmosphere, the aged sea-salt aerosols are acidic, dechlorinated, and nitrate and sulphate enriched compared to fresh sea-salt aerosols. Meanwhile, during all these processes the amount of Na remains the same (Murphy et al., 1998a): so the sea salt aerosol "aging" can be detected from changes in the seawater ratios of the others ions respect to Na. For this reason in this study Na/Cl ratio will be used as an index of the aerosol "age".

Thus, using the experimental $[Cl^-]/[Na^+]$ mass ratio in the aerosol collected at Lampedusa we identified fresh and aged SeaSA. In order to characterize these two different types of sea salt particles the results obtained from the 8 - stage impactor data will be presented. In particular two days were selected on the basis of $[Cl^-]/[Na^+]$ mass ratio and of the relative chloride depletion percentage: 17th May 2005 as an example of fresh sea salt aerosol ($[Cl^-]/[Na^+]$ = 1.60, chloride depletion percentage = 11,67%) and 30th May 2005 as aged SeaSA type ($[Cl^-]/[Na^+]$ = 0.51, chloride depletion percentage = 71.47%).

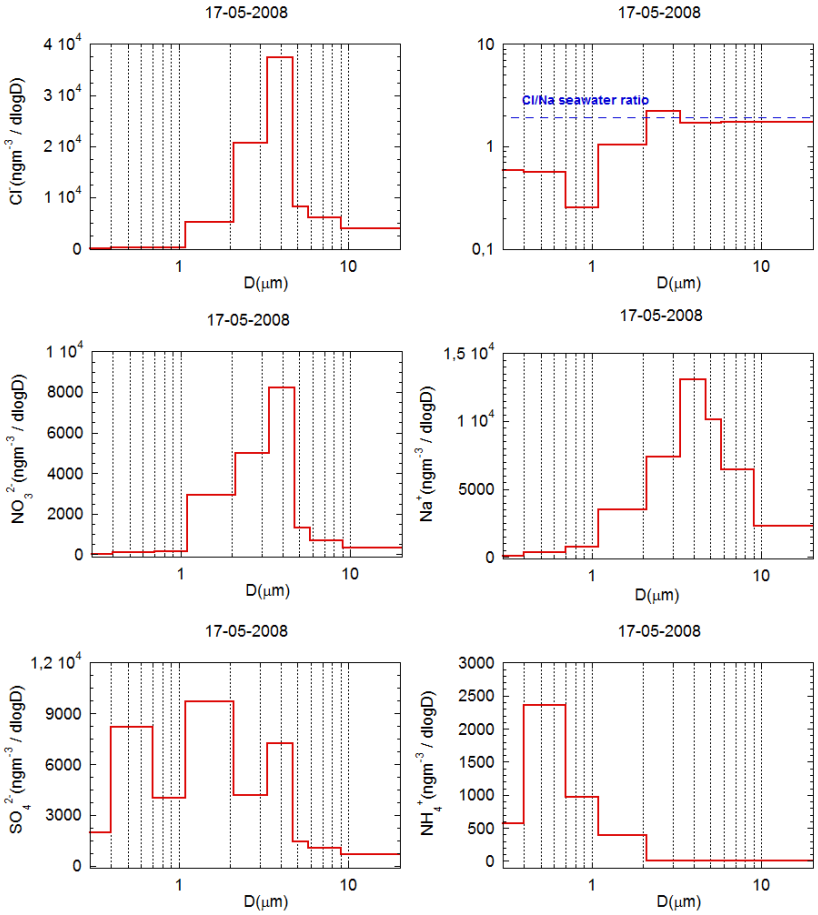

Figure 8.8 – *Size distribution of Cl^- Na^+ NO_3^- SO_4^{2-} NH_4^+ and [Cl^-/Na^+] mass ratio in the fresh SeaSA sampled on 17th May 2008.*

Figures 8.8 and 8.9 show the size distribution of the main SeaSA ionic compounds in those two days. As can be seen from the figure 8.8 fresh SeaSA is interested by chloride depletion processes only in the finest classes of particles and the main ionic species involved is sulphate.

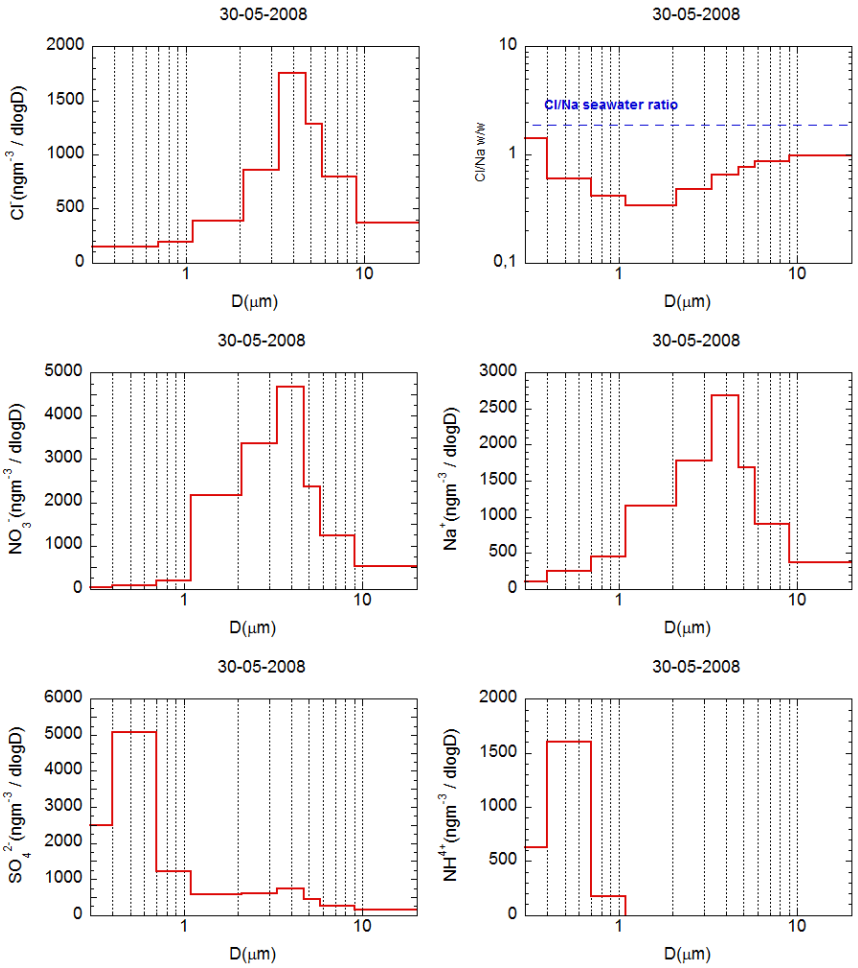

Figure 8.9 – *Size distribution of Cl^- Na^+ NO_3^- SO_4^{2-} NH_4^+ and [Cl^-/Na^+] mass ratio in the the aged SeaSA sampled on 30th May 2008.*

In particular it must be noticed how sulphates in fresh aerosol are characterized by a tri-modal size distribution while in the aged sample they are principally present in the finest size range (see fig. 8.9). This fact confirm that during aging processes H2SO4 belong to the fine fraction react with other species in the same size range (e.g NH_4^+), but react also

with the fraction of Cloride present in this fine size classes. Indeed, the CL/Na ratio is lower than theoric Na/Cl in sea water in these fine classes.

Also the size distribution of the aged aerosol type confirm this evidence, but in this case dechlorination occurs both in the coarse and finest fraction. Nitrate present higher concentration in the coarse fraction, for this reason it is the main responsible for dechlorination in the classes from 1 to 10 µm, instead sulphates, presenting maximum concentration in fine fraction are involved for dechlorination in the finest dimensional classes.

CHAPTER 9 – Ship emissions identification

Although the remoteness of this site, aerosol's anthropic sources are not negligible at Lampedusa. In particular emissions of heavy metals (such as Pb, V and Ni) from fossil fuel combustion are found to be relevant for this site as explained in chapter 5.5. It is known that for a marine remote site as Lampedusa, where population and industrialization are scarce, maritime traffic is the main source for this type of pollution. In this chapter results from an intensive PM10 sampling campaign, carried out from 1 June to 3 August 2013 at 12-hour resolution are reported with the aim of isolating the ship source (Becagli et al., 2016).

Indeed, ship emissions may significantly affect atmospheric concentrations of several important pollutants, especially in maritime and coastal areas (e.g. Endresen et al., 2003). Main emitted compounds from this source are carbon dioxide (CO2), nitrogen oxides (NOx), sulfur dioxide (SO2), carbon monoxide (CO), hydrocarbons, and primary and secondary particles. Thus, ship emissions impact the greenhouse gas budget (Stern, 2007), acid rain (through NOx and SO2 oxidation products; Derwent at al., 2005), human health (CO, hydrocarbons, particles; Lloyd's Register Engineering Services, 1995; Corbett et al., 2007) and solar radiation budget through aerosol direct and indirect effects (black carbon and sulfur containing particles; Devasthale et al., 2006; Lauer et al., 2007; Coakley and Walsh, 2002).

Heavy oil fuels used by ships contain varying transition metals originating from the fuel. The aerosol emitted by ship engines is formed at high temperature (>800°C) from V, Ni, Fe compounds (Sippula et al.,

2009). The thermodynamics predict that these species mainly form oxides, but when the flue gas dew point is reached, sulfuric acid (which was found to form a liquid layer on the ultra-fine particles) condenses on it leading to partial dissolution of the ultra-fine seeds, probably increasing the toxicity of the particles when inhaled.

Several studies have been carried out to determine the detailed chemical composition of shipping emissions (Agrawal et al., 2008a and b, Moldanová et al., 2009, Murphy et al., 2009, Lyyränen et al 1999, Cooper, 2003, Sippula et al. 2014); however, in comparison to on-road vehicles, the ships emissions are still poorly characterized.

In this context, studies performed at a remote Mediterranean site as Lampedusa, where it is possible to distinguish ship emission from other sources of heavy fuel oil combustion that are scarce, are important to investigate the current impact of the ship emissions on primary and secondary aerosols.

9.1. The ship emissions unambiguous identification

Vanadium and Nickel are markers for heavy fuels oil (HFO) combustion: in particular at Lampedusa their presence in the atmosphere is principally caused by maritime traffic (Becagli et al. 2012). In literature several authors assume 3.5 w/w V/Ni ratio as specific for ship emissions (Mazzei et al. 2008), conversely their characteristic ratio in the upper earth's crust is 2.06 w/w.

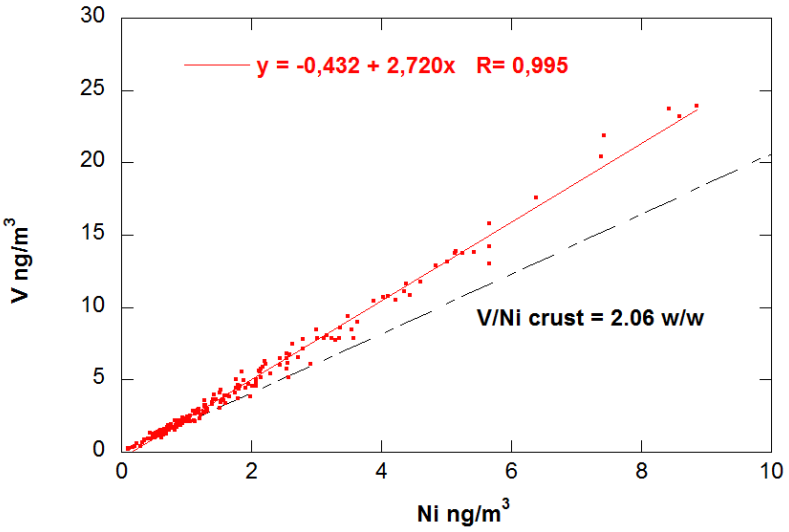

Figure 9.1 - *Correlation between the atmospheric concentration of V and Ni obtained by ICP-AES analysis after extraction with HNO_3 at pH 1.5 for the samples selected as no crustal event (< 75th percentile of crustal oxides content).*

Figure 9.1 shows the correlation between the atmospheric concentration of V and Ni obtained by ICP-AES analysis after extraction with HNO_3 pH 1.5 for the samples selected as no crustal event over all the 2013 (< 75th percentile of crustal oxides content). The very good correspondence between the two data set (R = 0.995) and the V/Ni experimental ratio (2.72 w/w) higher than the earth's crust ratio demonstrate the relevance of this anthropic source.

Moreover, as showed in tab. 5.1, the solubility percentage of these two metals at pH1.5 is very close to that reported by Becagli et al. 2012 for V and Ni from heavy oil combustion sources (about 80% and 70% for V and Ni respectively in the samples directly influences by ship emissions). The temporal evolution of V and Ni atmospheric concentration shows a

seasonal pattern with higher content in spring-summer both for the data obtained by ICP-AES analysis after weak and strong extraction method to those obtained by PIXE measurements (see Fig. 5.5). Indeed the marine boundary layer is generally more stable in summer than in winter (e.g., Dayan et al., 1989), and this effect may produce elevated concentrations of sulphate and metals during this season (Becagli et al. 2012). Moreover, since that seasonal changes in maritime traffic is primarily connected with touristic activities/passenger transport that are higher in spring summer, also the variability of the traffic ship may play a role in determining the observed annual cycle.

The ship source, however, could not be unequivocally separated from possible influences from refineries and power plants (which use similar fuels) through the V/Ni ratio. At this purpose, an intensive additional sampling campaign was carried out from 10th June to 31st August 2013 in the framework of the ChArMEx international project. For those aerosol samples the analysis is complemented with measurements of Rare Earth Elements (REEs), trajectories from a high resolution regional model, and actual observations of ship traffic. The combination of these approaches allows unambiguously identifying and providing constraints for the ship contribution to PM10 in the central Mediterranean (Becagli et al., 2016).

9.1.1. PM10 chemical composition during the intensive ChArMEx campaign in summer 2013

Before the evaluation of the ship emissions contribute to PM10 during the additional sampling campaign carried out in summer 2013 (in the

ChArMEx framework) also the impact of the others aerosol source was evaluated.

As described in chapter 5 in order to determine metals content two solubilisation method (the weak and the UNI EN 14902) were carried out on the filters before the ICP-AES measurements both for metals and REEs (see section 3.3). The sea salt aerosol (SeaSA) component of PM10 was estimated as the sum of the sea salt (ss) fractions of Na+, Mg2+, Ca2+, K+, sulfate and chloride. Details on this calculation are reported in chapter 8. The crustal component is calculated from Al, which represents 8.2% of the upper continental crust, UCC (Henderson and Henderson 2009). In this case measurements of the soluble Al concentration obtained by ICP-AES after the strong extraction procedure were used instead of the total Al content. Indeed, although this solubilisation procedure is not able to completely dissolve the silicate species, is able to recover at least 70% of the same analites measured by PIXE also for elements having dominant crustal source (see chapter 5). Therefore, the crustal contribution is underestimate by about 30%. However, it must be emphasized that the crustal aerosol contribution was very low throughout this additional campaign.

Figure 9.2 shows the time series of the main PM10 components in aerosol samples from 10th June to 31st July 2013.

It must be noticed that an intense Mistral event occurred from 22nd June to 1st July (for the characterization of Mistral events at Lampedusa see chapter 8.1). Thus, in those days elevated values of SeaSA and low concentrations of other compounds are found. Average concentrations of

PM10 and of the different aerosol components for the whole measurement campaign and for the non-Mistral conditions are reported in Table 9.1. The largest PM10 values were linked to elevated SeaSA during the Mistral event.

The PM10 measured during this campaign was significantly smaller than its long-term average at Lampedusa (27.6 μg/m3 as reported in chapter 6). No Saharan dust transport events occurred at low altitude in this period and the crustal aerosol contribution remained very low and almost constant (average < 1 μg/m3). SeaSA accounted for about 26% and during the periods non influenced by the Mistral its contribution was about 14%. Non-sea salt SO_4^{2-} was the most abundant among the secondary inorganic species.

During this intensive campaign also measurements of Elemental carbon (EC) and Organic Carbon (OC) on quartz filters were carried out by the use of a thermo-optical Analyser (for the analytical methodology see chapters 3.2 and 4.4).

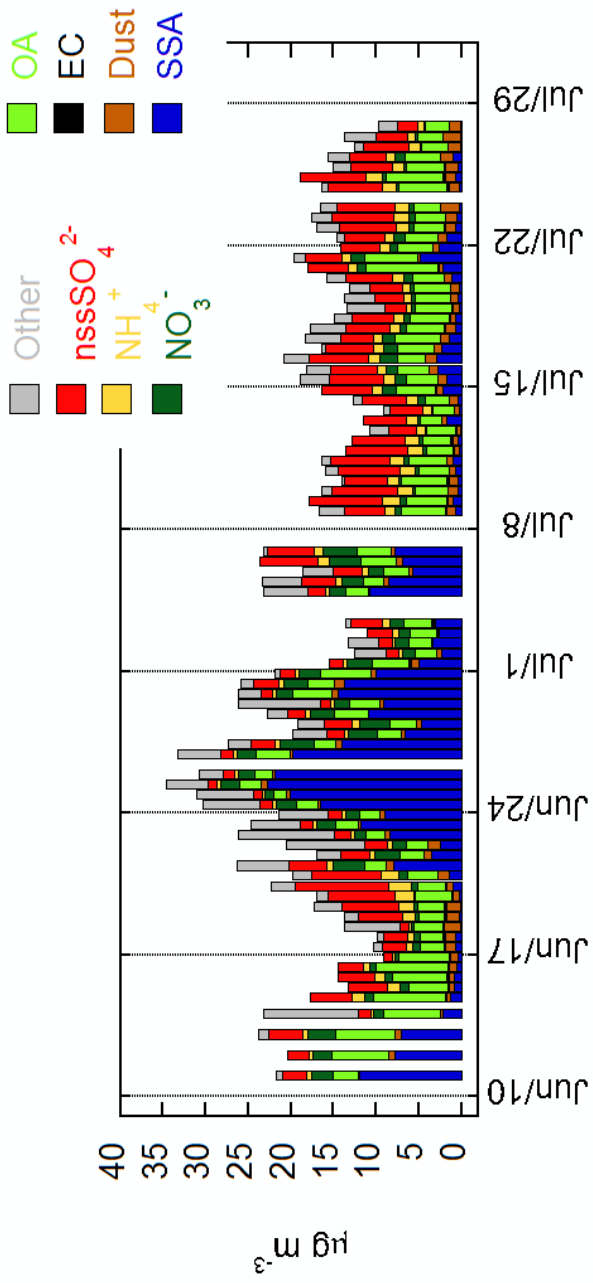

Figure 9.2 – *Time series of the main aerosol components at Lampedusa from 10th June to 31st July 2013.*

	All data	Mistral excluded
PM_{10} (µg/m^3)	18.0±6.6	16.3±5.2
Sea Salt Aerosol (µg/m^3)	4.63±6.30 (25.7%)	2.33±3.21 (14.3%)
Crustal Aerosol (µg/m^3)	0.82±0.44 (4.6%)	0.90±0.43 (5.5%)
nssSO_4^{2-} (µg/m^3)	3.95±2.28 (21.9%)	4.40±2.22 (27.0%)
NH_4^+ (µg/m^3)	0.98±0.56 (5.5%)	1.09±0.55 (6.7%)
NO_3^- (µg/m^3)	1.25±1.00 (7.0%)	1.02±0.02 (6.2%)
OA (µg/m^3)	3.86±1.56 (21.4%)	4.04±1.59 (24.8%)
EC (µg/m^3)	0.15±0.08 (0.8%)	0.15±0.08 (0.9%)
Unknown (µg/m^3)	2.52±3.26 (14.0%)	2.20±3.40 (13.5%)

Table 9.1 - *Mean PM10 load and composition with the related standard deviation and percentage with respect to PM10 (in bracket) at Lampedusa Mean, standard deviation and percentage are calculated the common sampling ("all data" columns) and excluding the mistral events ("Mistral excluded" columns).*

Regarding to EC and OC they show the behaviour typical of remote sites. Indeed from the plot of of OC versus EC reported in fig. 9.3 OC was not correlated with EC, indicating a strong impact of OC secondary and/or natural sources. Thus, we used a conversion factor of 2.1 (typical for remote sites characterized by high impact of secondary sources, Turpin and Lin, 2001) to estimate the total organic aerosol (OA) amount from

the measured values of OC. Once estimated OA with this method, the sum of the various species accounted to more than 85% of the measured mass. The unreconstructed mass could be due to an underestimation of OA from OC, or to the presence of bound water not removed by the desiccation procedure at 50% relative humidity (Tsyro, 2005; Canepari et al., 2013).

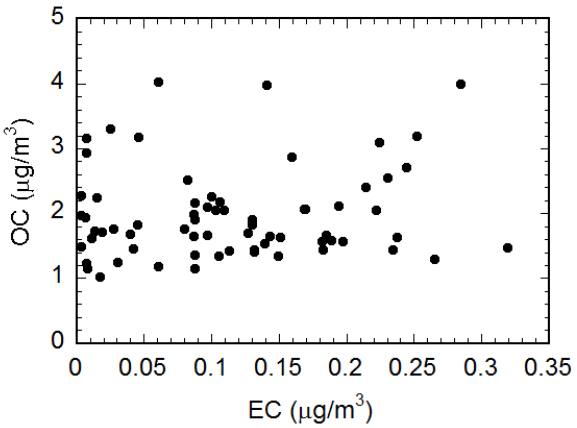

Figure 9.3 - *Scatter plot of OC vs. EC from 10th June to 31st July 2013.*

9.1.2. Ship emission markers: V, Ni and Rare Earth elements

As exposed before, several studies focused on the identification of specific tracers of shipping emissions (Viana et al., 2008; Becagli et al., 2012, Isakson et al., 2001, Hellebust et al., 2010) considered Vanadium and Nickel the best markers for this source since that after sulfur, they are the main impurities in heavy fuel oil (Agrawal et al., 2008a and b). Furthermore, as reported in Becagli 2012 the soluble fraction of these metals (i.e. that obtained after weak extraction procedure at pH 1.5) is even more representative for the ship source (see chapter 5.3) since that

the metals content such derived is not influenced by mineral dust. In the data set here considered the V_{sol} and Ni_{sol} ratio with respect to Al were always more than 10 times larger than for UCC, as expected for cases dominated by heavy oil combustions sources (ships, refineries, power plants, stainless steel production plants). Figure 9.4 shows the time series of the V soluble fraction and correlation parameters (as slope, correlation coefficient and number of samples) of the linear regression between V_{sol} and Ni_{sol} for the aerosol samples collected during the intensive ChArMEx campaign. As illustrated previously in section 9.1, even for those sample V_{sol} and Ni_{sol} are highly correlated, suggesting a common source. The obtained slope of the regression line (2.8-2.9, that increases to 3.0 for samples with V_{sol} >6 ng/m^3) is typical for heavy fuel oil combustion sources (3.5). The behaviour of V, Ni, and their ratio are then representative of heavy fuel oil combustion. As already said It is however difficult to distinguish V and Ni originating from power plants, refineries, or ship engines. Moreover, several refineries are present in Sicily (Siracusa, Gela, Milazzo) and in Sardinia (Cagliari) which may potentially influence the sampling sites. A combination of methods is thus used in this thesis to unequivocally identify the ship source. The analysis is based on: additional chemical tracers, like the Rare Earth Elements, whose behaviour is specific for the refinery and the ship sources; high resolution back-trajectories, based on data from the high resolution regional model; information on the vertical mixing in the atmospheric boundary layer; coincidences between the high resolution back-trajectories and the position of different types of ships in the Sicily Channel.

As regarding the additional chemical tracers of ship emissions rare earth elements content was investigated. Indeed, few studies propose the use of lanthanoid elements (La to Lu) to distinguish refinery from ship emissions (Moreno et al., 2008a and b; Du and Turner, 2015; Kulkarni et al., 2006). In particular, the ratio between the La and Ce concentrations and between La and V can be used to identify specific sources.

Ship emissions are characterised by values of La/Ce between 0.6 and 0.8 and La/V < 0.1 (Moreno et al., 2008a, 2008b). Conversely, crustal aerosols are characterized by La/Ce ranging from 0.4 to 0.6 and La/V usually in the range 0.2-0.3 (Moreno et al., 2008 a and b). The differences in dust source areas and collected aerosol fraction induce a scarce variability of La/Ce, but La/V exhibits a more large range of values reaching La/V=0.9 for the aerosol coarse fraction (>10 μm) arising from certain aereas of Sahara (Hoggar Massif) (Handerson and Handerson, 2009; Moreno et al., 2006; Castillo et al, 2008).

Elevated values of La/Ce (from 1 to 13) are associated with emissions from refineries (Moreno et al., 2008a; Du and Turner, 2015). This is because zeolitic fluidised-bed catalytic cracking (FCC) unit enriched in La are used to crack long-chain olefin in crude oil to shorter-chain product (Bozlaker et al., 2013; Du and Turner 2015; Kulkani et al 2006; Moreno et al., 2008a, 2008b). In this case the large variability of La/Ce is due to the mix of different aerosol sources having different La/Ce. The larger is La/Ce the larger is the impact of the source from refinery.

The time series of La/Ce and La/V at Lampedusa during this intensive campaign is displayed in figure 9.4. The range of values expected for

crustal aerosol are highlighted in the figure. La/Ce was generally around the value expected for crustal aerosol (dashed grey area in figure 9.4), but 10 samples show La/Ce values higher than 1 and for only one sample La/Ce is higher than >1.5. demonstrating that the impact of aerosol from refinery if present is low.

A previous study (Moreno et al., 2008b) has shown that it is possible to identify aerosol from refineries based on V, La, Ce three-component plot. This type of plot is shown in figure 9.5 for the data set obtained during the intensive campaign. La and Ce were scaled in order to have the typical UCC composition in the centre of the plot.

By comparison, the typical UCC composition and that of uncontaminated and La-contaminated (Refinery) Asian dust collected at Mauna Loa, Hawai'i by Olmez and Gordon (Olmez and Gordon, 1985) are also displayed in figure 9.5.

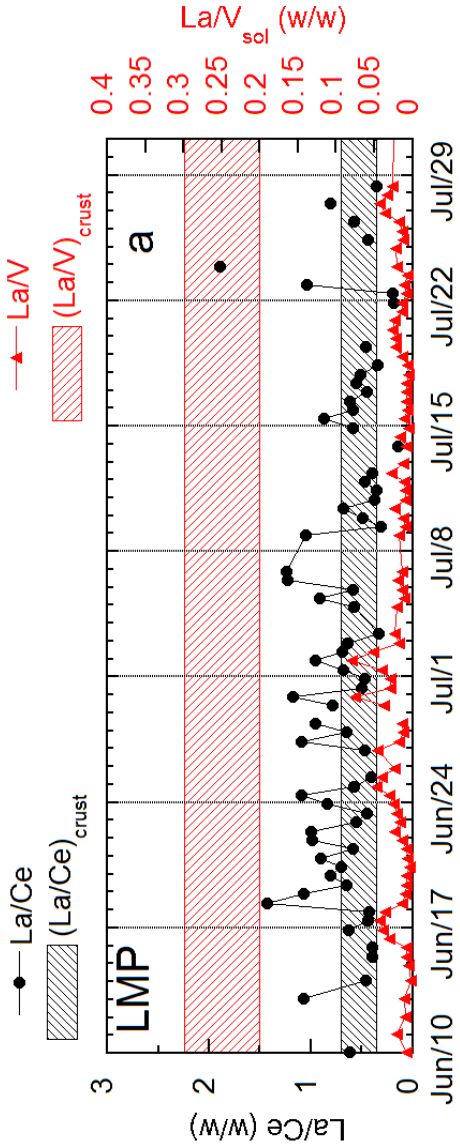

	Slope (± uncertainty)	R^2	n.
All data	2.94±0.03	0.986	124
V_{sol} > 6ng/m^3	2.99±0.03	0.994	44

Figure 9.4 - *Time series of La/Ce and La/V at Lampedusa. The horizontal red and grey shadow areas in each plot represent the ranges of values for upper continental crust of La/V ratio and La/Ce ratio, respectively. Correlation parameters between V and Ni in PM_{10} for all the samples and for samples with V concentration higher than 6 ng/m^3 are also reported.*

The data points from Lampedusa are grouped in a region with elevated values of V, and marked different amounts of La and Ce with respect to V, differently from UCC and refineries. The behaviour of the different chemical tracers support the conclusion that the V due to ship emissions is largely dominant in the PM_{10} measured at Lampedusa during the measurement campaign. Thus, cases with elevated V can be used to identify cases with a large contribution from the ship source.

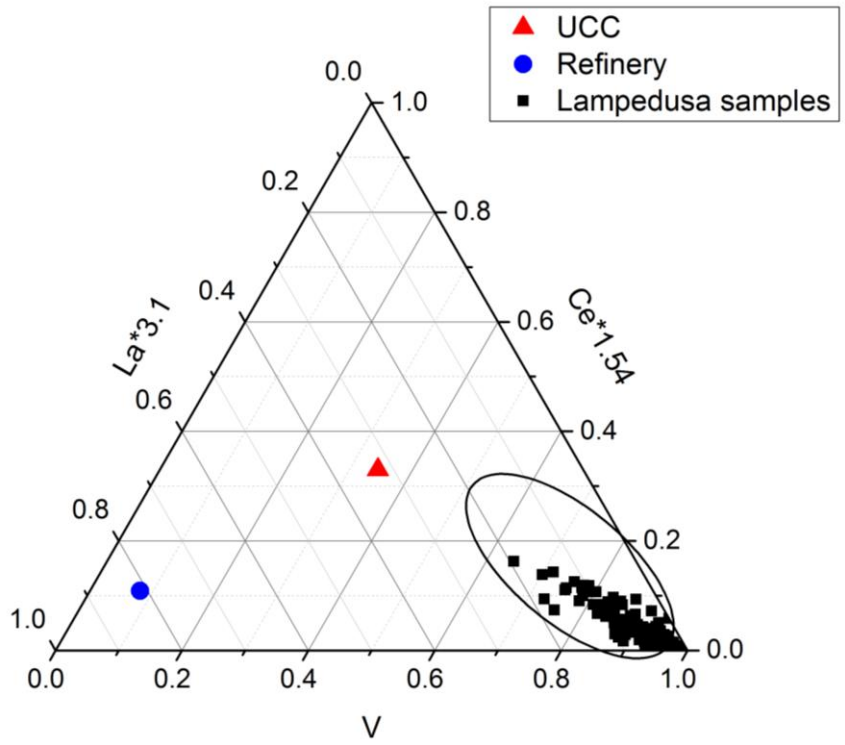

Figure 9.5- *Three-component Ce-La-V plots. The UCC composition is marked with a red triangle in the centre of the plots. The blue dot represents the composition of refinery-contaminated Asian dust (Olmez and Gordon, 1985). The black encircled area represents the ship emission composition.*

9.1.3. Trajectories and ship traffic

To further investigate the mechanisms determining the V enhancement at Lampedusa we examined the relationships among the amount of V, the back-trajectory pattern, the effective number of ships influencing the air mass, and the stability of the boundary layer in the ship source region (i.e., the Sicily Channel).

In order to characterize the meteorological conditions during the intensive campaign the Weather Research and Forecasting (WRF) model (Skamarock et al., 2008) outputs, provided by the Department of Physics of the University of Genoa, were used. In particular, the WRF 3-D hourly meteorological fields were used to perform a backward trajectory analysis with the NOAA HYbrid Single-Particle Lagrangian Integrated Trajectory Model (HYSPLIT; Stein et al. 2015), aimed at assessing the origin of air masses impacting the monitoring sites. Specifically, 48-h long back trajectories were computed from a reference height of 10 m above ground level, starting every six hours for the whole period of the campaign, from 10th June to 31st July 2013.

Figure 9.6 shows all the trajectories arriving at Lampedusa, calculated with the HYSPLIT model driven by the WRF meteorological fields, in an aggregated way where the trajectory frequency at each point of the computing grid is shown for the whole period (upper panel) and for the June 10th – June 30th interval (lower panel).

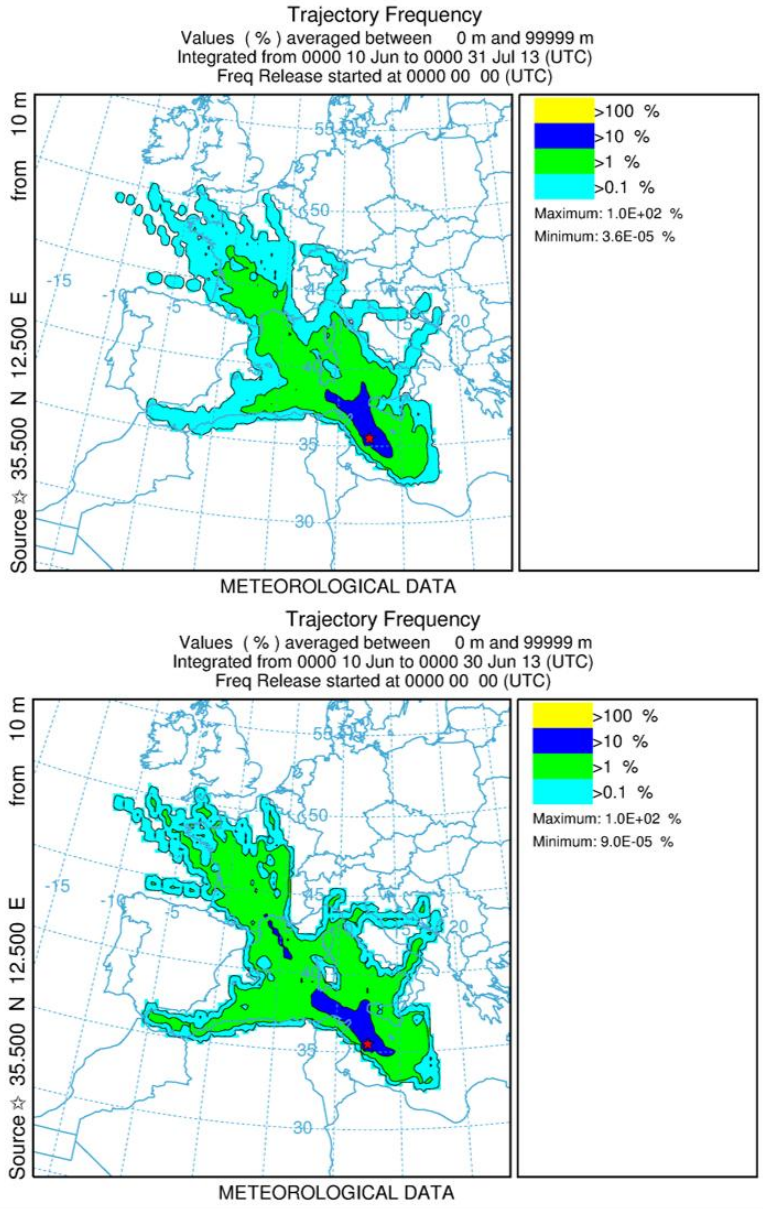

Figure 9.6- *Trajectory frequency computed at each grid cell with starting points at Lampedusa. Upper panel show values averaged over the whole period of the campaign (10th June – 31st July 2013), while lower panel is relative to the June 10th –June 30th interval.*

It can be seen that the trajectory frequency pattern is quite elongated in the NW-SE direction: the predominance of air masses coming from the northwest is particularly evident in June (lower panel), when areas with trajectory frequencies exceeding 10% are found farther to the north, up to the Gulf of Lion. During the first part of the campaign (June 2013), indeed, the synoptic situation was characterized by a “dipolar” sea level pressure anomaly pattern, with positive anomalies in the western Mediterranean and negative ones in the eastern part of the basin (Denjean et al., 2016). This situation induced stronger and more frequent than usual north-westerly winds (i.e. Mistral episodes, see chapter 8) over the Sardinia and Sicily Channels.

Furthermore, the position and the main characteristics of the ships travelling in the central Mediterranean were derived from the Marine Traffic database (http://www.marinetraffic.com/), which provides the position of the ships with a high temporal resolution (about 3-5 minutes) by means of the Automatic Identification System (AIS). Three classes of ships defined by the AIS classification were considered: all the ships, the merchant (i.e. cargo and tanker), and the fishing vessels. The merchant and fishing vessels are the most frequent ships in Sicily Channel and the former are expected to produce the highest impact on the V concentration due to their higher emissions).

In this analysis all back-trajectories arriving at Lampedusa were considered and all trajectory-ship coincidences occurring within the last 36 hours before sampling were taken into account. In particular it was assumed that the ship plume influenced the sampled air mass if the

trajectory passed at less than 15 km from the position of the ship and together the altitude of the air mass was lower than 500 m. The total number of ships satisfying these criteria was associated to each trajectory. The analysis was based on the available 1-hour time resolution meteorological fields (a ship influencing a trajectory was counted once every hour).

The atmospheric stability is also expected to play a large role in modulating the V amounts (Becagli et al. 2012). A temperature inversion, TI index, was calculated based on the 3D atmospheric fields from the WRF model at three sites in the Sicily Channel. The temperature inversions have been used as a proxy to identify the periods characterized by a stable boundary layer. The three sites, A (37.2°N, 11.5°E), B (37.0°N, 12.4°E), and C (36.3°N, 13.3°E), were selected in the regions of most frequent ship passage and crossing with the trajectories from Lampedusa. The TI index was calculated as the difference between the temperature at the altitude of the maximum T, and the surface T (for this reason it is indicated as dT in figure 9.7). A positive TI indicates an inversion, and the TI value provides an indication of the intensity of the inversion. Only positive values are considered in this analysis. Figure 9.7 summarizes the results of this analysis taking into account ship traffic, atmospheric stability and V atmospheric content. In fact It shows the times series of the number of the ships influencing the trajectories arriving at Lampedusa and the corresponding measured values of V. Results are shown for the three classes of ships. The TI intensity is also shown as dT.

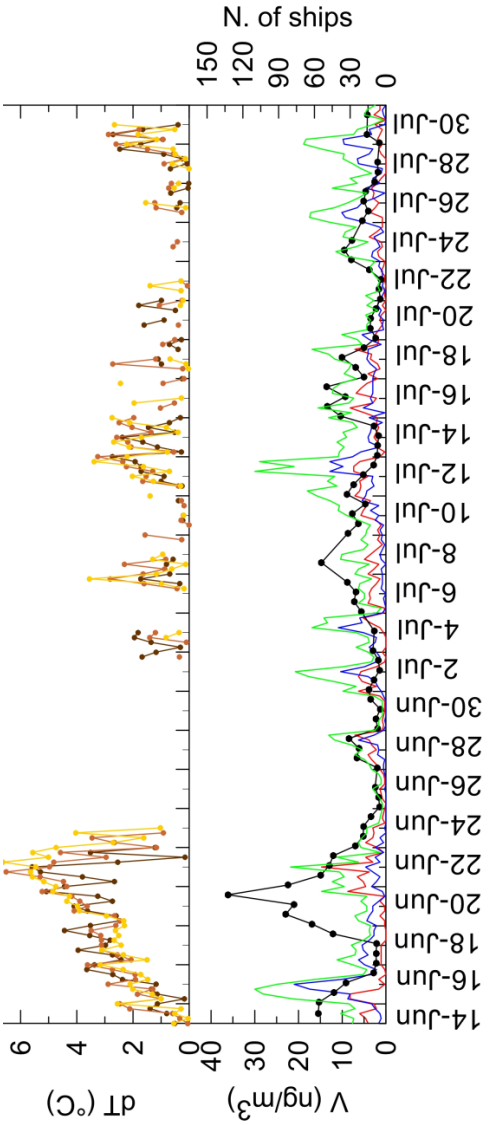

Figure 9.7 - *Time series of Vanadium content (black line with dots) and number of ships affecting the air masses sampled at Lampedusa. Green, red and blue lines indicate respectively the total number of ships, the number of merchant and of fishing vessels. The time evolution of the temperature inversion index (dT in the figure) at three different locations in the Sicily Channels is shown: brown, red, and yellow curves correspond to sites A, B, and C (see text).*

In general, there is a rather good correspondence between the measured values of V and the number of ships encountered along the associated air mass trajectory.

The analysis of the event with elevated V concentration registered between 18th and 21st June, provides further information to understand the link between the ship traffic and measured V concentration. Maxima of V in this event was measured on 21st June (36.1 ng/m3) and this episode resulted to be the largest occurred at Lampedusa during the intensive campaign both for duration and V concentration. Though, especially at the beginning of the event, large values of V do not correspond with an increase of the number of ships along the air mass trajectories. A possible explanation for this behaviour is provided by the temporal evolution of TI in the Sicily Channel. The temperature inversion started to develop on 14 June, and gradually increased in intensity until 22 June; the TI persistence and progressive increase in intensity provided suitable conditions for the trapping of the ship plumes in the boundary layer, with a consequent build-up of the ship aerosol and V concentration. A similar combined dependency on number of ships and TI appears also at Lampedusa around 7 July. Moreover, it is interesting to note that V seems to depend more directly on the number of merchant ships (see, e.g., the lack of V peaks on 17 June, 12 and 29 July, when the number of fishing vessels was high and the number of merchant ships was low) than on the total or the fishing ships.

Thus, the trajectory analysis carried out in combination with the available information on the ship tracks confirms that the ship emissions

are the main responsible for the moderate and elevated values of V measured at this site during the campaign. This analysis also clearly suggests that the boundary layer structure plays a very important role in determining the impact produced by the emissions. This simplified approach confirms the importance to carefully characterize the emission scenario and the meteorological conditions in studies on the impact of ships emissions on the air quality.

9.2. Sulphates, nitrates and organic carbon from ships

SO_2 is one of the main species emitted in the ship plume in the gas phase (Agrawal et al., 2008a, b). SO_2 is produced through oxidation of the S contained as impurity in heavy fuel oil, and is an aerosol precursor. A previous study performed at Lampedusa over 5 years (Becagli et al., 2012) showed that the behaviour of non-sea salt sulfate is not directly correlated with V and Ni because several other SO_4^{2-} sources (anthropic, marine biogenic, crustal, volcanic) contribute to the non-sea salt sulfate in the Central Mediterranean Sea. The same study suggests a lower limit of about 200 for the $nssSO_4^{2-}/V$ ratio for particles originating from heavy oil combustion at Lampedusa. Figure 9.8 shows $nssSO_4^{2-}/V$ versus V at Lampedusa for the samples collected from 10th June to 31st July 2013: it must be noticed that $nssSO_4^{2-}/V$ decreases for increasing V and reaches a lower limit of about 200 at elevated values of V (> 15 ng/m^3). We assume that the ship emission is the dominant source of the sampled particles for these cases with elevated V. This implies that in these cases virtually all sulphate originated from the ship source, and the observed lower limit for $nssSO_4^{2-}/V$ can be considered the lower limit for the sulphate to V

ratio in the ship plume. We use a value of 200 in this work as a rough estimate of the sulphate to V ratio, based on the values obtained in the previous study and confirmed by the data set used in this study.

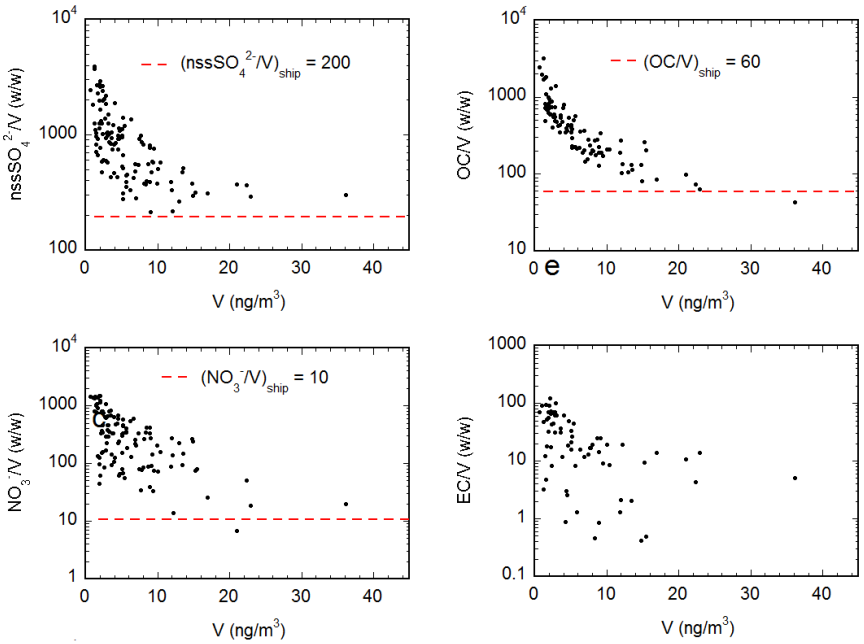

Figure 9.8 - *Scatter plots of $nssSO_4^{2-}/V$ (a and b), NO_3^-/V (c and d), OC/V (e and f) and EC/V (g and h) vs. V concentration at LMP (plots on the left) and CGR (plots on the right) sites. The dashed lines in the plot represent lower limits for the characteristic ratio in the ship plume.*

NOx are among the main compounds emitted in gas phase acting as aerosol precursors. The photochemistry of NO_x leading to NO_3^- formation in the particulate phase is complex, especially in summer due to the presence of high amounts of OH radical (see e.g., Chen et al., 2005), and the NOx contribution to the particulate phase is not easy to be quantified. Here we try to use the same approach used for sulphate for

the determination of a lower limit for the NO_3^-/V ratio in the ship plume. Figure 9.8 shows the NO_3^-/V ratio versus V at Lampedusa: similarly to sulphates, the NO_3^-/V ratio tends to a lower limit value (around 10 for V higher than 15 ng/m^3). The NOx concentration is about two times larger than that of SO_2 in the ship plume close to the source (Agrawal et al 2008b) and lifetime of NOx is extremely low (1.8 hour during day and 6.5 hour during night, Chen et al., 2005). However, the NO_3^-/V limit ratio values is low compared to the limit ratio for SO_4^{2-}. It has to be considered that NO_3^- takes part in other photochemical atmospheric reactions that lead to its removal. Besides, the presence of HNO_3 in gas phase not neutralized by NH_3 or by sea salt could explain the low NO_3^-/nssSO_4^{2-} ratio in the aerosol. Indeed, the NO_3^- concentration measured at Lampedusa is 4 times lower than that of nssSO_4^{2-} (table 9.2). Low amount of NO_3^- with respect to SO_4^{2-} from ship emissions are found in model simulations in Southern California (Dabdub, 2008). Indeed, Dabdub (2008) shows that the contribution to aerosol from ship emissions is 0.05% for NO_3^-, and 44% for SO_4^{2-}.

Elemental and Organic Carbon are also present in the ship plume (Shah et al., 2004). In particular, OC constitutes about 15-25% and EC is generally lower than 1% of the PM sampled at the plume of main ship engine powered by heavy fuel oil (Agrawal et al., 2008b). Figure 7.9 shows EC/V and OC/V versus V at Lampedusa: similarly to sulphate and nitrate, OC/V decreases with increasing V and appears to reach a minimum value for V > 15 ng/m^3. Thus, we assume that the OC/V value obtained at Lampedusa for V>15 ng/m^3 is representative of cases

dominated by ship emissions, and this ratio is used to estimate the OC contribution due to ships at this site. The pattern of the ratio EC/V versus V is less clear; in particular, several very low values of EC/V appear also at small values of V. This result is unexpected because V and EC are both markers of the primary ship aerosol, but the data here presented seem to suggest that non negligible EC contributions from other sources were present, or that different fractionating effects acted during the transport.

9.3. Contribution of the ship aerosol to PM_{10}

With all the limitations above described, by using the lower limits for the ratios ($nssSO_4^{2-}/V$), (NO_3^-/V), and (OC/V) representative for ship aerosol it is possible to estimate the minimum contribution of $nssSO_4^{2-}$, NO_3^- and OC emitted by ships to the total budget of these component, and also to the total PM_{10} mass.

	$nssSO_4^{2-}$ ($nssSO_4^{2-}/V)_{min}$=200	**NO_3^-** ($NO_3^-/V)_{min}$=10	**OA** $(OC/V)_{min}$=40	**PM_{10}**
Average contribution µg/m³ (%)	1.3 (33%)	0.065 (4.5%)	0.55 (14%)	1.9 (11%)
Maximum contribution µg/m³ (%)	7.2 (66%)	0.36 (50%)	3.0 (92%)	10.6 (48%)

Table 9.2 - *Estimated minimum ratio of nssSO42-, NO3-, OA with respect to V, minimum contribution of each species from ship emissions averaged over the considered time period and for the cases with highest ship impact of nssSO42-, NO3, OA and PM10.*

The minimum ratio of each specie with respect to V, the minimum estimated contribution of ship emissions, for the average amount and for

the maxima, to the total concentration of these species and to PM_{10}, are reported in Table 9.2. As previously discussed, the measured OC contribution is multiplied by 2.1 to obtain the total organic aerosol contribution.

At Lampedusa, the estimated minimum concentration of non-sea-salt sulphate from ship emissions was 1.3 μg/m^3, on average during this campaign. Marmer and Langmann (2005) estimate that ship emissions contribute by 50% to the total amount of $nssSO_4^{2-}$ in the Mediterranean.

This value is larger than the one we derive (about 30%); however, our data show that in cases with largest ship impact the $nssSO_4^{2-}$ from ship contributes at least by 66% to the total $nssSO_4^{2-}$.

Ships appear to contribute by small fractions to the total budget of NO_3^-. As previously mentioned, the atmospheric chemistry of NO_3^- is complex and the contribution of nitrate from ship emission could be highly variable especially in the Mediterranean region where high amount of UV radiation and highly reactive radical species are present.

Organic aerosol from ships also contributes significantly to the total OA amount and to the total PM; in particular, at Lampedusa at least about 92% of the total OA may be attributed to the ship source in the case with maximum ship impact.

By summing these three contributions, it is possible to estimate the total aerosol mass due to ship emissions, and its contribution to the total mass of PM_{10}. The lower limit for the ship contribution was 1.9 μg/m^3 corresponding to 11% of PM_{10} at this site. In cases with maximum ship impact, the estimated lower limit for the ship contribution was between

40% and 48% of the total PM_{10}. It must be notice that these percentages refer to the summer season, when the ship contribution in the Mediterranean region is higher.

CHAPTER 10 - Characterization of PM10 sources from PMF analysis

In this chapter, the source apportionment based on the application of the Positive Matrix Factorization (PMF) model is applied to a 2-year long data set of PM_{10} mass concentration and chemical composition obtained during 2007 and 2008 sampling campaigns at Lampedusa. This statistical analysis was performed in collaboration with the Florence section of INFN (National Institute of Nuclear Physics) and complete the experimental work presented in this thesis confirming the aerosol sources identification given in previous chapters.

The Positive Matrix Factorization (PMF) is a receptor model allowing the determination of the chemical profiles of the aerosol sources affecting the receptor site and the estimation of their contributions to the aerosol load, using as input data the atmospheric concentrations of different chemical species (Calzolai et al., 2015). With more detail, PMF model may be written as $X=G \cdot F+E$, where X is the n x m matrix of the m measured chemical species in n samples and G and F are factor matrices to be determined: G is the n x p matrix of source contributions to the samples; F is the p x m matrix of factor composition (source profiles); E is the residual matrix.

Input data were handled according to (Polissar et al., 1998): measured data were weighted with their analytical uncertainty increased by one third of the detection limit (DL); data below the DL were substituted with a value corresponding to DL/2, and a DL*5/6 uncertainty was associated

to them. Missing data were handled filling the gaps with the geometric mean value calculated over the days with data and associating to them a 400% uncertainty.

Mass concentration was put in the PMF analysis as a variable, with very high (400%) uncertainty (Norris et al., 2009), as it is suggested when significant portions of the mass (not directly correlated with the other input variables) are not measured/available: in our case, no data on the carbonaceous fraction, which is known to be a major component of the aerosol, is available for the whole considered period.

The PMF model was applied to the data set of mass concentration and chemical composition relative to the 562 samples collected in the years 2007-2008, considering 21 chemical species as measured by either PIXE (Mg, Al, Si, K, Ca, Ti, Mn, Fe, Cu, Br, Sr), ICP-AES (V_{sol}, Ni_{sol}) or IC (Na^+, NH_4^-, Cl^-, NO_3^-, SO_4^{2-}, Oxalates, Glycolate, MSA). The soluble fraction of V and Ni (V_{sol}, Ni_{sol}) was used instead of their total fraction due to the lower DLs of ICP-AES compared to PIXE, and because, as already illustrated in chapter 9, it is a more representative marker for anthropogenic sources.

Briefly, the analysis allowed the identification of 7 different sources which are identified as sea-salt, mineral dust, biogenic emission aerosol, secondary nitrate particles, secondary sulphate particles, primary particulate ship emissions, and combustion emission aerosol (see the following sections).

Profiles of the seven sources identified are reported in Figure 10.1: the left y-axis displays the fraction of the elemental mass concentration, reported in the graph as blue column, whereas the right y-axis refers to

the explained variation of each element, depicted as red squares (the contribution of one element in all the profiles sum up to one, when the variation of the element is completely reconstructed by the model). The evolution of the daily contribution of each identified source is shown in Figure 10.2.

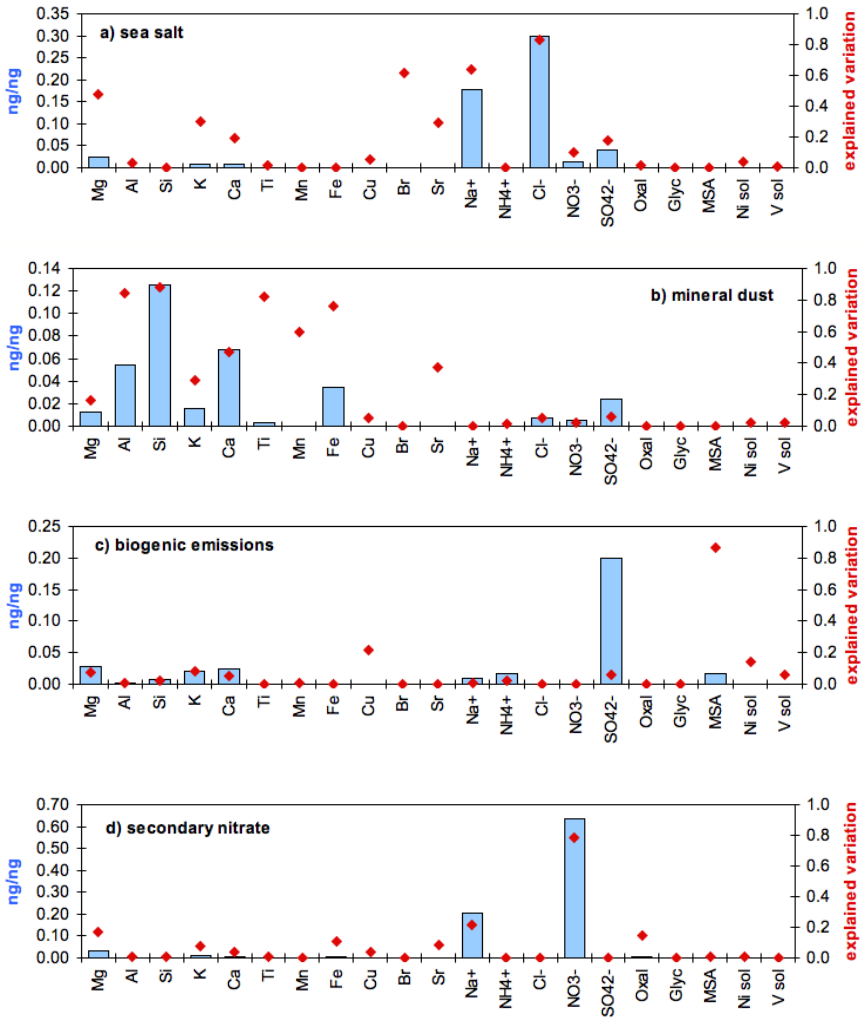

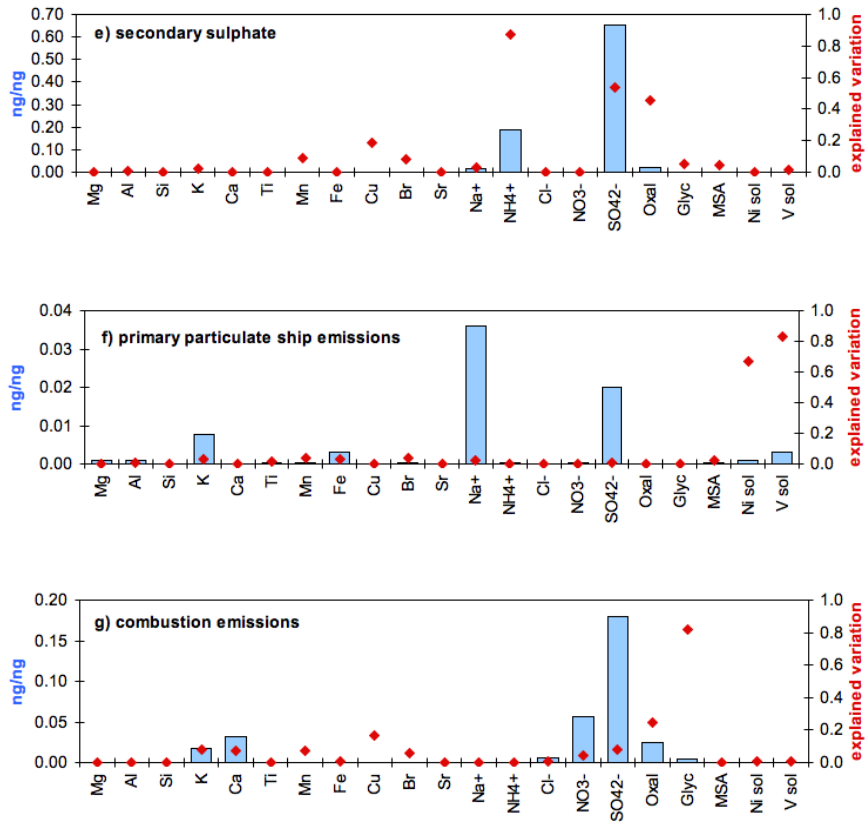

Figure 10.1 - *Profiles (fraction of the elemental mass concentration, blue columns) and explained variations (red squares, referring to the right y-axis) of the identified PM10 sources.*

Figure 10.2 - *Temporal evolution of the PM_{10} contributions from the identified sources.*

The seven aerosol sources identified by the PMF analysis are described in the following sections.

10.1. Sea Salt

Na^+, Cl^-, Mg, K and Br are the characterizing elements for this factor (figure 10.1, panel a); most of their mass concentration is explained by this source (explained variations: 64%, 83%, 48%, 30% and 61%

respectively). Some SO_4^{2-} is also present. The elemental ratios are in good agreement with those measured in marine water, suggesting a common marine origin for the species characterizing this factor. More in detail, the source profile elemental ratios are reported in Table 1 together with the sea salt literature elemental ratio (Henderson and Henderson, 2009). Thus, this factor of the PMF is identified with the primary marine aerosol, sea salt aerosol.

As for the SeaSA profile obtained as the sum of the main marine ionic components over all the ten years covered by sampling (see fig. 8.2), the temporal evolution shows no clear seasonality. As already said in chapter 8 this evidence is largely expected for this source, since that sea-salt aerosol is strongly related to wind intensity.

10.2. Mineral Dust

Several crustal elements such as Al, Si, Ti, Mn, Fe, Sr, Ca, K an Mg characterize this factor (figure 10.1, panel b). This source reconstructs almost completely the mass concentration of some of these elements, such as Al, Si and Ti (more than 80% of their signal).

Enrichment factors (EF) with respect to Al in this profile were calculated using the average Earth's soil composition reported by (Mason, 1966). The values of these EFs, all near to 1 (with a moderate enrichment only for Ca and Sr which is usually associated with Ca in carbonates), strengthen the identification of this source as "mineral dust". The temporal evolution of this factor shows no clear seasonality, being dominated by many narrow peaks. Sixty-hour backward trajectories ending at Lampedusa at 50 m a.s.l. corresponding to the start, middle,

and end time of the sampling interval were calculated for the peaks in PM_{10} concentrations due to mineral dust larger than the 95° percentile (about 32 µg/m^3), using the NOAA Air Resource Laboratory HYSPLIT transport model (see chapter 7).

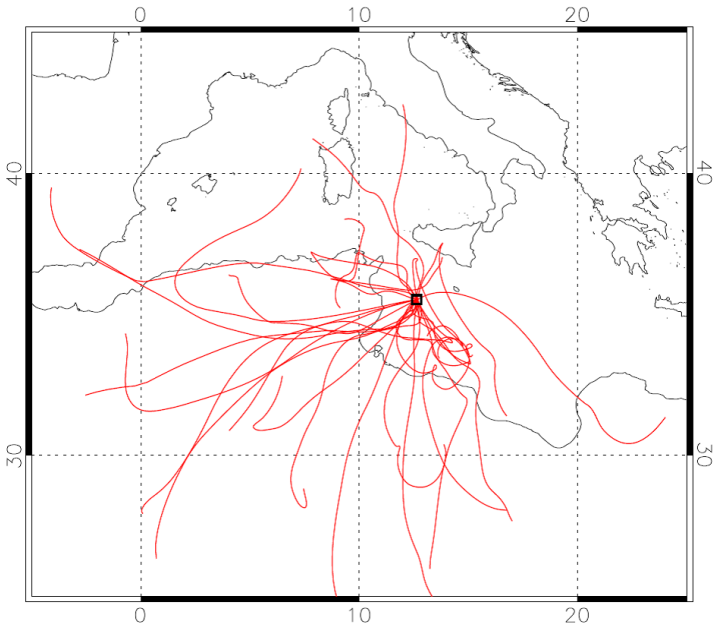

Figure 10.3 - *HYSPLIT backward trajectories ending at Lampedusa at 50 m a.s.l. corresponding to the peaks in the PM_{10} contributions due to mineral dust source (see text for the details).*

The analysis showed that in about 86% of the cases at least one of the three trajectories associated to the sampling overpassed Northern Africa (see Figure 10.3). It has to be notice that the mineral dust temporal pattern obtained by PMF on the 2007-2008 data set did not display a seasonal trend in agreement with results already showed in chapter 7 about the seasonality of Saharan dust input. Indeed, since that African

desert dust transports often occur above the boundary layer (mainly in summer), despite the strong seasonality observed for the aerosol optical depth, at the ground level no evident seasonal trend was observed for PM_{10} or crustal markers content.

10.3. Biogenic emissions

This factor is mainly characterized by MSA (Methanesulfonic Acid), and explains almost completely (87%) its mass concentration. A small percentage (6%) of the total mass of SO_4^{2-} is also accounted by this source, and constitutes however the prevalent absolute mass contribution to this factor. Indeed, as already said in chapter 8 MSA is used as a tracer for biogenic sulphur emissions (from phytoplankton processes), as it is solely produced by oxidation of dimethylsulfide (DMS). The strong seasonality observed for this factor, with minima during winter and maxima in summer, is also supporting its attribution to the biogenic emissions source (see fig. 10.1 panel c). A recent study investigated the role of biogenic aerosols in the PM at Lampedusa (Becagli et al., 2013) with respect to the phytoplancton productivity, suggesting that the seasonal evolution of methanesulfonate, with a very evident summer maximum, is mainly driven by phytoplankton physiology and cell stress factors, such as high irradiance and shallow depth of the marine upper mixed layer.

10.4. Secondary nitrate

This factor is characterized by NO_3^- and Na^+, with the mass concentration of NO_3^- being explained almost for the 80% by it. This result confirm the

interpretation of the atmospheric acidic neutralizing processes illustrated in chapter 8. Indeed even in this data set the ionic balance for this source is neutral, when taking into account NO_3^- and the two cations Na^+ and Mg^+, as in a marine environment the neutralization of HNO_3 can occur to a large extent on sea-salt components as also resulted from previous studies (Bardouki et al., 2003; Metzger et al., 2006).

The temporal evolution shows a small seasonality, with somewhat larger values during summer (see fig. 10.1 panel d). A similar seasonal behaviour was observed by (Querol et al., 2009) in Eastern Mediterranean Basin (EMB) sites. The same study evidenced that in the EMB nitrate is mainly present in the coarse mode, chemically bound to alkaline ion species, while in the Western Mediterranean Basin (WMB) it is largely in the fine mode, as it is most frequently present as ammonium nitrate. As well demonstrated in chapter 8 in Lampedusa, as in the EMB, the observed seasonality appears to be mainly regulated by the combination of nitrates with sea-salt cations (Metzger et al., 2006).

10.5. Secondary sulphate

NH_4^+, SO_4^{2-}, and Oxalates are the characterizing elements for this source, with most of their signals explained by this factor (explained variations are 87%, 54%, and 45%, respectively). The major absolute contribution to the profile is given by SO_4^{2-}; the SO_4^{2-}/NH_4^+ ratio of 3.4 indicates that both the compounds $(NH_4)HSO_4$ and $(NH_4)_2SO_4$ are present. The temporal evolution shows maxima during summer, when the marine boundary layer is more stable and the photochemistry leading to the production of secondary aerosols is enhanced (see fig. 10.1 panel e). The

same behaviour was observed by (Querol et al., 2009) for sulphate both at Eastern and Western Mediterranean sites. Further, it is worthy to note that sulphate neutralization with NH_4^+ may leave very low amounts of NH_3 available for the neutralization of nitrate, which thus occurs favourably on sea-salt aerosol confirming what was showed in chapter 8 (see also section 10.4).

10.6. Primary particulate ship emissions

This factor explains most of the mass of V_{sol} and Ni_{sol}, even if the predominant mass contributions are from Na^+ and SO_4^{2-}. The V_{sol}/Ni_{sol} ratio for this source is 3.40, in good agreement with the aforementioned literature and experimental data (see chapter 9). Moreover, the interpretation of this factor as "primary ship emissions" is strengthened by the fact that the observed SO_4^{2-}/V_{sol} ratio (6.2 w/w; as V has been found to have a 80% solubility in ships exhausts, such value corresponds to a SO_4^{2-}/V ratio of 5.0) is of the same order of magnitude as the ones reported by (Agrawal et al., 2008) for the particulate matter freshly emitted from the main engine of an ocean going container vessel (SO_4^{2-}/V ranging from 8.9 to 11.9 depending on the engine operating conditions for the considered vessel). Much higher SO_4^{2-}/V values are reported when secondary aerosols (mainly SO_4^{2-}) are formed from the oxidation of the gaseous precursors (e.g., SO_2) (Becagli et al., 2012).

A clear seasonal evolution, with maxima during summer, is evident for this source (see fig. 10.1 panel f); this is in agreement with the temporal evolution of ship emissions markers (Ni_{sol}, V_{sol}, $nssSO_4^{2-}$) observed in previous chapter of this thesis. As explained, this temporal evolution is

due to three possible causes: a) an increased photochemical activity in summer leading to a faster production of secondary aerosols; b) a stronger stability of the marine boundary layer during summer, leading to an increase of their concentrations at the ground level; c) prevalent winds from the Strait of Sicily (one of the main ship paths) during summer. Due to the primary origin of this factor, such seasonal behaviour appears to be more probably linked to the two latter phenomena.

10.7. Combustion emissions

Several compounds, as K, Cu, NO3-, SO42- and short carboxilic acids as Oxalates and Glycolates, whose signal is mostly explained by this source, characterize this factor. K and SO42- are commonly associated with biomass burning, and short carboxilic acids have been recently associated with coal/waste/biomass burning (Wang et al., 2007). Enhancements of Cu in the aerosol produced by wood combustion have also been reported by several studies (Dall'Osto et al., 2013). Therefore this factor has been interpreted as a generic combustion source, which includes biomass burning. The temporal evolution (fig. 10.1 panel g) of this factor shows no clear seasonality, even if important contributions during summer may be observed and may be linked to the more frequent occurrence of fires in the Mediterranean region. During spring and autumn the contributions from this source are generally low, while several high contribution days may be observed during winter.

Figure 10.4 shows the combined evolution of the desert dust and combustion emissions contributions to PM_{10}, and some selected cases with airmass trajectories and satellite observations of active fires. Most

of the winter cases characterized by elevated contributions of combustion sources display also a high contribution from the mineral dust source (see Figure 10.4).

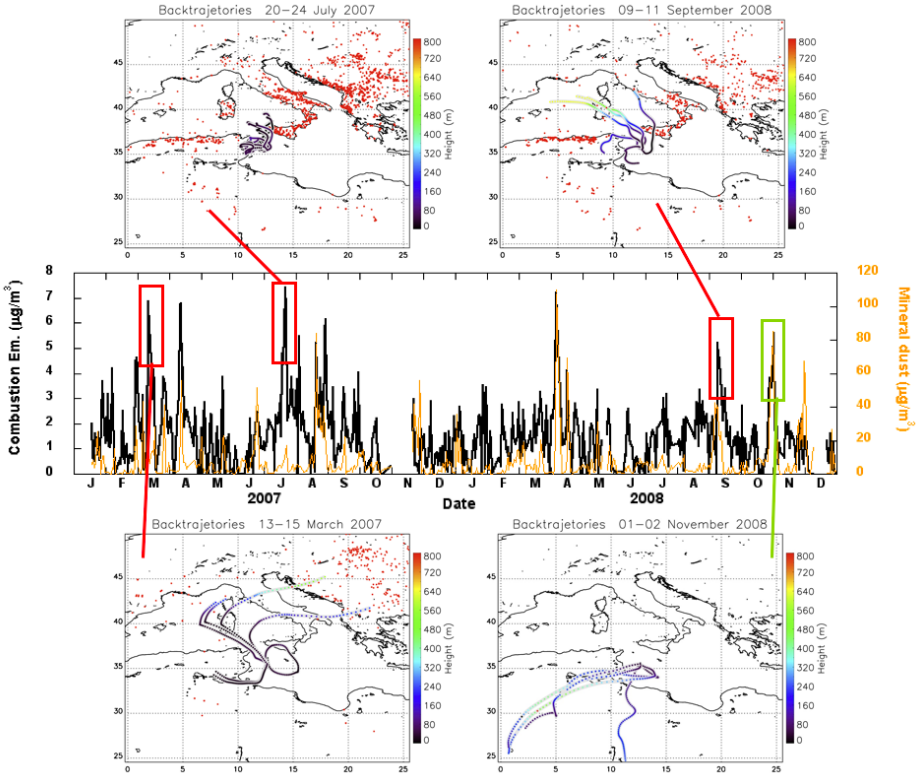

Figure 10.4 - *Temporal evolution of the "combustion emissions" and "mineral dust" sources; examples of trajectories from fires are evidenced in red, together with an example of advection from the Saharan region (green).*

The analysis of the backtrajectories shows that these days were mostly interested by African dust advection episodes. Several studies report that dust particles plumes from the Saharan area also export biomass-burning particles (Tesche et al., 2011; Rodriguez et al., 2011), mainly during the dry winter season. Further, small fires, often occurring in biomes as

croplands, wooded savannas and tropical forests, are usually below the detection limit of the current generation of surface reflectance/thermal imagery instruments (Randerson et al., 2012). Therefore, winter contributions from this source are likely to be mainly due to small scale biomass burning activity in north Africa; nonetheless, some winter peaks of this source appear also connected with fires and/or biomass burning activity in Central-Eastern Europe (e.g., 13-15/3/2007, Figure 10.4).

Summer peaks have been clearly connected by backtrajectory analysis to fires mainly in South Italy and Sicily, thus supporting the interpretation of this factor as a combustion source, with a main contribution from biomass burning.

As previously reported, additional data on the carbonaceous fractions in PM_{10} are available for limited periods in the years 2007-2008. In particular, samplings of PM_{10} on quartz filters for EC/OC analysis were performed from 15 May to 13 August 2007 with integration times ranging from 24 to 72 h. The starting time of the sampling was set in the morning/early-afternoon (between 8 am and 2 pm) due to manual filter change operations. In Figure 10.5, the EC and OC contents are plotted together with the estimates of the contributions from the combustion emission source as obtained by PMF.

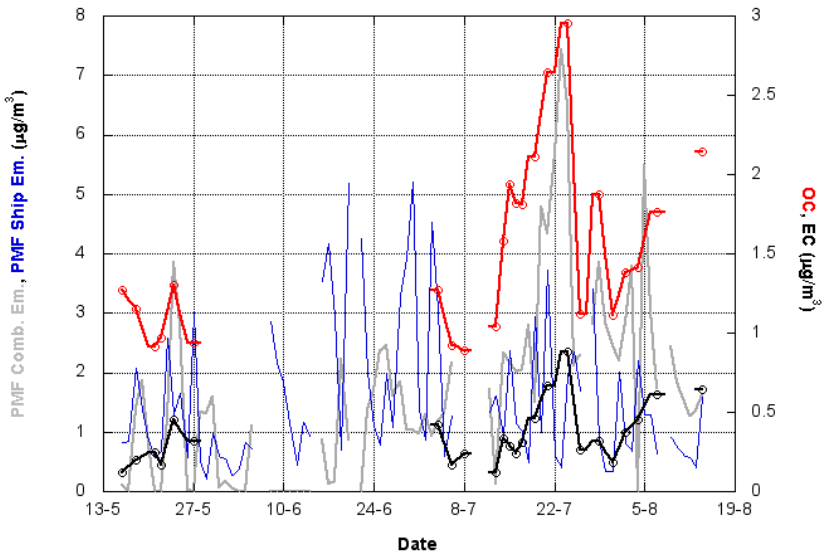

Figure 10.5 - *Comparison between EC and OC data and PMF estimates of the contributions of combustion emissions and primary particulate ship emissions in the period of EC/OC data availability. Results for EC and OC are reported with solid lines, black and red, respectively, referring to the secondary axis (empty rounds report the single sample result attributing it to the central sampling day).*

EC and OC are produced in combustion processes of both fossil fuels and biomasses, while OC may have also a biogenic origin. Therefore, EC and, to a smaller extent, OC are good markers of combustion sources, while additional information from other chemical tracers (such as K, levoglucosan, glycolates or radiocarbon (Bernardoni et al., 2013)) is needed for the assessment of the burnt fuel (biomass or fossil). As shown in Figure 10.5, EC and OC are highly correlated with the combustion emission contribution estimated by the PMF, thus strengthening the attribution of the seventh PMF factor to a combustion source. Small discrepancies, as the one occurring at the beginning of July, may be

attributed to episodic important contributions to EC and OC from heavy oil combustion, that is from the primary particulate ship emission source, also reported in figure 10.5.

10.8. PM10 source apportionment

Figures 10.6 and 10.7 report the relative and absolute seasonal contributions of the seven identified sources (winter – December, January, February; spring – March, April, May; summer – June, July, August; fall – September, October, November). During all the seasons, natural sources (seas-salt, mineral dust, and biogenic emissions) give the largest contribution to PM_{10}, accounting for a minimum of 62% in spring to a maximum of 76% during fall. The maximum relative and absolute contribution of sea-salt is observed in winter, while relative contributions during the other seasons are comparable. This is consistent with a higher wind velocity during the winter months (7.4 m/s, versus 5.6 m/s in summer, 6.5 m/s in spring, and 6.1 m/s in fall during 2007 and 2008). The mineral dust maximum relative contribution is found during fall (37%), and is around 20% in the other seasons. As expected, the maximum relative contribution of biogenic emissions is during summer, and is negligible in winter. Among the anthropogenic sources, primary particulate ship emissions and secondary sulphate display a clear and similar seasonality, with maxima in summer. No significant dependence on the season is observed for the relative contributions of secondary nitrate and combustion emissions. It is worth to note that the not explained mass is around 10% across the seasons.

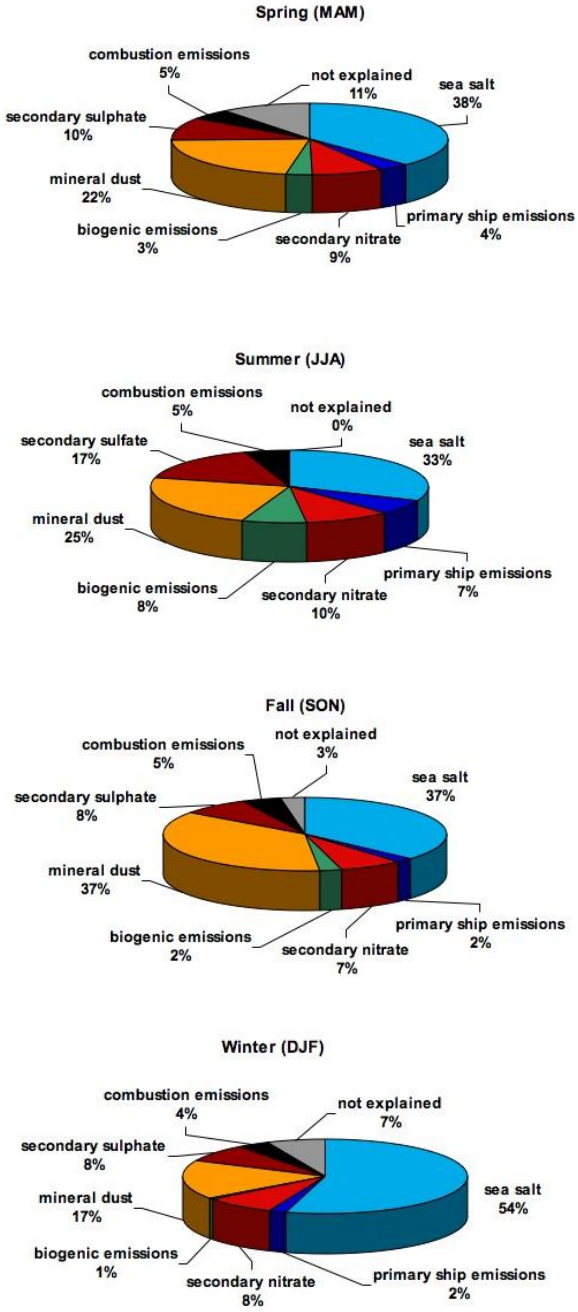

Figure 10.6 - *Seasonal relative contributions to PM_{10} concentration (average over the years 2007-2008).*

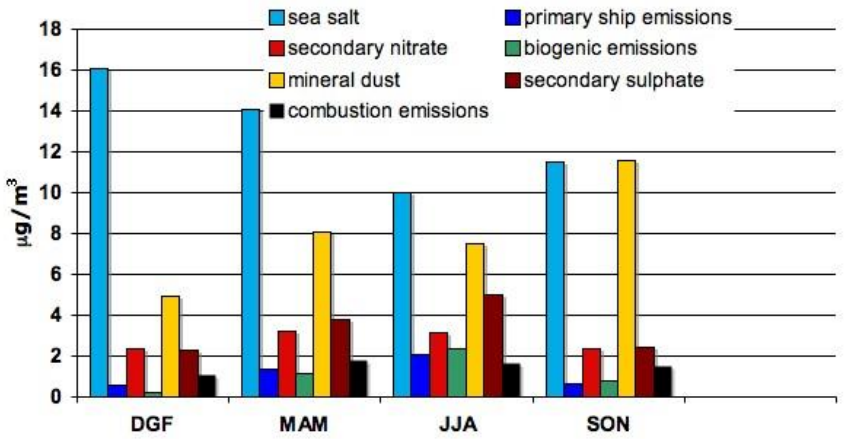

Figure 10.7 - *Seasonal absolute contributions to PM10 concentration (average over the years 2007-2008).*

The annual average relative contributions are reported with their uncertainties in Figure 10.8: the main contribution to aerosol comes from sea-salt, accounting for 40% of the mass; the second contribution is from mineral dust (25%). Taking into account also of the biogenic emissions, accounting for 4% of the mass, the contribution of natural sources to the PM_{10} in Lampedusa is estimated to be around 68% on average. As concerns secondary nitrates and sulphates, they are estimated to contribute by 9% and 11% to the total PM_{10}, respectively. Finally, primary particulate ship emissions have been observed to give an average 4% contribution, while 5% of PM_{10} was found to be due to combustion emissions. Uncertainties on the contributions were estimated propagating the uncertainties obtained by the PMF model on the G matrix. In absolute terms, the following contributions were estimated: sea-salt, 12.9 ± 1.1 µg/m^3; mineral dust, 7.8 ± 0.5 µg/m^3; biogenic emissions, 1.1 ± 0.2 µg/m^3; secondary nitrate, 2.8 ± 0.3 µg/m^3; secondary

sulphate, 3.4 ± 0.4 μg/m^3; primary particulate ship emissions, 1.2 ± 0.2 μg/m^3; combustion emissions, 1.5 ± 0.3 μg/m^3 (Calzolai et al., 2015).

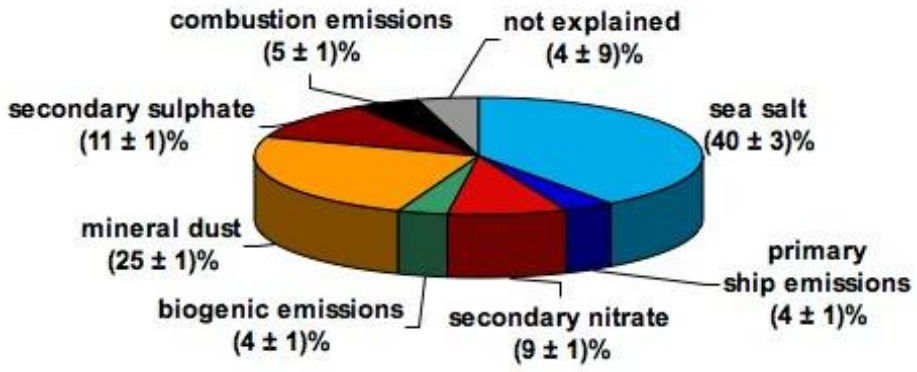

Figure 10.8 - *Relative annual contributions to the PM10 concentration (average over the years 2007-2008).*

The PMF estimates of the contributions from sea-salt and mineral dust were compared with those obtained from the same dataset assuming the average composition of seawater and Earth's soil as reported in chapter 7 and 8. More in detail, sea-salt concentration (i.e. [sea-salt]) was evaluated, for every day, according to the expression:

[sea-salt] = [Cl-] + [ssNa+] + [ssCa] + [ssMg] + [ssK] + [ssSO42-]

and the contribution of mineral dust ([mineral dust]) was calculated as sum of the metal oxides:

[mineral dust] = 1.35 [nssNa+] + 1.66 [nssMg] + 1.89 [Al] + 2.14 [Si] + 1.21 [nssK] + 1.40 [nssCa] + 1.67 [Ti] + 1.43 [Fe]

The mineral dust estimate from the PMF analysis is about 30% higher than the crustal content calculated as the metal oxides sum. It must be pointed out that information on carbonates is lacking, and that the used analytical techniques are not sensitive to the Oxygen content, thus the estimated metal oxide mass is based on the assumption of an oxygen fraction according to the prevalent oxides of the crustal elements. Nevertheless, PMF may slightly overestimate the source contribution as a consequence of some profile interferences: in this case, the PMF retrieval associated a small amount of SO_4^{2-} and Cl^- to the crustal dust profile, probably due to their co-linearity in case of long-range transport episodes.

Coming to sea-salt, the stoichiometric approach gives an estimate of the average contribution of 8.3 µg/m3, to be compared with the PMF estimated contribution for the sea-salt source of 12.9 µg/m3. Since all the sea-salt elements are measured, this discrepancy is likely to be due to other compounds not visible with the applied analytical techniques, such as water or, to a lesser extent, organic compounds. In fact, although gravimetric measurements are performed in a controlled atmosphere (50% relative humidity, 25°C), some water may endure and it is likely to be bound to hygroscopic aerosol components such as sea-salt. Therefore, taking into account for water, the PMF contribution from the sea-salt source may be possibly split in two contributions, namely “dry sea-salt” and “H_2O”, accounting for about 26% and 14% of the PM10 mass in Lampedusa, respectively.

Conclusions

In this thesis chemical composition of PM10 sampled at daily resolution on the Island of Lampedusa (35.5°N, 12.6° E) over a ten years' period (from 2004 to 2014) was presented. In particular, PM10 ionic content was obtained by Ion chromatography analysis whereas metal content evaluation was carried out by the use of two different analytical techniques: ICP-AES and PIXE. Finally carbonaceous fraction (EC-OC and TC) was determined by a thermo-optical Analyser.

Saharan dust inputs, Sea Salt aerosols and anthropic emissions from maritime traffic at Lampedusa were identified and characterized both from the PM10 chemical composition and from others parameters as aerosol optical properties, backward trajectories and meteorological data. Moreover studies on the solubility and the sizing of the main components of these aerosol sources were presented.

1. Comparison between PIXE and ICP-AES results

The use of both PIXE and ICP-AES technique allowed to compare two different extraction methods: a "weaker" one, able to determine the metal fraction available to the ecosystems, and a "stronger" according to the EN14902 methodology. This experimental work aimed to find correlation between the metal solubility and the aerosol sources: the obtained results were pointed out below.

- As expected the efficiency of the extraction resulted to be strongly dependent on the aerosol sources: metals emitted by anthropic sources were found to be more soluble (because of their chemical speciation and their occurrence in the finest particle fraction);

conversely crustal markers such as Fe and Al showed lower solubility since they are strongly linked to the silica matrix.

- Both the weaker and the stronger extraction methods showed a very high reproducibility. Moreover the EN14902 method revealed to have an efficiency extraction percentage of about 70% even for Al which is the main crustal marker and more resilient to chemical digestion. This evidence is particularly interesting and has a potential for addressing further analytical work due to the complexity of the instrumentation required for the total metal content determination.

2. Atmospheric aerosol load determination

The daily aerosol load at Lampedusa was obtained by the gravimetric method and some important considerations about the PM10 content in the considered data set are here summarized.

- The mean PM10 content over all the sampling period was 27.6 μg/m3. This value revealed to be in agreement with the increasing PM gradient from the NW to the SE of the Mediterranean Basin reported in literature.
- In spite of the remoteness of this site, on the whole dataset 147 days (corresponding to 6.8% of the total number of the data) exceeding the daily threshold value established by the European Commission for PM (50 μg/m3, European Community, EC/30/1999) were identified. Many of those exceedances were caused by strong natural aerosol input as Saharan dust or sea spray events.

3. Saharan dust aerosol identification and characterization

- Saharan dust content was calculated as the sum of the main crustal oxides (Al, Si, Fe, Ti and non-sea-salt Ca, Na, Mg, K) where PIXE measurements were available (2007-2008): in that data set crustal content accounted for the 18% of the total PM10 mass (the mean crustal oxides content was 5.42 μg m^{-3} but could reach 67.9 μg m^{-3} during a strong Saharan dust event).
- In order to extend the evaluation of the crustal content to the whole data set another marker for this source was identified: in particular elevated Saharan dust events are identified from the non-sea-salt Ca (nssCa) concentration determined by ion chromatography (nssCa presented a strong correlation with crustal aerosol content determined as the sum of the metal oxides).
- Some considerations about Saharan dust and PM10 content seasonality were highlighted by comparison between the aerosol chemical composition measured at ground level and on the entire air column. Indeed, desert dust column burden identified from optical properties displayed an evident annual cycle, with a strong summer maximum; conversely, the crustal aerosol amount contribution to PM_{10} and the percentage of Saharan dust events at ground level did not show any evident seasonal pattern. This experimental result was explained through the study of the behaviour of both the boundary layer on the sea surface and on the Sahara desert during the year's seasons. Indeed in summer Saharan dust transport occurs above the

marine boundary layer, and no significant mixing between inside and above the boundary layer takes place.

- Backward trajectories arriving at 50 m a.g.l. were analyzed in connection with the dust chemical composition to identify possible differences in the properties of the dust source areas. Two main areas were identified, corresponding to the Tunisia-Algeria region, and to Libya (transport from these regions takes place mainly in winter, when low altitude transport occurs). Dust from the two source areas identified presented Ca/Al and Mg/Al ratios higher than for the mean upper crust composition. This fact is due to the presence of carbonate and palygorskite (a Mg-bearing clay mineral) in areas with higher carbonate contents in North Africa region.
- Although Ca/Al and especially (Ca+Mg)/Fe ratios presented a large variability, they displayed a somewhat different behaviour in the two sources. Indeed, the retrieved median value of Ca/Al and (Ca+Mg)/Fe were 2.5±1.0 and 4.7±2.0, respectively, for dust aerosol arising from Tunisia-Algeria; they were 1.9±0.7 and 3.3±1.1 (Ca/Al and (Ca+Mg)/Fe, respectively) for Libyan dust.

4. Sea Salt aerosol evaluation

The sea salt aerosol (SeaSA) fraction was calculated as the sum of the main components of sea water content: sea-salt Na^+, $ssMg^{2+}$, $ssCa^{2+}$, ssK^+, $ssSO_4^{2-}$ and chloride. As expected, this aerosol source was found to be the most important at Lampedusa.

- In the ten year data set presented, the SeaSA average contribution percentage to PM10 and the mean level of sea spray content were

27.53% and 7.38 μg/m^3 respectively (these values are in consistent with those founded in others sites of the Mediterranean Basin). Furthermore, it must be noticed that the daily SeaSA content in this data set could reach the level of 42.74 μg/m^3 (up to the 70% of PM10 content) during an intense sea spray event.

- Since that SeaSA production mainly depends on wind speed (Kisha et al., 2012), the SeaSA temporal trend and the occurrence of strong marine aerosol inputs did not show a seasonal trend.
- In this data set, several days interested by sea spray input of very high intensity were found during the occurrence of Mistral winds. In particular, two events of this type recorded on the 25th and 26th June 2013 were identified and characterized both from the aerosol chemical composition and from backward trajectories analysis.
- It is known that, once emitted in the atmosphere, sea salt particles undergoes into several reactions that change their original composition from a mixture of sulphates and chlorides to a mixture of sulphates and nitrates. These processes caused changes in the deliquescence point and optical properties of the aerosol particles and may also have affected atmospheric acidic deposition. Thus, chloride depletion, that is the most relevant of these processes at Lampedusa, was studied. Indeed, chloride depletion was found to be not negligible at Lampedusa even though it is a marine remote site: its mean level percentage over all the ten years covered by sampling was 39.03%. Furthermore the [Cl^-/Na^+] mass ratio temporal variation showed a marked seasonal trend indicating that this process

principally occurred in later spring-summer (in this period the mean chloride depletion percentage was 50.16%). This evidence can be ascribed mainly to the higher atmospheric acidity that is found at this site during later spring-summer with respect to the others periods of the year.

- To estimate the potential maximum contribution of each acidic species to chloride depletion, the concentration of NO_3^- and $nssSO_4^{2-}$ was studied. In particular their size distributions were used to understand the role played by both these two species in these types of processes. The interesting evidence is that in the range from 1 to 10 μm, nitrate is the only ion compensating the chloride loss, beside sulphates are the mainly responsible for chloride depletion occurred in the finest particle classes.

5. Ship emissions identification

The contribution of the ship emissions to PM_{10} at Lampedusa was evaluated from the results obtained by an intensive campaign carried out in summer 2013 in the framework of the Chemistry and Aerosol Mediterranean Experiment (ChArMEx). The identification of aerosol originating from ships was based on an integrated analysis of chemical analyses, calculations of backward trajectories using a high resolution regional model, and on tracking of ship traffic in the Mediterranean through the Automatic Identification System. Results are summarized as follows.

- Moderate and elevated values of V and Ni in the aerosol were unambiguously associated with the ship source. In particular this

attribution was based on the V to Ni ratio which corresponded to what expected for heavy fuel oil combustion; low amounts of La and Ce with respect to V, and La/Ce ratio similar to those in the UCC, which allowed to exclude power plants or refineries as sources significantly contributing to the observed aerosol; coincidences between air mass trajectories and travelling ships.

- In addition to travelling ships, also the planetary boundary layer vertical structure was found to play an important role in determining the dispersion of aerosols from the ship source. Indeed, temperature inversions appeared to be associated with large amounts of ship emissions tracers, suggesting that they favoured the build-up of aerosol concentration in the lowest atmospheric layers.
- Merchant ships (cargo and tankers) appeared to produce a larger impact on the measured aerosol than fishing vessels.
- By using lower limits for the ratios $nssSO_4^{2-}/V$, NO_3^-/V, and OC/V identifying the ship-dominated emission cases, the lower limits to the contribution of the ship source to $nssSO_4^{2-}$, NO_3^-, OA, and to PM_{10} were estimated. In particular ship emissions contributed by at least 30% to the total amount of sulfate, by at least 4-7% to the total amount of NO_3^-, and by at least 8-14% to the total amount of organic aerosol. All these contributions correspond at least to 11% of PM_{10} at Lampedusa. In cases with largest ship impact, ships contributed up to 12 $\mu g/m^3$ to PM_{10}, and by about 48% of PM_{10}.

6. Application of the PMF analysis to the PM10 content and its chemical composition at Lampedusa

Finally the application of a statistical model (The Positive Matrix Factorization - PMF) to 2-year long data set (2007 and 2008) of PM10 mass concentration and chemical composition was presented. In particular, seven sources were resolved: sea-salt, mineral dust, biogenic emissions, primary particulate ship emissions, secondary sulphate, secondary nitrate, and combustion emissions. These results confirmed the experimental data set and its interpretation illustrated in this thesis.

References

Agrawal, H., Malloy, Q.G.J., Welch, W.A., Miller, J.W., Cocker, D.R.: In-use gaseous and particulate matter emissions from a modern ocean going container vessel. Atmos. Environ., 42, 5504−5510, 2008a.

Agrawal, H., Welch, W.A., Miller, J.W., Cocker, D.R.: Emission measurements from a crude oil tanker at sea. Environ. Sci. Technol., 42, 7098−7103, 2008b.

Avila, A., and Rodà , F.: Assessing decadal changes in rainwater alkalinity at a rural Mediterranean site in the Montseny mountains (NE Spain), Atmos. Environ., 36, 2881–2890, 2002.

Baker, A. R., and Croot, P.L.: Atmospheric and marine controls on aerosol iron solubility in seawater, Mar. Chem., 120, 4–13, 2010.

Bardouki, H., Liakakou, H., Economou, C., Sciare, J., Smolík, J., Ždímal, V., Eleftheriadis, K., Lazaridise, M., Dyef, C. and Mihalopoulos, N., Chemical composition of size-resolved atmospheric aerosols in the eastern Mediterranean during summer and winter, Atm. Env. 37, 195–208, 2003.

Bates, T. S., J. A. Calhoun, and P. K. Quinn,: Variations in the Methanesulfonate to Sulfate Molar Ratio in Submicrometer Marine Aerosol-Particles over the South Pacific Ocean, J. Geophys. Res., 97(D9), 9859-9865, 1992.

Becagli, S., Sferlazzo, D. M., Pace, G., di Sarra, A., Bommarito, C., Calzolai, G., Ghedini, C., Lucarelli, F., Meloni, D., Monteleone, F., Severi, M.,

Traversi, R., and Udisti, R.: Evidence for heavy fuel oil combustion aerosols from chemical analyses at the island of Lampedusa: a possible large role of ships emissions in the Mediterranean, Atmos. Chem. Phys., 12, 3479–3492, 2012.

Becagli, S., L. Lazzara, F. Fani, C. Marchese, R. Traversi, M. Severi, A. di Sarra, D. Sferlazzo, S. Piacentino, C. Bommarito, U. Dayan, R. Udisti.: Relationship between methanesulfonate (MS-) in atmospheric particulate and remotely sensed phytoplankton activity in oligo-mesotrophic Central Mediterranean Sea, Atmos. Environ., 79, 681-688, 2013.

S. Becagli, F. Anello, C. Bommarito, F. Cassola, G. Calzolai, T. Di Iorio, A. di Sarra, J.-L. Gómez-Amo, F. Lucarelli, M. Marconi, D. Meloni, F. Monteleone, S. Nava, G. Pace, M. Severi, D. M. Sferlazzo, R. Traversi, R. Udisti.: Constraining the ship contribution to the aerosol of the Central Mediterranean. Atmospheric Chemistry and Physics Discussions, 489 - 2016.

Bernardoni, V., Vecchi, R., Valli, G., Piazzalunga, A., and Fermo, P.: PM10 source apportionment in Milan (Italy) using timeresolved data, Sci. Total Environ., 409, 4788-4795, 2011.

Bernardoni, V., Calzolai, G., Chiari, M., Fedi, M., Lucarelli, F., Nava, S., Piazzalunga, A., Riccobono, F., Taccetti, F., Valli, G. and Vecchi, R.: Radiocarbon analysis on organic and elemental carbon in aerosol samples and source apportionment at an urban site in Northern Italy, J. Aer. Sci. 56, 88-99, 2013

Bethoux, J. P., Morin, P., and Ruiz-Pino, D. P.: Temporal trends in nutrient ratios: chemical evidence of Mediterranean ecosystem changes driven by human activity, Deep Sea Res. II, 49, 2007–2015, 2002.

Birch, M. E. and Cary, R. A.: Elemental Carbon–Based Method for Monitoring Occupational Exposures to Particulate Diesel Exhaust, Aerosol Sci. Tech., 25, 221–241, 1996.

Bozlaker, A., Buzcu-Güven, B., Fraser, M.P., Chellam, S.: Insights into PM10 source in Houston, Texas: Role of Petroleum refineries in enriching lanthanoid metal during episodic emission events. Atmos. Environ., 69, 109-117, 2013.

Bonnet, S. and Guieu, C., Atmospheric forcing on the annual iron cycle in the western Mediterranean Sea: A 1-year survey, J. of Geophys. Res., 111, 2006.

Boucher, O.: Atmospheric Aerosols Properties and climate impacts, XVII, 311, 2015.

J.L. Campbell, N.I. Boyd, N. Grassi, P. Bonnick, J.A. Maxwell, Nucl. Instr. Meth. B 268 (2010) 3356–3363.

Calzolai G., Chiari, M., García Orellana, I., Lucarelli, F., Migliori, A., Nava, S., and Taccetti, F.: The new external beam facility for environmental studies at the Tandetron accelerator of LABEC, Nucl. Instr. Meth. B, 249, 928–931, 2006.

Calzolai G., M. Chiari, F. Lucarelli, S. Nava, F. Taccetti, S. Becagli, D. Frosini, R. Traversi, R. Udisti,: PIXE–PIGE analysis of size-segregated aerosol samples from remote areas, Nucl. Instr. Meth. B, 318, Part A, pp. 125–129, 2014.

Calzolai, G., S. Nava, F. Lucarelli, M. Chiari, M. Giannoni, S. Becagli, R. Traversi, M. Marconi, D. Frosini, M. Severi, R. Udisti, A. di Sarra, G. Pace, D. Meloni, C. Bommarito, F. Monteleone, F. Anello, and D. M. Sferlazzo, Characterization of PM10 sources in the central Mediterranean, Atmos. Chem. Phys., 15, 13939–13955, 2015.

Canepari, S., Farao, C., Marconi, E., Giovannelli, C., and Perrino, C.:. Qualitative and quantitative determination of water in airborne particulate matter, Atmos. Chem. Phys., 13, 1193–1202, 2013.

Casasanta, G., di Sarra, A., Meloni, D., Monteleone, F., Pace, G., Piacentino, S., and Sferlazzo, D.: Large aerosol effects on ozone photolysis in the Mediterranean, Atmos. Environ., 45, 3937-3943, 2011.

Castillo, S., Moreno, T., Querol, X., Alastuey, A., Cuevas, E., Herrmann, L., Mounkaila, M., and Gibbons, W.: Trace element variation in size-fractionated African desert dusts, J. Arid Environ., 72, 1034–1045, 2008.

Chen, G., Huey, G., Trainer, M.: An investigation of the chemistry of ship emission plumes during ITCT 2002. J. Geophys. Res. 110, D10S90, 2005.

Clarke, A. D.; Owens, S. R.; Zhou, J. C. An ultrafine sea-salt flux from breaking waves: Implications for cloud condensation nuclei in the remote marine atmosphere. J. Geophys. Res.-Atmos., 111 (D6), D006565, 2006.

Coakley Jr., J. A. and Walsh, C. D.: Limits to the aerosol indirect radiative effect derived from observations of ship tracks, J. Atmos. Sci, 59, 668–680, 2002.

Cooper, D.A.: Exhaust emissions from ships at berth. Atmos. Environ., 37, 3817−3830, 2003.

Corbett, J.J., Winebrake, J.J., Green, E.H., Kasibhatla, P., Eyring, V., and Lauer, A.: Mortality from Ship Emissions: A Global Assessment, Environ. Sci., Technol., 41, 8512–8518, doi:10.1021/es071686z, 2007.

Criado, C., and Dorta, P.: An unusual “blood rain” over the Canary Islands (Spain). The storm of January 1999, J. Arid Environ., 55, 765–783, 2003.

Dabdub, D., Air quality impacts of ship emission in south coast air basin of California. Final report for State of California Air Resources Board Planning and Technical support division. 2008.

D'Almeida, G. A.: A Model for Saharan Dust Transport, J. Climate Appl. Meteor., 25, 903–916, 1986.

Dayan, U., Heffter, J. L., and Miller J. M.: Meteorological and climatological data from surface and upper measurements for the assessment of atmospheric transport and deposition of pollutants in the Mediterranean Basin: Part B: Seasonal distribution of the planetary boundary layer depths over the Mediterranean Basin, UNEP. Mediterranean Action Plan Technical Reports Series no. 30, Athens, Greece, 1989.

Dayan, U., Heffter, J., Miller, J., and Gutman, G.: Dust intrusion events into the Mediterranean Basin, J. Appl. Meteorol., 30, 1185–1199, 1991.

Dayan, U., and I. Levy,: Relationship between synoptic-scale atmospheric circulation and ozone concentrations over Israel. J. Geophys. Res., 107, 4813, 2002.

Dayan, U., and D. Lamb,: Global and synoptic-scale weather patterns controlling wet atmospheric deposition over central Europe. Atmos. Environ., 39, 521–533, 2005.

G. De Leeuw, E. L. Andreas, M. D. Anguelova et al.,: Production flux of sea spray aerosol, Reviews of Geophysics, vol. 49, no. 2, 2011.

Denjean, C., Cassola, F., Mazzino, A., Triquet, S., Chevaillier, S., Grand, N., Bourrianne, T., Momboisse, G., Sellegri, K., Schwarzenbock, A., Freney, E., Mallet, M., and Formenti, P.: Size distribution and optical properties of mineral dust aerosols transported in the western Mediterranean, Atmos. Chem. Phys., 16, 1081-1104, 2016.

Dentener, F. J., Carmichael, G. R., Zhang, Y., Leleieveld, J., and Crutzen, P. J.: Role of mineral aerosols as a reactive surface in the global troposphere, J. Geophys. Res., 101, 22869–22889, 1996.

Derwent, R., Stevenson, D. S., Doherty, R. M, Collins, W. J., Sanderson, M. G., Amann, M., and Dentener, F.: The contribution from ship emissions to air quality and acid deposition in Europe, Ambio, 34, 54–59, 2005.

Desboeufs, K.V., and Cautenet, G.: Transport and mixing zone of desert dust and sulphate over Tropical Africa and the Atlantic Ocean region, Atmos. Chem. Phys. Discuss., 5, 5615-5644, 2005.

Devasthale, A., Kr¨uuger, O., and Graßl, H.: Impact of ship emissions on cloud properties over coastal areas, Geophys. Res. Lett., 33, L02811, doi:10.1029/2005GL024470, 2006.

Di Iorio, T., di Sarra, A., Sferlazzo, D. M., Cacciani, M., Meloni, D., Monteleone, F., Fuà, D., and Fiocco, G.: Seasonal evolution of the tropospheric aerosol vertical profile in the central Mediterranean and role of desert dust, J. Geophys. Res., 114, D02201, 2009.

Di Sarra, A., Di Biagio, C., Meloni, D., Monteleone, F., Pace, G., Pugnaghi, S., and Sferlazzo, D.: Shortwave and longwave radiative effects of the intense Saharan dust event of 25–26 March 2010 at Lampedusa (Mediterranean sea), J. Geophys. Res., 116, D23209, 2011.

Draxler, R.R. and Rolph, G.D.: HYSPLIT (HYbrid Single-Particle Lagrangian Integrated Trajectory) Model access via NOAA ARL READY Website (http://ready.arl.noaa.gov/HYSPLIT.php). NOAA Air Resources Laboratory, Silver Spring, MD. 2012.

Du, l., Turner, J.:Using PM2.5 lanthanoid elements and nonparametric wind regression to track petroleum refinery FCC emissions. Sci. of Tot Environ, 529, 65-71. 2015.

Duce, R. A., Liss, P. S., Merrill, J. T., Buat-Menard, P., Hicks, B. B., Miller, J. M., Prospero, J. M., Arimoto, R., Church, T. M., Ellis, W., Galloway, J. N.,

Hanson, K., Jickells, T. D., Knapp, A. H., Rienhart, K. H., Schneider, B., Soudine, A., Tokos, J. J., Tsunogai, S., Wollast, R. and Zhou, M.: The atmospheric input of trace species to the world ocean, Global Biogeochemical Cycles, 5, 193-259, 1991.

Eldred, R. A., Cahill, T. A., and Feeney, P. J.: Particulate monitoring at US National Parks using PIXE, Nucl. Instr. Meth. B, 22, 289-295, 1987.

Endresen, Ø., Sørg°ard, E., Sundet, J. K., Dalsøren, S. B., Isaksen, I. S. A., Berglen, T. F., and Gravir, G.: Emissions from international sea transportation and environmental impact, J. Geophys. Res., 108, 4560, 2003.

Engelstaedter, S., and. Washington, R.: Atmospheric controls on the annual cycle of North African dust, J. Geophys. Res., 112, D03103, 2007.

Erel, Y., Dayan, U., Rabi, R., Rudich, Y., and Stein, M.: Trans boundary transport of pollutants by atmospheric mineral dust, Env. Sci.e & Tech., 40, 2996–3005, 2006.

Escudero, M., Querol, X., Avila, A., and Cuevas, E.: Origin of the exceedances of the European daily PM limit value in the regional background areas of Spain, Atmos. Environ., 41, 730-744, 2007.

Escudero, M., Stein, A. F., Draxler, R. R., Querol, X., Alastuey, A., Castillo, S., and Avila, A.: Source apportionment for African dust outbreaks over the Western Mediterranean using the HYSPLIT model, Atmos. Res., 99, 518–527, 2011.

Evans, C.D., Chadwick T., Norris D., Rowe, E.C., Heaton, T.H.E., Brown, P., Battarbee, R. W.,: Persistent surface water acidification in an organic soil-dominated upland region subject to high atmospheric deposition: The North York Moors, UK. Ecological Indicators 37, 304–16. 2014.

A. T. Evan, C. Flamant, M. Gaetani, F. Guichard.: The past, present and future of African dust. Nature, 531, 493-495, 2016.

Fairlie, T. D., Jacob, D. J., Dibb, J. E., Alexander, B.,. Avery, M. A, van Donkelaar, A., and Zhang, L.: Impact of mineral dust on nitrate, sulphate, and ozone in transpacific Asian pollution plumes, Atmos. Chem. Phys., 10, 3999-4012, 2010.

Fenger, J.: Urban Air Quality. Atmos. Environ. 33: 4877-4900, 1999.

Finlayson-Pitts, B., J.N., Pitts,: Chemistry of the Upper and Lower Atmosphere: theory, experiment, and application - chapter 9, Academic Press, 381–391 pp., 2000.

Gallisai, R., Peters, F., Basart, S., and Baldasano, J. M.: Mediterranean basin-wide correlations between Saharan dust deposition and ocean chlorophyll concentration, Biogeosciences Discuss., 9, 8611–8639, doi:10.5194/bgd-9-8611-2012, 2012.

Gerasopoulos, E., Kouvarakis, G., Babasakalis, P., Vrekoussis, M., Putaud, J. -P., and Mihalopoulos, N.: Origin and variability of particulate matter (PM10) mass concentrations over the Eastern Mediterranean, Atmos. Environ., 40, 4679–4690, 2006.

Guerzoni, S., Chester, R., Dulac, F., Herut, B., Loye-Pilot, M-D., Measures, C., Migon, C., Molinaroli, E., Moulin, C., Rossini, P., Saydam, C., Soudine, A., and Ziveri, P.: The role of atmospheric deposition in the biogeochemistry of the Mediterranean Sea. Prog. Oceanogr., 44, 147–190, 1999.

Harrison, R.M. and Yin, J.: Particulate Matter in the Atmosphere: Which Particle Properties are Important for Its Effects on Health? Sci. Total Environ. 249: 85-101, 2000.

Hellebust, S., Allanic, A., O'Connor, I.P., Jourdan, C., Healy, D., Sodeau, J.R.: Sources of ambient concentrations and chemical composition of PM2.5-0.1 in Cork Harbour, Ireland. Atmos. Res. 95, 136-149. 2010.

Henderson, P. and Henderson, G. M.: Earth science data, Cambridge University Press, 92–97, 2009.

Henne, S., Brunner, D., Folini, D., Solberg, S., Klausen, J. and Buchmann, B.: Assessment of parameters describing representativeness of air quality in-situ measurement sites, Atmos. Chem. Phys., 10, 3561-3581, 2010.

Hinds, W.C.: Aerosol Technology: Properties, Behavior and Measurement of Airborne Particles, John Willey and Sons, 1999.

Hou X. and Jones B.T., Inductively Coupled Plasma/Optical Emission Spectrometry, Encyclopedia of Analytical Chemistry, R.A. Meyers (Ed.) pp. 9468–9485, John Wiley & Sons Ltd, Chichester, 2000.

Isakson, J., Persson, T.A., Lindgren, E.S.: Identification and assessment of ship emissions and their effects in the harbour of Goteborg, Sweden. Atmos. Environ. 35, 3659-3666. 2001.

Israelevich, P. L., Levin, Z., Joseph, J. H., and Ganor, E.: Desert aerosol transport in the Mediterranean region as inferred from the TOMS aerosol index, J. Geophys. Res., 107(D21), 4572, 2002.

Intergovernmental Panel on Climate Change (IPCC) 2001 In Climate change 2001: The scientific basis (eds J. T. Houghton, Y. Ding, D. J. Griggs, M. Noguer, P. J. van der Linden & D. Xiaosu), New York, NY: Cambridge University Press, 2001.

IPCC: Climate Change 2007: The Physical Science Basis, Contribution of Working Group I to the Fourth Assessment Report of the IPCC, ISBN 978 0521 88009-1 Hardback; 978 0521 70596-7 Paperback, 2007.

Fifth Assessment Synthesis Report of IPCC (2014) by Myles R. Allen, Vicente R. Barros, John Broome, et al. edited by Paulina Aldunce, Thomas Downing, Sylvie Joussaume, et al., Cambridge University Press, 2014.

Jiang, Q., Smith, R.B., Doyle, J.: The nature of the mistral: Observation and modelling of two MAP events. Q. J. R. Meteorol. Soc. 129, 857–875, 2003.

Kallos, G., P. Kassomenos, and R. A. Pielke,: Synoptic and mesoscale weather conditions during air pollution episodes in Athens, Greece. Bound.-Layer Meteor., 62, 163–184, 1993.

Kallos, G., and A. Papadopoulos,: On the long-range transport of air pollutants from Europe to Africa. Geophys. Res. Lett., 25, 619–622, 1998a.

Kallos, G., A. Papadopoulos, P. Katsafados, and S. Nickovic,: Trans-Atlantic Saharan dust transport: Model simulation and results. J. Geophys. Res., 111, D09204, 2006.

Kallos, G., Astitha, M., Katsafados, P., and Spyrou, C.: Long-Range transport of Anthropogenically and Naturally Produced particulate matter in the Mediterranean and north Atlantic: current State of Knowledge, J. Appl. Meteorol. Clim., 46 (8), 1230–1251, 2006.

Khiri, F., Ezaidi, A., and Kabbachi, K.: Dust deposits in Souss–Massa basin, South-West of Morocco: granulometrical, mineralogical and geochemical characterization, Journal of African Earth Sciences 39, 459–464, 2004.

Kishcha P., Nickovic, S., Starobinets, B., di Sarra, A., Udisti, R., Becagli, S., Sferlazzo, D., Bommarito, C. and Alpert, P.: Sea-salt aerosol forecasts compared with daily measurements at the island of Lampedusa (Central Mediterranean), Atmos. Res., 100, 28–35, 2011.

P. Kishcha, B. Starobinets, R. Udisti, S. Becagli, A. di Sarra, D. Sferlazzo, C. Bommarito, and P. Alpert,: Sea-Salt Aerosol Mass Concentration Oscillations after Rainfall, Derived from Long-Term Measurements in Lampedusa (Central Mediterranean), ISRN Meteorology, Volume 2012, Article ID 679120, 8 pages, 2012.

Koirtyohann S.R., J.S. Jones, C.P. Jester, D.A. Yates,: Use of Spatial Emission Profiles and a Nomenclature System as Acids in Interpreting Matrix Effects in the Lowpower Argon Inductively Coupled Plasma, Spectrochim. Acta, 36B(1), 49–59, 1981.

Kopanakis, I., Eleftheriadis, K., Mihalopoulos, N., Lydakis-Simantiris, N., Katsivela, E., Pentari, D., Zarmpas, P. and Lazaridis, M.: Physico-chemical characteristics of particulate matter in the Eastern Mediterranean, Atmospheric Research 106, 93–107, 2012.

Koulouri, E., Saarikoski S., Theodosi C., Markaki Z., Gerasopoulos, E., G. Kouvarakis , Mäkelä, T., Hillamo, R., and Mihalopoulos, N.: Chemical composition and sources of fine and coarse aerosol particles in the Eastern Mediterranean, Atmos. Environ., 42, 6542–6550, 2008.

Kouvarakis, G., Tsigaridis, K., Kanakidou, M., and Mihalopoulos, N.: Temporal variations of surface regional background ozone over Crete Island in southeast Mediterranean, J. Geophys. Res., 105, 4399–4407, 2000.

Kulkarni, P., Chellam, S., Fraser, M.P.: Lanthanum and lanthanides in atmospheric fine particles and teir apportionment to refinery and petrochemical operations in Houston, TX. Atmos. Environ., 40, 508-520, 2006.

Lauer, A., Eyring, V., Hendricks, J., J¨ockel, P., and Lohmann, U.: Global model simulations of the impact of ocean-going ships on aerosols, clouds, and the radiation budget, Atmos. Chem. Phys., 7, 5061–5079, 2007.

Lee T., Yu X.Y., Ayres B., Kreidenweis S.M., Malm W.C., Collett Jr J.L.: Observations of fine and coarse particle nitrate at several rural locations in the United States. Atmos Environ; 42 (11): 2720–32, 2007.

Lelieveld, J, and Dentener, F. J.: What controls tropospheric ozone?, J. Geophys. Res., 105, 3531-3551, 2000.

Levin, Z., Ganor, E., and Gladstein, V.: The effects of desert particles coated with sulfate on rain formation in the Eastern Mediterranean, J. Appl. Meteorol., 35, 1511–1523, 1996.

Lewis, E.R., Schwartz, S.E.,: Sea salt aerosol production: mechanisms, methods, measurements, and models—a critical review. Geophys. Monogr. Ser. 152 AGU, Washington, D.C., 412 p., 2004.

Li, Z. and Aneja, V. P.: Regional analysis of cloud chemistry at high elevations in the eastern United States, Atmos. Environ., 26A, 2001–2017, 1992.

Linke, C., Möhler, O., Veres, A., Mohácsi, Á., Bozóki, Z., Szabó, G., and Schnaiter, M.: Optical properties and mineralogical composition of different Saharan mineral dust samples: a laboratory study, Atmos. Chem. Phys. Disc., 6, 2897–2922, 2006.

Lloyd's Register Engineering Services,: Marine Exhaust Emissions Research Programme, London. pp. 63, 1995.

F. Lucarelli, G. Calzolai, M. Chiari, M. Giannoni, D. Mochi, S. Nava, L. Carraresi, The upgraded external-beam PIXE/PIGE set-up at LABEC for

very fast measurements on aerosol samples, Nucl.Instr.&Meth. B318, 55-59, 2014.

Luria, M., and Coauthors,: Atmospheric sulphur over the east Mediterranean region. J. Geophys. Res., 101, 25 917–25 930, 1996.

Lyyränen, J., Jokiniemi, J., Kauppinen, E.I., Joutsensaari, J.: Aerosol characterisation in medium-speed diesel engines operating with heavy fuel oils. J. Aerosol Sci. 30, 771−784, 1999.

Maheras P., Xoplaki, E., Kutiel, H.: Wet and Dry monthly anomalies across the Mediterranean basin and their relationship with circulation 1860-1990, Theor. Appl. Climatol., 189-199, 1999.

Malm, W. C., Sisler, J. F., Huffman, D., Eldred, R. A., and Cahill, T. A.: Spatial and seasonal trends in particle concentration and optical extinction in the United States, J. Geophys. Res., 99, 1347-1370, 1994.

Marcazzan, G. M., Vaccaro, S., Valli, G., and Vecchi, R.: Characterisation of PM10 and PM2.5 particulate matter in the ambient air of Milan (Italy), Atmos. Environ., 35, 4639-4650, 2001.

Marconi, M., Sferlazzo, D.M., Becagli, S., Bommarito, C., Calzolai, G., Chiari, M., di Sarra A., Ghedini, C., Gómez-Amo, J.L., Lucarelli F., Meloni D., Monteleone F., Nava S., Pace G., Piacentino S., Rugi F., Severi M., Traversi R., and Udisti R.: Saharan dust aerosol over the central Mediterranean Sea: PM10 chemical composition and concentration versus optical columnar measurements Atmos. Chem. Phys., 14, 2039–2054, 2014.

Marmer, E., Dentener, F., Aardenne, J.V., Cavalli, F., Vignati, E., Velchev, K., Hjorth, J.,Moldanová, J., Fridell, E., Popovicheva, O., Demirdjian, B., Tishkova, V., Faccinetto, A., Focsa, C.: Characterisation of particulate matter and gaseous emissions from a large ship diesel engine. Atmos. Environ., 43, 2632−2641, 2009.

Marticorena, B., Bergametti, G., Aumont, B., Callot, Y., N'Doumé C. and Legrand M.: Modelling the atmospheric dust cycle : 2-Simulations of Saharan dust sources, J. Geophys. Res., 102, 4387-4404, 1997.

Mayer, H.: Air Pollution in Cities. Atmos. Environ. 33: 4029-4037, 1999.

Mazzei F., D'Alessandro, A., Lucarelli, F., Nava, S., Prati, P., Valli, G., and Vecchi R.: Characterization of particulate matter sources in an urban environment. Sci. of Tot. Environ., 401, 81–89, 2008.

McFiggens, G., Plane, J. M. C., Allan, B. J., Carpenter, L. J., Coe, H. & O'Dowd, C. D.: A model study of Iodine chemistry in the marine boundary layer. J. Geophys. Res. 105, 14 371–14 386, 2000.

Meloni, D., di Sarra, A., Fiocco, G., and Junkermann, W.: Tropospheric aerosols in the Mediterranean: III. Measurements and modeling of actinic radiation profiles, J. Geophys. Res., 108 (D10), 4323, 2003.

Metzger, S., Mihalopoulos, N., and Lelieveld, J.: Importance of mineral cations and organics in gas-aerosol partitioning of reactive nitrogen compounds: case study based on MINOS results, Atmos. Chem. Phys., 6, 2549–2567, 2006.

Millán, M., and G. Kallos,: Photo oxidant dynamics in the Mediterranean Basin in summer: Results from European research projects. J. Geophys. Res., 102, 8811–8823, 1997.

Millán, and Coauthors,: Climatic feedbacks and desertification: The Mediterranean model. J. Climate, 18, 684–701, 2005.

Miranda, J., Cahill, T. A., and Morales, J. R.: Determination of elemental concentrations in atmospheric aerosols in Mexico City using proton induced X-Ray emission, proton Elastic scattering and Laser absorption, Atmos. Environ., 28, 2299-2306, 1994.

Moldanová, J., Fridell, E., Popovicheva, O., Demirdjian, B., Tishkova, V., Faccinetto, A., Focsa, C. Characterisation of particulate matter and gaseous emissions from a large ship diesel engine. Atmos. Environ. 2009, 43, 2632−2641.

Moreno, T., Querol, X., Castillo, S., Alastuey, A., Cuevas, E., Herrmann, L., Mounkaila, M., Elvira, J., and Gibbons, W.: Geochemical variations in aeolian mineral particles from the Sahara–Sahel dust corridor, Chemosphere, 65, 261–270, 2006.

Moreno, T., Querol, X., Alastuey, A., Pey, J. Cruzminguillon, M., Perez, N., Bernabe, R., Blanco, S. Cardenas, B., Gibbons, W., :Lanthanoid geochemistry of urban atmospheric particulate matter, Environ. Sci. Technol. 42, 6502–6507, 2008a.

Moreno, T., Querol, X., Alastuey, A., Gibbons, W.: Identification of FCC refinery atmospheric pollution events using lanthanoid- and vanadium-bearing aerosols. Atmos. Environ., 42, 7851-7861, 2008b.

Murphy, D., J. Anderson, P. Quinn, L. McInnes, F. Brechtel, S. Kreidenweis, A. Middlebrook, M. Posfai, D. Thomson, and P. Buseck, Influence of sea-salt on aerosol radiative properties in the Southern Ocean marine boundary layer, Nature, 392(6671), 62-65, 1998a.

Murphy, S., Agrawal, H., Sorooshian, A., Padró, L.T., Gates, H., Hersey, S., Welch, W. A., Jung, H., Miller, J. W., Cocker, D.R. III, Nenes, A., Jonsson, H.H., Flagan, R.C., Seinfeld, J.H.: Comprehensive simultaneous shipboard and airborne characterization of exhaust from a modern container ship at sea. Environ. Sci. Technol. 43, 4626−4640, 2009.

Nava, S., Becagli, S., Calzolai, G., Chiari, M., Lucarelli, F., Prati, P., Traversi, R., Udisti, R., Valli G., and Vecchi R.: Saharan dust impact in central Italy: An overview on three years elemental data Records, Atmos. Environ., 60, 444-452, 2012.

Norris, G. A., Vedantham, R., Wade, K., Zhan, P., Brown, S., Paatero, P., Eberly, S. I., Foley, C.: Guidance Document for PMF Applications with the Multilinear Engine. U.S. Environmental Protection Agency, Washington, DC, EPA/600/R-09/032 (NTIS PB2009-107895), 2009

O'Dowd, C. D., Smith, M. H., Consterdine, I. E. & Lowe, J. A.: Marine aerosol, sea salt, and the marine sulphur cycle: a short review. Atmos. Environ. 31, 73–80, 1997.

C. D. O'Dowd and G. de Leeuw,: Marine aerosol production: a review of the current knowledge, Phil. Trans. R. Soc. A , 365, 1753–1774, 2007.

M.P. Pavageau, A. Morin, F. Séby, C. Guimon , E. Krupp , C. Pécheyran, J. Poulleau and O. F. X. Donard,: Partitioning of Metal Species during an Enriched Fuel Combustion Experiment. Speciation in the Gaseous and Particulate Phases, Environ. Sci. Technol., 38 (7), pp 2252–2263, 2004.

Pace, G., di Sarra, A., Meloni, D., Piacentino, S., and Chamard, P.: Aerosol optical properties at Lampedusa (Central Mediterranean). 1. Influence of transport and identification of different aerosol types, Atmos. Chem. Phys., 6, 697–713, doi:10.5194/acp-6-697-2006, 2006.

Pederzoli, A., Mircea, M., Finardi, S., di Sarra, A., and Zanini, G.: Quantification of Saharan dust contribution to PM10 concentrations over Italy in 2003-2005, Atmos. Environ, 44, 4181-4190, 2010.

Perrino, C., Canepari, S., Cardarelli, E., Catrambone, M., and Sagolini, T.: Inorganic constituents of urban air pollution in the Lazio region (Central Italy), Environ Monit. Assess., 136, 69–86, 2008.

Pey, J., Querol, X., and Alastuey, A.: Variations of levels and composition of PM10 and PM2.5 at an insular site in the Western Mediterranean, Atmos. Res., 94, 285–299, 2009.

Pey, J., Querol X., Alastuey, A., Forastiere, F., and Stafoggia, M.: African dust outbreaks over the Mediterranean Basin during 2001–2011: PM10 concentrations, phenomenology and trends, and its relation with

synoptic and mesoscale meteorology, Atmos. Chem. Phys., 13, 1395-1410, doi:10.5194/acp-13-1395-2013, 2013.

A. Piazzalunga, V. Bernardoni , P. Fermo , G. Valli , and R. Vecchi, Technical Note: On the effect of water-soluble compounds removal on EC quantification by TOT analysis in urban aerosol samples, Atmos. Chem. Phys., 11, 10193–10203, 2011.

Polissar, A. V., Hopke, P. K., Paatero, P., Malm, W. C. and Sisler, J. F.: Atmospheric aerosol over Alaska – 2. Elemental composition and sources, J. Geophys. Res. 103, 19045-19057, 1998.

Querol, X., Alastuey, A., Pey, J., Cusack, N. Pérez, N., Mihalopoulos, N., Theodosi, C., Gerasopoulos, E., Kubilay, N. and Koçak, M.: Variability in regional background aerosols within the Mediterranean, Atmos. Chem. Phys., 9, 4575–4591, 2009.

Rodríguez, S., Alastuey, A., Alonso-Pérez, S., Querol, X., Cuevas, E., Abreu-Afonso, J., Viana, M., Perez, N., Pandolfi, M., and de la Rosa, J.: Transport of desert dust mixed with North African industrial pollutants in the subtropical Saharan Air Layer, Atmos. Chem. Phys., 11, 6663–6685, doi:10.5194/acp-11-6663-2011, 2011.

Rodríguez, S., Alastuey, A., and Querol, X.: A review of methods for long term in situ characterization of aerosol dust, Aeolian Res., 6, 55–74, 2012.

Rodríguez, S., Querol, X., Alastuey, A., Kallos, G., and Kakaliagou, O.: Saharan dust contributions to PM10 and TSP levels in Southern and Eastern Spain, Atmos. Environ., 35, 2433–2447, 2001.Scheuvens, D.,

Schütz, L., Kandler, K, Ebert, M., and Weinbruch, S.: Bulk composition of northern African dust and its source sediments — A compilation, Earth-Science Rev., 116, 170–194, 2013.

Randerson, J. T., Chen, Y., van der Werf, G. R., Rogers, B. M. and Morton, D. C.: Global burned area and biomass burning emissions from small fires, J. Geophys. Res., 117, G04012, doi:10.1029/2012JG002128, 2012.

Rodríguez, S., Alastuey, A., Alonso-Pérez, S., Querol, X., Cuevas, E., Abreu-Afonso, J., Viana, M., Pérez, N., Pandolfi, M. and de la Rosa, J.: Transport of desert dust mixed with North African industrial pollutants in the subtropical Saharan Air Layer, Atmos. Chem. Phys., 11, 6663–6685, 2011.

Rosenfeld, D., Lahav, R., Khain, A., Pinsky, M.,: The role of sea spray in cleansing air pollution over ocean via cloud processes. Science 297, 1667–1670, 2002.

Salvador, P., Alonso-Pérez, S., Pey, J., Artíñano, B., de Bustos, J. J., Alastuey, A., and Querol, X.: African dust outbreaks over the western Mediterranean Basin: 11-year characterization of atmospheric circulation patterns and dust source areas, Atmos. Chem. Phys., 14, 6759–6775, 2014.

Skamarock, W. C., Klemp, J. B., Dudhia, J., Gill, D. O., Barker, D. M., Huang, X. Z., Wang, W., and Powers, J. G.: A Description of the Advanced Research WRF Version 3. Technical report. Mesoscale and Microscale Meteorology Division, NCAR, Boulder, Colorado, 2008.

Sharif, S.: Chemical and mineral composition of dust and its effect on the dielectric constant, IEEE Trans. Geosci. Remote Sens., 33, 353–358, 1995.

Scheuvens, D., Schütz, L., Kandler, K., Ebert, M., and Weinbruch, S. (2013). Bulk composition of northern African dust and its source sediments—A compilation. Earth Sci. Rev. 116, 170–194, 2012.

Shah, S.D., Cocker, D.R., Miller, J.W., Norbeck, J.M.: Emission rates of particulate matter and elemental and organic carbon from in-use diesel engines. Environ. Sci. Technol., 38, 2544–2550, 2004.

Sippula, O., Hokkinen, J., Puustinen, H., Yli-Piril¨a, P., and Jokiniemi J: Comparison of particle emissions from small heavy fuel oil and wood-fired boilers. Atmos. Environ., 43, 4855–4864, 2009.

Sippula, O., Stengel, B., Sklorz, M., Streibel, T., Rabe, R., Orasche, J., Lintelmann, J., Michalke, B., Abbaszade, G., Radischat, C., Gröger, T., Schnelle-Kreis, J., Harndorf, H., and Zimmermann R.: Particle emissions from a marine engine: chemical composition and aromatic emission profiles under various operating conditions. Environ. Sci. Technol., 48, 11721−11729, 2014.

Stein, A. F., Draxler, R. R, Rolph, G. D., Stunder, B. J. B., Cohen, M. D., and Ngan, F.: NOAA's HYSPLIT atmospheric transport and dispersion modeling system, Bull. Amer. Meteor. Soc., 96, 2059-2077, 2015.

Stern, N.,: The Economics of Climate Change: The Stern Review. Cambridge and New York, Cambridge University press. 2007.

Tesche, M., Gross, S., Ansmann, A., Müller, D., Althausen, D., Fredenthaler, V. and Esselborn, M.: Profiling of Saharan dust and biomass-burning smoke with multiwavelength polarization Raman lidar at Cape Verde, Tellus, 63B, 649–676, 2011.

Tomadin, L., Cesari, G., Fuzzi, S., Landuzzi, V., Lenaz, R., Lobietti, A., Mandrioli, P., Mariotti, M., Mazzucotelli, A., and Vannucci, R.: Eolian dust collected in springtime (1979 and 1984 years) at the seawater–air interface of the Northern Red Sea. In: Leinen, M., Sarnthein, M. (Eds.), Palaeoclimatology and Palaeometeorology: Modern and Past Patterns of Global Atmospheric Transport. NATO ASI Series C, 282. Kluwer Academic Publishers, Dordrecht, The Netherlands. 1989.

Tsyro S. G.: To what extent can aerosol water explain the discrepancy between model calculated and gravimetric PM10 and PM2.5?. Atmos. Chem. Phys., 5, 515–532, 2005.

Traversi, R., Becagli, S., Calzolai, G., Chiari, M., Giannoni, M., Lucarelli, F., Nava, S., Rugi, F., Severi, M. and Udisti, R.: A comparison between PIXE and ICP-AES measurements of metals in aerosol particulate collected in urban and marine sites in Italy, Nucl. Instr. and Meth. B, 318, 130-134, 2014.

Viana, M., Amato, F., Alastuey, A., Querol, X., Moreno, T., Santos, S.G.D., Herce, M.D., Fernández-Patier, R.: Chemical tracers of particulate emissions from commercial shipping. Environ. Sci. and Tech. 43, 7472-7477, 2009.

Vignati, E., Facchini, M.C., Rinaldi, M., Scannell, C., Ceburnis, D., Sciare, J., Kanakidou, M., Myriokefalitakis, S., Dentener, F., O'Dowd, C.D. Global scale emission and distribution of sea spray aerosol: sea-salt and organic enrichment. Atmospheric Environment, 2009.

Vogt, R., Crutzen, P. J. & Sander, R.: A mechanism for halogen release from sea salt aerosol in the remote marine boundary layer. Nature 383, 327–330, 1996.

Wagener, T., Guieu, C., and Leblond N.: Effects of dust deposition on iron cycle in the surface Mediterranean Sea: results from a mesocosm seeding experiment, Biogeosciences, 7, 3769–3781, doi:10.5194/bg-7-3769-2010, 2010.

Wang, Y., Zhuang, G., Chen, S., An, Z. and Zheng, A.: Characteristics and sources of formic, acetic and oxalic acids in PM2.5 and PM10 aerosols in Beijing, China. Atmospheric Research 84, 169-181, 2007.

P. Warneck,: Chemistry of the Natural Atmosphere, Academic Press, San Diego, Calif, USA, 1988.

Wu P.M., Okada K.: Nature of coarse nitrate particles in the atmosphere—a single particle approach. Atmos Environ.; 28:2053–60, 1994.

Cheng Wu , X. H. Hilda Huang , Wai Man Ng , Stephen M. Griffith and Jian Zhen Yu.: Inter-comparison of NIOSH and IMPROVE protocols for OC and EC determination: implications for inter-protocol data conversion. Atmos. Meas. Tech., 9, 4547–4560, 2016

Zhao, Y., and Y. Gao (2008b),: Acidic species and chloride depletion in coarse aerosol particles in the US east coast, Sci. Total Environ., 407(1), 541-547, 2008.

Zender, C. S., Miller, R. L., and Tegen, I.: Quantifying mineral dust mass budgets: Terminology, constraints, and current estimates, Eos Trans. Amer. Geophys. Union, 85, 48, 509- 512, 2004.

Zhuang H., Chan C.K., Fang M., Wexler A.S., Formation of nitrate and non-sea-salt sulfate on coarse particles. Atmos Environ; 33:4223–33, 1999a.

Zhuang H., Chan C.K., Fang M., Wexler A.S.,: Size distributions of particulate sulfate, nitrate, and ammonium at a coastal site in Hong Kong., Atmos Environ; 33:843–53, 1999b.

SUMMARY